UC Irvine
UC Irvine Electronic Theses and Dissertations

Title

Quantitative Percussion Diagnostics For Evaluating Bond Integrity Between Composite Laminates

Permalink

https://escholarship.org/uc/item/28j257d2

Author

Poveromo, Scott

Publication Date

2015

Peer reviewed|Thesis/dissertation

UNIVERSITY OF CALIFORNIA,
IRVINE

Quantitative Percussion Diagnostics For Evaluating Bond Integrity Between Composite
Laminates

DISSERTATION

submitted in partial satisfaction of the requirements
for the degree of

DOCTOR OF PHILOSOPHY

in Materials Science and Engineering

by

Scott Leonard Poveromo

Dissertation Committee:
Professor James Earthman, Chair
Associate Professor Lorenzo Valdevit
Assistant Professor Daniel Mumm
Chancellor's Professor Reginald Penner

2015

DEDICATION

To my wife Sarah and two children Maria and Julia....
For waiting patiently and helping me persevere throughout the process

To my and parents, sister Jamie, and friends....
For providing encouragement and support during the ups and downs

To my late grandfather Leo.....
For always reminding me that working hard will be rewarded

TABLE OF CONTENTS

Page

LIST OF FIGURES

LIST OF TABLES

Page

ACKNOWLEDGMENTS

CURRICULUM VITAE

Scott Leonard Poveromo

<u>**EDUCATION**</u>
University of California, Irvine (2015)
The Henry Samueli School of Engineering, Ph.D. Materials Science and Engineering,
Thesis topic: **"Quantitative Percussion Diagnostics for Evaluating Bond Integrity between Composite Laminates"**

San Jose State University (2009)
College of Engineering, MS Materials Engineering,
Thesis topic: **"The Effect of Strain on the Electrical Resistivity of Carbon Filled Elastomers"**

University of Virginia, Charlottesville, VA (1999)
School of Engineering and Applied Science, BS Chemical Engineering,
Thesis topic: **"Analysis of Carbon Fibers in Order to Cost Effectively Repair Bridges: Scale-up of Vapor Grown Carbon Fiber Process"**

<u>**PROFESSIONAL EXPERIENCE**</u>
Northrop Grumman Engineering and Global Product Development, El Segundo, CA- June 2012-Present
Part Time Intern in Advanced Materials and Processes Group
- Development of advanced non-destructive inspection techniques for composite bonded structures
- Development of ceramic matrix composite materials for use in high temperature structural applications
- Development of open cell metallic sandwich structure for actively cooled thermal protection systems

Graduate Student, University of California, Irvine (UCI) – August 2010-Present
   Research
- Quantitative Percussion Diagnostics For Evaluating Bond Integrity Between Composite Laminates
    - Completed Northrop Grumman-UCI contract on non-destructive characterization of adhesive bonded composite structures
    - Worked with MSC Software on non-linear FEA analysis to examine bond integrity between composite laminates-published case study
- Worked on UCI/Advanced Systems and Technologies team to complete Navy Phase 1 STTR on nondestructive testing of bonded composite panels.
- Teamed with UC Riverside on project to characterize bonded silicon wafers using percussion diagnostics

Teaching
- Teaching assistant for the following classes:
CBEMS 155L Mechanical Behavior of Materials (twice), CBEMS 50L Principles of Materials Science and Engineering (once) and CBEMS 175 Design Failure Investigation (3 times)

BAE Systems, US Combat Systems, Santa Clara, CA- Sept. 2007-July 2010
Staff Materials Engineer, Supervisor of Composites Lab
- Developed composite prototyping capability at Santa Clara using out-of-autoclave processing
- Managed buying of new equipment and materials for composites lab to improve capabilities
- Conducted research and development activities in the composites lab focusing on improving various components on wheeled and tracked armored vehicles
- Taught non-metallic materials engineering tutorials for design engineers
- Completed several non-metallic failure analyses

Lockheed Martin Space Systems Company, Sunnyvale, CA- Nov. 1999-Sept. 2007
Materials Engineer Sr.
Special Programs (January 2002-September 2007)
- Principal materials and processes engineer for structures utilizing advanced fiber reinforced polymer matrix composites and adhesives
- Coordinated activities with vendors in selecting and ordering composite materials to meet specification requirements
- Fabricated, conditioned, and tested material coupons for multiple physical and mechanical properties
- Compared different NDT techniques (ultrasound, X-ray, thermography, dye penetrant) in determining the extent of damage of composite sandwich panels after exposure to different temperature extremes
- Worked in multidisciplinary teams to achieve technical milestones under an aggressive schedule

Qualification of Materials for SBIRS Program (June 2000-March 2002)
- Led the successful development and evaluation of thermal control materials
- Qualified a new thermal control paint process in-house for the program and performed all qualification and process control testing on schedule.

Advanced Technology Center R&D (March 2000-October 2000)
- Worked on a R&D team to develop a new thermal protection coating system
- Involved in the selection and characterization of materials that may be used to reduce the thermal mismatch stresses in the coating and improve durability.

RELEVANT PUBLICATIONS/PRESENTATIONS

- Poveromo, Scott and Earthman, James. "Development of Percussion Diagnostics in Evaluating 'Kiss' Bonds Between Composite Laminates." SAMPE Conference Proceedings: Education & Green Sky - Materials Technology for a Better World. Long Beach, CA. May 6-9, 2013. Society for the Advancement of Material and Process Engineering.
- Poveromo, Scott and Earthman, James. "Development of Percussion Diagnostics in Evaluating 'Kiss' Bonds Between Composite Laminates." TMS Conference Proceedings: Advanced Composites for Aerospace, Marine, and Land Applications. Edited by Tomoko Sano, T.S. Srivatsan and Michael W. Peretti. San Diego, CA February 16th-20th, 2014. The Minerals, Metals & Materials Society.
- Poveromo, Scott and Earthman, James. "Analysis of Kiss Bonds Between Composite Laminates." *Journal of Materials* 66 (2014): 970-978.
- Presentation only: MSC Aerospace and Defense Industry User Meeting September 17, 2014
- Case study published with MSC Software based on FEA Analysis performed at UCI http://mscdrupal.mscsoftwarecorpo.netdna-cdn.com/cdn/farfuture/kUQwp31pxDjeyR9A4XDfsINo0oCHKrt3sZ78KDJFMRU/mtime:1422990242/sites/default/files/cs_uci_ltr_w.pdf. 2015.
- Poveromo, Scott and Earthman, James. "Finite Element Analysis of Quantitative Percussion Diagnostics for Evaluating the Strength of Bonds Between Composite Laminates." TMS Conference Proceedings: Advanced Composites for Aerospace, Marine, and Land Applications II. Edited by Tomoko Sano and T.S. Srivatsan. Orlando, Fl March 15th-19th, 2015. The Minerals, Metals & Materials Society.

HONORS AND AWARDS
- Bronze Chairman Award, BAE Systems, 2009
- Special Recognition Team Award, Lockheed Martin, 2005
- Directors Team Award, Lockheed Martin, 2004

LEADERSHIP DEVELOPMENT
- Active in the Orange Coast (OC) chapter of the American Society for Materials (ASM) from 2011-present. Elected chairman of the OC chapter for the 2012-2013 term. Chairman for the First Annual ASM OC symposium on Biomaterials, Medical Devices and Tools: Challenges with Design, Fabrication and Testing on November 14th, 2011.
- Active in the northern California chapter of the Society for Advanced Materials and Process Engineering (SAMPE) 2000-2010. Workshop Chairman in 2002, Secretary 2007-2009.

ABSTRACT OF THE DISSERTATION

Quantitative Percussion Diagnostics For Evaluating Bond Integrity Between Composite
Laminates

By

Scott Leonard Poveromo

Doctor of Philosophy in Materials Science and Engineering

University of California, Irvine, 2015

Professor James Earthman, Chair

Conventional nondestructive testing (NDT) techniques used to detect defects in
composites are not able to determine intact bond integrity within a composite structure
and are costly to use on large and complex shaped surfaces. To overcome current NDT
limitations, a new technology was utilized based on quantitative percussion diagnostics
(QPD) to better quantify bond quality in fiber reinforced composite materials.
Experimental results indicate that this technology is capable of detecting 'kiss' bonds (very
low adhesive shear strength), caused by the application of release agents on the bonding
surfaces, between flat composite laminates bonded together with epoxy adhesive.
Specifically, the local value of the loss coefficient determined from quantitative percussion
testing was found to be significantly greater for a release coated panel compared to that for
a well bonded sample. Also, the local value of the probe force or force returned to the
probe after impact was observed to be lower for the release coated panels. The increase in
loss coefficient and decrease in probe force are thought to be due to greater internal
friction during the percussion event for poorly bonded specimens.

NDT standards were also fabricated by varying the cure parameters of an epoxy film adhesive. Results from QPD for the variable cure NDT standards and lap shear strength measurements taken of mechanical test specimens were compared and analyzed. Finally, experimental results have been compared to a finite element analysis to understand the visco-elastic behavior of the laminates during percussion testing. This comparison shows how a lower quality bond leads to a reduction in the percussion force by biasing strain in the percussion tested side of the panel.

CHAPTER 1: INTRODUCTION

1.1 What is a Kissing Bond?

Examining defects within composite structures using nondestructive testing (NDT) is critical in evaluating the integrity of composite components. One such area in which an increase in knowledge of defects within a composite structure is sorely needed is in bonded structures. Bonding composite structures together using adhesives provides many advantages over other joining methods. These advantages include distributing the load over a large bond area, reduced weight, an ability to join dissimilar materials together, higher stiffness and toughness over the bond area and in many cases lower manufacturing cost[1,2]. However, a significant limitation when using adhesives is the inability to determine in a nondestructive manner whether or not the cohesive strength of a bond joint meets structural requirements. Unfortunately, this leads to a conservative design approach and the application of fasteners through the bond to ensure joint integrity. The addition of fasteners increases cost and weight and greatly diminishes the aforementioned advantages. Furthermore, fasteners cannot be the solution to attach materials that are being bonded within composite laminates that act as toughening aids or sensors for creating multifunctional materials.

In order to address this limitation, a new NDT method is needed that can detect adhesive 'kissing' bonds, where the adhesive shear strength is low, typically less than 10% of its ultimate shear strength, due to contamination on the bonding surfaces or improper handling, mixing, or curing of the adhesive. It is believed that most 'kissing' bonds result from poor surface preparation of as-molded surfaces due to excess fluorocarbons, silicones,

plasticizers, etc. introduced from the manufacturing process[2–4]. If these contaminants are not removed, they will decrease the surface energy which will decrease the contact angle between the adhesive and the bonding surface causing a decrease in shear strength. As a result, the bond that is formed will not be able to carry load as both substrates will in essence be 'kissing' one another.

1.2 State of the Art Nondestructive Testing (NDT) for Bonded Composite Structures

State of the art non-destructive testing (NDT) used to detect defects in bonded composite structures are focused on ultrasonic techniques and optical-non-contact methods such as thermography and shearography[5–12]. A quick review of how these techniques work and descriptions of how these methods are being used to inspect bonded composite structures will be discussed.

Ultrasound is one of the most common techniques used in aerospace where sound waves are created and sent through the specimens to be inspected[12–14]. The interaction of the sound waves with the internal structure of the specimen provides feedback to the user about the properties of the material. Two of the most common types of ultrasound techniques are pulse echo and through transmission. Pulse echo uses a single transducer to introduce sound waves into the part on one side. The same or second transducer on the same side will then measure the reflection amplitude or echo after interacting with the internal structure of the specimen. An illustration of this type of detection method is shown in Figure 1. The ultrasonic transducer is coupled to the unit under test (UUT) using water or gel in order to ensure the ultrasonic pulse is transmitted directly to the specimen without any attenuation[15].
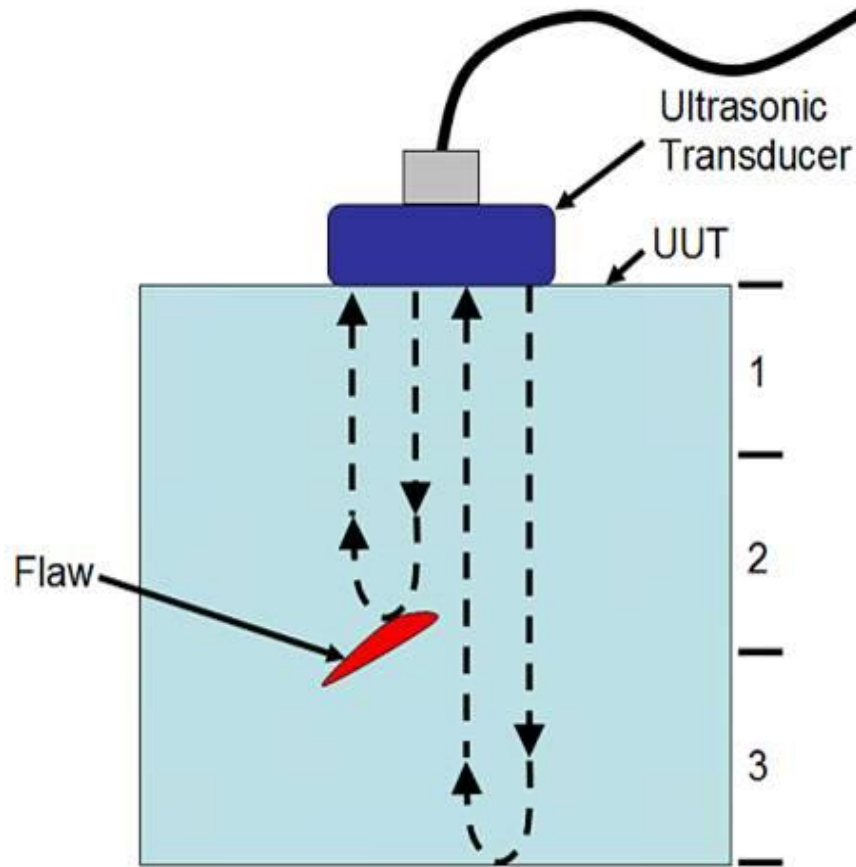
Figure 1 Illustration of how ultrasound works in pulse echo mode (Figure reproduced with permission from National Instruments)[15]

The other common ultrasound technique is through transmission which uses two transducers, one on each side of the part, and measures the amount of attenuation the sound wave experiences through the total thickness. The reflection amplitude will change when interacting with an interface between two materials with different density and stiffness. For instance, if a delamination within a composite laminate exists there will be a reflection caused by the change in acoustic impedance between air within the delamination and the laminate material itself. There also will be a loss in transmission of the sound wave through the thickness of the part. The location of the delamination can be determined

based on when the reflection occurred and measuring the time of flight (TOF) of the sound wave. TOF measurements are also very useful to measure the thickness variation of composite laminates and adhesive bondlines. For that reason, ultrasound measurements shall be taken of all panels fabricated in this study. When the sounds waves interact with a localized defect, such as porosity, the difference in density causes the wave to scatter and hence is easier to detect using through transmission mode. A plot of attenuation of the sound wave vs percent porosity at specific frequencies can help characterize these types of composite defects[12].

Ultrasound studies on bonded structures are mainly focused on metal to metal structures because of the higher acoustic impedence difference between the metal structure and polymer adhesive. An example is Roach et al. who explored using ultrasound to characterize bond integrity of single steel lap shear specimens bonded together with epoxy adhesive[16]. Bond strength was varied by adding different types of contamination to the bonding surface. Pulse echo and through transmission ultrasound showed promise in detecting low levels of bond integrity. However, the contamination layers applied to the surface were observed to be relatively thick and resembled physical defects which are easier to characterize. Inspecting polymer matrix composite laminates bonded together is more difficult since they are similar in stiffness and density to the adhesive layer through the thickness of the material. To combat this limitation, Kumar et al. used oblique incidence ultrasonic inspection to inspect carbon fiber reinforced polymer composite lap shear specimens bonded with a 2-component epoxy adhesive[17]. Poly-vinyl alcohol (PVA) was mixed with the epoxy adhesive to create samples with varying bond strengths. The oblique incidence ultrasonic technique produces shear waves to interrogate the bonded

specimen and it was found that the shear wave amplitude increased as the amount of PVA was increased in the adhesive mix. The PVA/epoxy mix most likely caused an increase in defects at the interface of the bond that changed the bond strength and was detected by shear waves. However, this method of creating a weak bond (discussed in chapter one) is not representative of how bond joints fabricated in a manufacturing environment could be compromised. Also, in many instances, determining the bond integrity of film adhesive bonds are more prevalent than paste adhesive bonds which could not be degraded by mixing with PVA. Finally, the frequency of 20MHz used in the experimentation is very high and will be difficult to characterize composite laminates due to noise created from porosity (out of autoclave processing) and will be limited to thinner substrates.

Active infra-red thermography is a common optical NDT method used to characterize adhesive bonded structures in aerospace applications[18-24]. In this method an external heat source is applied to the test specimen and the variation in surface temperature is captured by an IR camera. Temperature differences are due to changes in thermal diffusivity within the substructure being investigated. For example, active thermography can detect a delamination between two parts that have been bonded together because the cooling rate associated to the defect will be slower (lower thermal diffusivity) than the bulk well bonded material. Figure 2 illustrates a thermogram showing a large disbond within the side walls of a composite pick-up truck box[21]. IR thermography has the advantage of being able to inspect large surface areas in a short amount of time compared to other state of the art techniques. However, the main limitation with this technique is it can only be used to inspect small depths (a few millimeters).

The source of the thermal excitation; heat lamp, optical flash lamp, ultrasonic excitation; can be varied in order to optimize sensitivity based on material and defect type. Also, the form in which the thermal excitation is applied to the specimen to be inspected can be varied. Pulsed thermography heats a sample with a short pulse (step function) from a xenon flash lamp[21]. The heating and the cooling of the specimen during and after the pulse is captured by an IR camera. Lock-in thermography is a continuous thermal excitation of the specimen, usually in a sinusoidal pattern, from a halogen lamp. The lock-in method has the advantage of allowing the user to monitor the specimen for a longer time since the thermal decay is never lower than the sensitivity of the IR camera due to the continuous excitation applied[19].
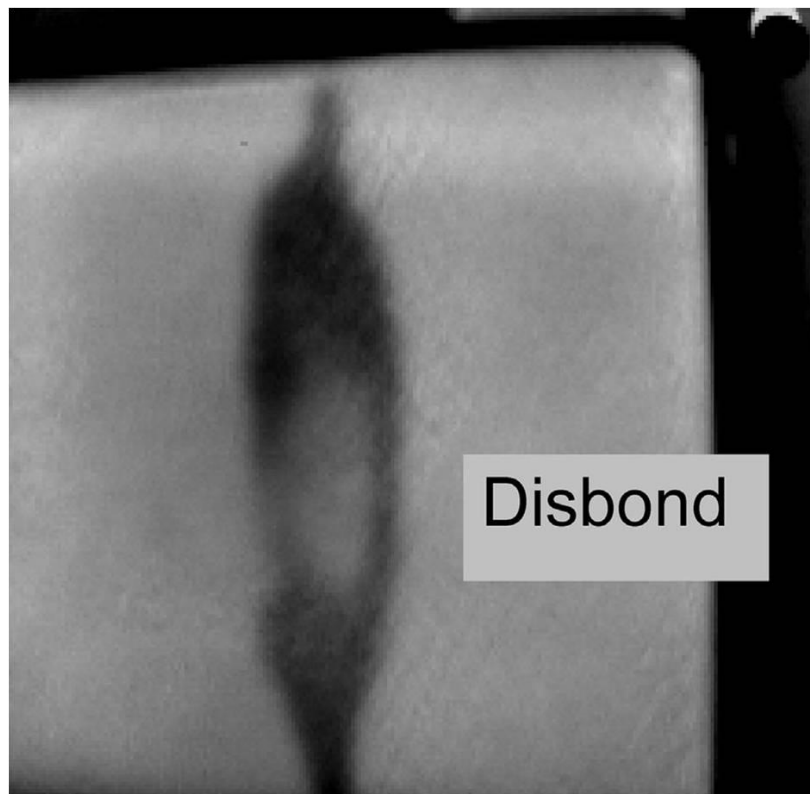
Figure 2 Illustration of a disbond detected using active thermography to inspect the side walls on a composite pick-up truck box
(Figure reproduced with permission from Elsevier)[21].

Active thermography studies on bonded structures are mainly focused on detecting delaminations within carbon fiber reinforced composite laminates or between the facesheets and core in composite honeycomb structures[20]. Also, defects resulting from impact damage (cracks and delaminations) are characterized using active thermography. To improve the resolution of IR thermography, Rantala et al used vibrothermography to inspect bonded composite structures where the source of energy came from mechanical vibrations[25]. The specimen to be inspected is shaken at a specific frequency. The energy resulting from this vibration is converted to thermal energy caused by acoustical damping from the specimen and is measured using an IR camera. Areas with defects should have higher acoustical damping values which will cause a measurable change in thermal energy. This method has the potential to inspect for physical defects within an adhesive by measuring both stress and thermal changes. However, the method is limited to polymer materials where the acoustical material damping is high (measurable thermal profile) and is dependent on identifying an optimal vibration frequency which will allow good contrast between the bulk material to be inspected and defect type.

Finally, laser shearography is another optical method that has been used to characterize composite structures[26–31]. In this method a digitized speckle image is taken of the specimen to be inspected. Next, the specimen is stressed causing out-of-plane surface displacement changes across the part. The stress can be applied by many different methods including pressure, vibration and vacuum. A second digitized speckle image is taken after the stress is applied and compared to the baseline digitized image. Any anomaly in the fringe pattern created when comparing the two speckle patterns can be related to a subsurface defect in the test specimen. The stress causes the part to have a

surface strain concentration where a subsurface defect is located. An example of a

shearography image showing several delaminations within a honeycomb sandwich panel

where the facesheets are made of graphite/epoxy is shown in Figure 3[31].
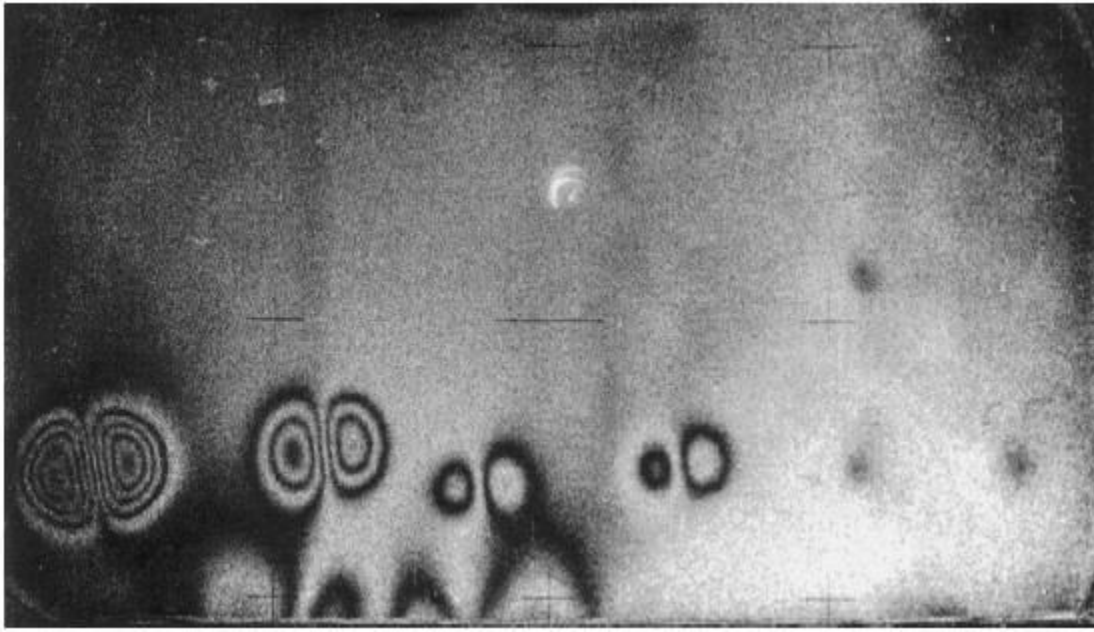
Figure 3 Shearography image depicting delaminations within a composite honeycomb
sandwich structure where partial vacuum was used as the stress source (Figure
reproduced with permission from Elsevier) [31].

The advantage of the technique is that it is much faster in inspection time over large areas

than standard ultrasound and insensitive to environmental conditions. However, the stress

level needed to obtain the appropriate out-of-plane surface displacement to observe

specific defects needs to be iteratively determined. Also, the technique is dependent on

how deep below the surface the defect is located. The closer the defect is to the surface, the

higher the probability an anomaly in the fringe pattern will be detected.

Another example of using shearography to inspect bonded composite sandwich

panels was described by Guo et al[27]. The composite sandwich panel was made up of 3

alternating layers of carbon fiber/epoxy and two layers of nomex core. Defects were

created by drilling flat bottom holes at specific depths on the backside of the sandwich panel to determine how sensitive shearography was to different size defects. Stress was applied varying vacuum loading from 10 to 30 inch of Hg. It was determined that shearography was able to detect holes as small as 25 mm under the outer facesheet and holes bigger than 38 mm between the top layer honeycomb and center facesheet. Based on this study the resolution for this technique was determined based on a minimum of 1 um of out-of-plane displacement which would allow accurate inspection without excess noise in the shearography output.

The state of the art techniques have a difficult time detecting kiss bonds within a polymer composite structure because there is no observable defect between the adhesive and bonding surfaces. Also, the state of the art techniques used are either costly, time consuming or difficult to use on large and complex shaped surfaces. For bonded structures it is necessary not only to be able to detect kiss bonds but also determine the shear strength of the adhesive. One of the main obstacles in this testing is in the heterogeneity of the composite materials being tested. Also, the heterogeneity of polymer matrix composite laminates and potential defects that can be found outside of the adhesive layer makes assessing the adhesive layers properties difficult. To combat some of these limitations lower technical readiness level (TRL) techniques have been examined and summarized below.

1.3 Low TRL NDT Methods for Bonded Composite Structures

Several low TRL NDT methods have been used to inspect bonded composite structures. One cost effective method that has shown promise to detect differences in bond integrity of aluminum and steel lap shear joints is vibration analysis[32–37]. In vibration

analysis, lap shear specimens are vibrated in a fixed free condition where one end of the specimen is fixed and the other end is free to vibrate. An impact force was applied to the specimen and the frequency response was measured. From the frequency response, the loss modulus can be computed dividing the resonant frequency by the half power band width. Changes in loss modulus or resonant frequency can be compared to the shear strength of different metal to metal bond joints. For example, Srivatsan et al. examined the effects of percent debond (released) area on the strength of steel double lap shear specimens bonded together with epoxy adhesive[34]. The authors discovered as the percent debond area increases, both the loss modulus (see Figure 4) and resonant frequency showed significant changes. As the percent debond area increased, the loss modulus increased and the resonant frequency decreased, while the joint strength decreased. The authors attributed the increases in damping capacity to friction caused by the opening and closing of the debonded interfaces during the vibration test. The decrease in resonant frequency is attributed to the decrease in stiffness of the overall bonded structure due to the higher debond area.

Although the results from the vibration analysis technique are promising, the measurements were taken on metal adherends that are typically homogenous and have high loss modulus values in the thickness direction and subsequently easier to examine than composite substrates. Yang et al. used modal parameters to measure the damping loss factor at different frequencies for polyisocyanurate structural reaction injection molding (SRIM) composite panels bonded together with polyurethane adhesive[2]. The amount of bond area between double lap shear SRIM panels was sanded at different area percentages and the loss coefficient was compared. As the percent area sanded was

increased, the loss factor decreased. This result was similar to what was published by

Srivatsan et al. for metal adherends. These comparable results are encouraging but still

need to be tested on aerospace grade woven and unidirectional carbon fiber/epoxy

laminates bonded together with epoxy adhesive. Also, vibration analysis is performed on

specific specimen geometry and is limited to a small specimen size. A technique which can

be used on large components in a manufacturing environment is desirable.
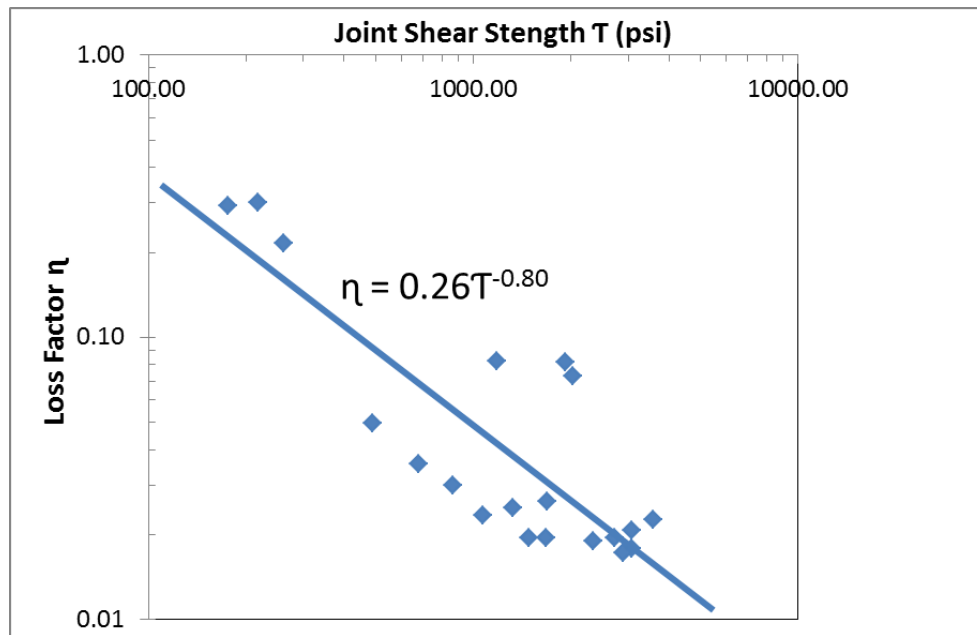
Figure 4 Loss factor vs joint shear strength for steel double lap shear specimens. Data
points gathered for different porosity levels in the adhesive, different cure conditions, and
different % debond areas (modified from Srivatsan) [34].

A recent method developed by Bossi et al. uses a high peak powered pulsed laser to

provide a localized dynamic proof test for bonded structures[38]. This laser bond method has

shown to be able to detect differences in adhesive shear strength (see Figures 5 and 6); it is

destructive if the adhesive bond is weak and is non-destructive if the bond is strong. The

damage parameter is 0 when there is no detectable damage from the laser pulse when

inspecting with ultrasound, 0.5 is assigned when there is a discernible change in the

ultrasound scan and 1 is when there is complete delamination. One of the major disadvantages of this system is that it is a destructive test. The user must clearly know the bond strength threshold of the part that will be acceptable and not go over this limit. Also, the laser fluence used is high which is costly to operate, difficult to set-up in a manufacturing environment and cannot be used in hard to access areas. There are also concerns about repeated measurements causing progressive damage to the composite structure; once one location has been tested, that same location cannot be re-tested.
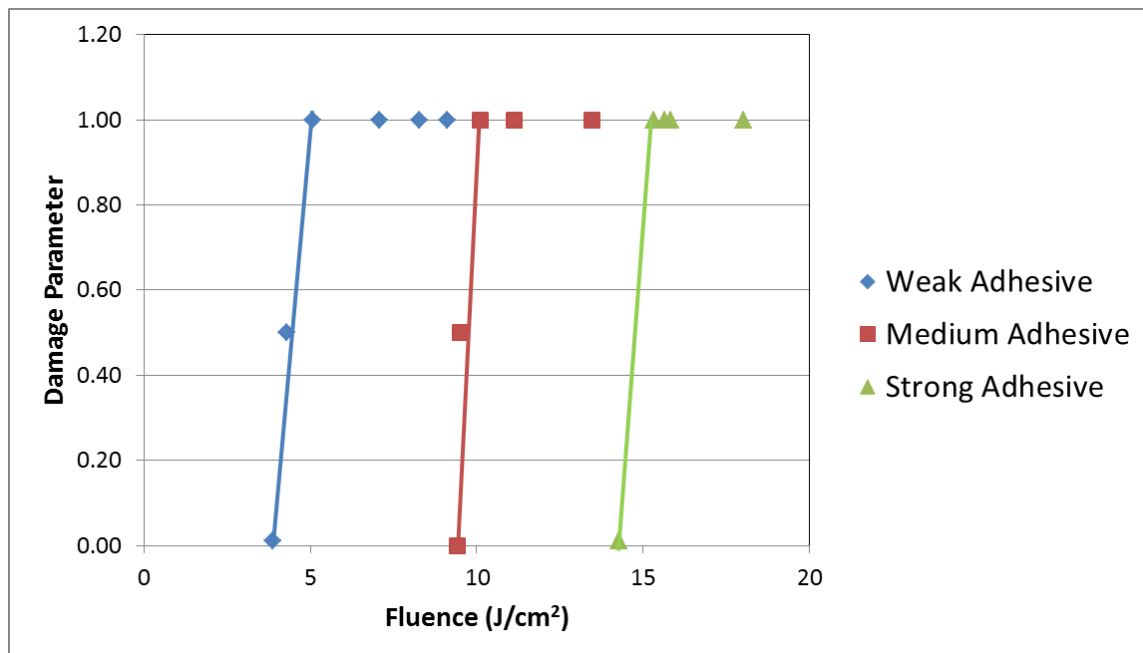
Figure 5 Damage parameter vs fluence for various strengths of EA 9394 paste adhesive bonded composite laminates (modified from Bossi)[38].
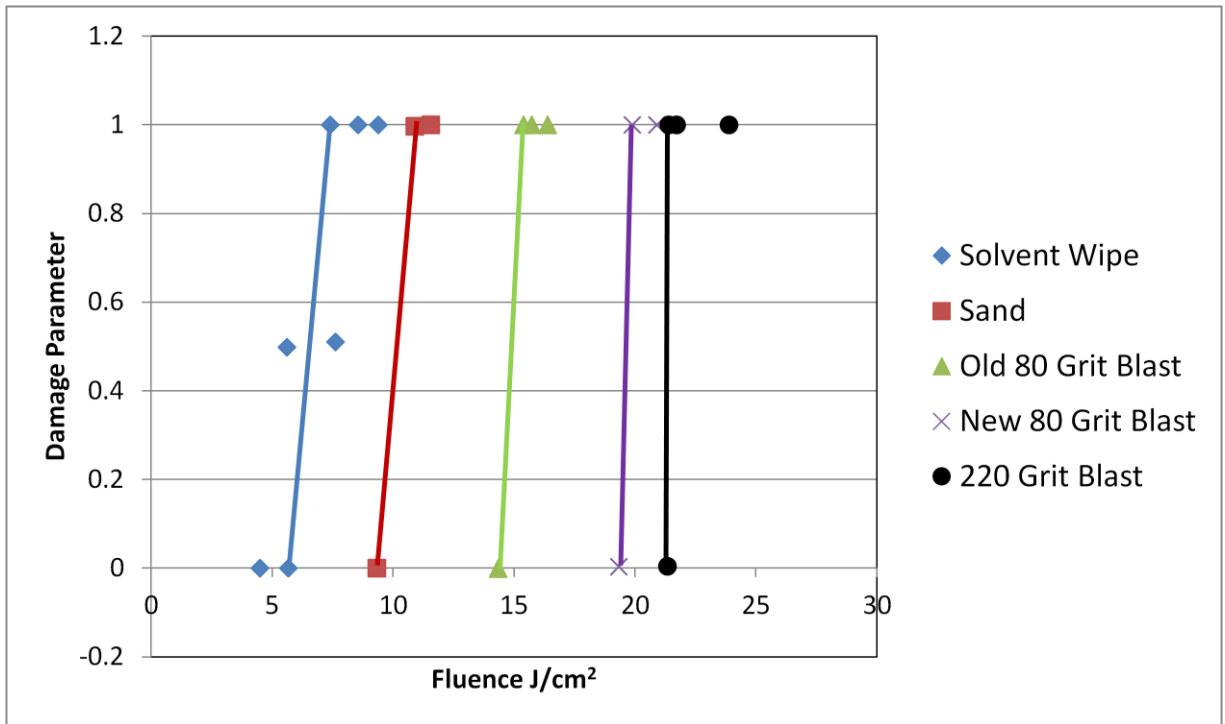
Figure 6 Damage parameter vs fluence for various surface treatments on composite laminates (modified from Bossi)[38].

Another method which has shown promise in investigating kiss bonds in composite bonded structures is digital image correlation[39]. Digital image correlation (DIC) is an optical method that uses digital images of a specimen's surface to obtain full-field deformation maps as that specimen is loaded to failure   Kumar et al. fabricated E-glass fiber/epoxy single lap shear joints that were bonded together with a two-part epoxy adhesive[39]. Kissing bonds were introduced into these specimens using fluoropolymer films of different sizes and placed in the 1" overlap bond area. This method to produce a kiss bond is not representative of how a kiss bond will form in service since the film is an actual physical defect that should be detectable by ultrasound. However, with the addition of the film the resulting bond strength of the lap joint should be decreased. The specimens in this study were loaded incrementally every 0.5 kN and a deformation map of the specimen was

created based on the digital images that were processed. Four strain fields were captured

in Figure 7 as a single lap shear was loaded to failure with a kissing bond area of 70 %.

Localized strain fields are shown in images b-d which illustrates the effect of the kiss bond.

Although this technique cannot be used to inspect composite components in service it may

be useful as a complementary technique to analyze tag end parts or test specimens.
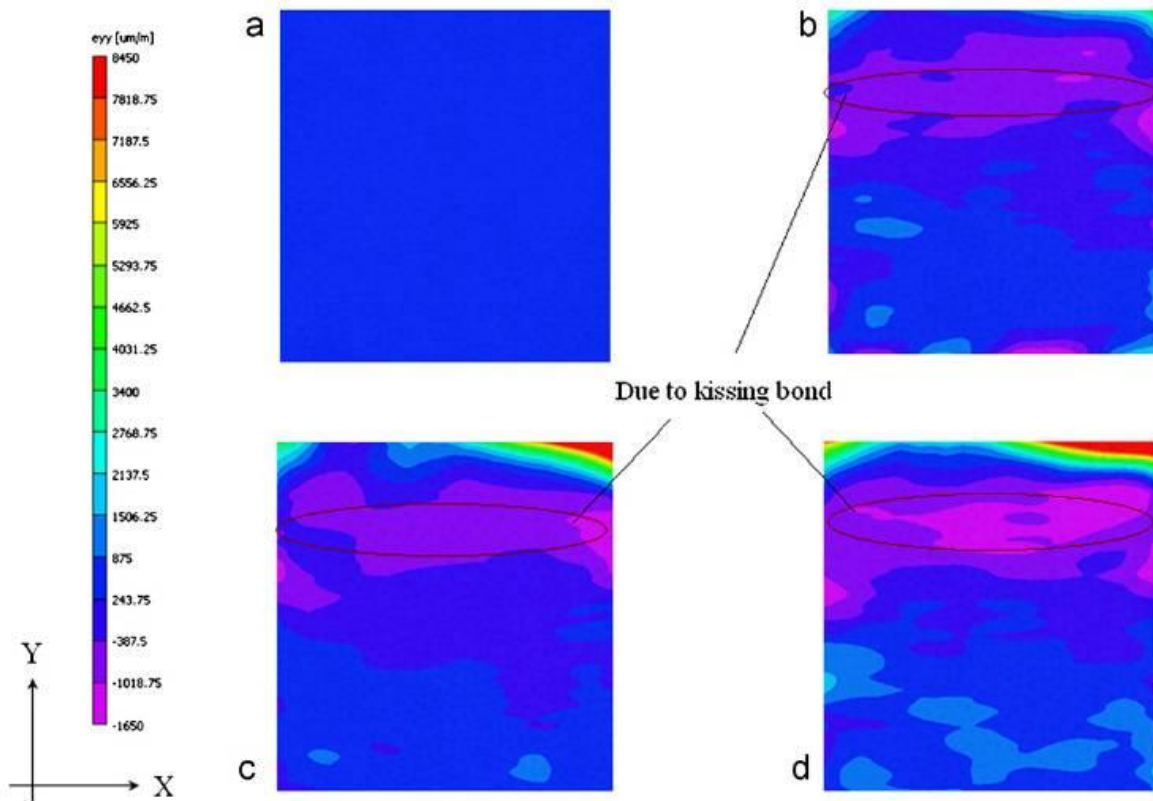
Figure 7 DIC strain field images based on a kissing bond area of 70%. 7a = 0% of failure load, 7b =25% of failure load, 7c = 75% of failure load, and 7d = right before failure (Figure reproduced with permission from Elsevier) [39].

Also, lamb waves have the potential to characterize damaged composite parts in a

low cost rapid technique[40-46]. A lamb wave is a guided wave that can travel long distances

longitudinally across the surface of a structure. When the waves come in contact with a

defect the properties will change such as the time history of the propagation, wave velocity,

and/or attenuation. In theory each type of defect in a bonded composite structure should result in a different change in the wave characteristics. Frequency, wavenumber, and other cycling characteristics should be examined before choosing specific Lamb modes to conduct the diagnostic testing. Also, the heterogeneity of the composite specimen as well as edge effects and complex geometrical boundaries causing wave dispersion will make deciphering changes in wave characteristics due to manufacturing defects challenging.

Lamb waves can be introduced into the structures by several methods including laser interferometers, piezoelectric transducers and ultrasonic probes. Each method type has its advantages and disadvantages depending on the structure geometry, budget, defect types trying to characterize as well as the shape and size of the sensor itself. For example, Samaratunga et al., used a piezoelectric transducer bonded to a composite laminate to create 3.5 cycle tone bursts to interrogate the structure for delaminations[44]. A simulation was created using ABAQUS that enabled the authors to estimate the size and location of a delamination within the center section of the laminate. The delamination causes the wave velocity to decrease and can be located based on the time it takes for the wave to return to the excitation point. Lamb waves propagating over areas with no delaminations will have a shorter arrival time back at the point of excitation. An example of a simulation using NASTRAN showing a lamb wave propagating throughout a flat composite bonded structure is shown in Figure 8. Here the transducer is modeled as a half circle and as result the wave propagating across the structure is done so in a radial pattern. An ideal sensor would create lamb waves that have low dispersion, low attenuation, and high sensitivity to the defects of interest.
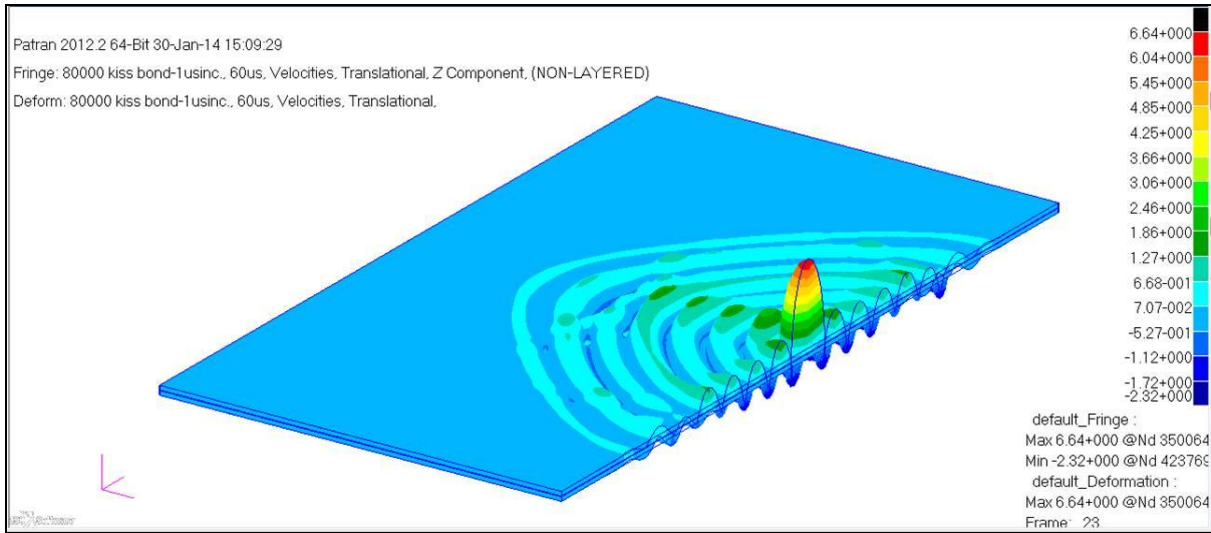
Figure 8 Simulation of an 80 khz 5 cycle sinusoidal pulse propagating through a composite structure with a kiss bond located at the center right edge. The pulse radiates out from its origin at around a wavelength of 13 mm. The fringe plot shows out-of-plane velocity at 800μs using a 1μs time increment to collect data.

Finally, percussion techniques in composite damage assessment have been conducted previously using electronic tap testing. The three devices created which perform 'electronic tap testing' are as follows: Woodpecker (Mitsui-Japan), RD[3] (Boeing), and the computer aided tap tester (CATT) developed by Iowa State University[47-50]. The goal of all three devices is to provide a quantitative way to measure damage of composite laminates and sandwich structures in a non-destructive manner using a portable low cost device.

The first automated 'tap-test' method that was patented as a low cost portable option for NDT of composites was an instrument named the Woodpecker sold by Mitsui Industries[49]. The Woodpecker was sold as an electronic hammer controlled by the use of a solenoid. A manual option was also developed by Mitsui. The Woodpecker measured the stiffness of the specimen by recording the force/time peak of each impact using an

16

accelerometer located in the hammer head. The stiffness was computed based on assuming a simple harmonic oscillation model. An LED light system was designed to notify the user whether the region of inspection was acceptable or defective. If the light turned green, the contact time was similar to what a good area should be. If the light turned yellow, the contact time was longer by a specific interval that can be adjusted. If the light turned red, a warning buzzer sounded signifying that the condition was considered abnormal as the contact time was measured significantly longer than for the impact on a good area.

An example application is the woodpecker being utilized to determine how loose a bolt was torqued into a part[49]. Specifically, the asymmetry of the force/time curve was used to detect differences in torque of the bolt. When the bolt was very loose the force/time curve was asymmetrical and the b/a ratio ('a' is the distance from the start of the curve to the peak and 'b' is the distance from the peak to the end of the event) was far away from 1. Also, two peaks were identified after testing. When the bolt was very tight, the force/time curve was symmetrical, the b/a ratio was close to 1 and only one curve was identified. The Woodpecker was used to also identify the degree of peeling in a honeycomb structure. The ratio of b/a was once again used to identify good and bad areas. As the ratio of b/a decreased, the force/time curve became more symmetrical and the degree of peeling in the honeycomb structure was greater (force/time curve became broader). The authors of the Woodpecker patent believed that the sensitivity of their instrument could be enhanced by increasing the mass of the hammer used to apply the impact on the specimen. As the mass increased, the percent change in contact time would be easier to measure. Also, an increase in impact force was needed to detect damage in thicker specimens.

Another patent for an automated tap tester was created by Boeing and called the RD[3] [47,48]. This instrumented hammer is manually operated and shown in Figure 9.

Figure 9 Illustration of RD[3] automated tap tester (Image reproduced with permission from WichiTech Industries)[51].

The RD[3] calculates the contact time and derives the stiffness of the specimen, but instead of using the asymmetry of the force/time peaks, it uses the entire width of the impulse above a specific force/time threshold. The reason the instrument was designed to be manual was based on testing performed by Boeing showing that impulse width was relatively independent of impact force. As the impact force was increased, the impulse width only changed around 5% when tested on composite structures. The output on the RD[3] can read pass/fail or impulse time (pulse width). A tap on a known good region is compared to a tap on an unknown region and the difference is determined and can then register a

pass/fail reading. The tap must also reach a specific high force threshold or a reading of 0 will result meaning the tap was not acceptable. Finally, the RD[3] was compared to the Woodpecker and found to be more sensitive to changes in signal for thicker composite laminates (4, 6, and 7 plies). The maximum thickness the RD[3] can be used on carbon fiber/epoxy laminates is 6 mm.

A third automated tap testing machine developed was the CATT, computer automated tap tester, invented at Iowa State University[50]. The CATT is unique in that it is designed to create a stiffness map of the structure based on contact time calculations over a specific region of the composite. A mylar template grid is created where specific areas are tapped and the data is recorded on a computer that has the grid spacing programmed into the software. First, a known good area is tapped 5-10 times and the average contact time (calculated stiffness) is recorded. Then the grid is set-up over an unknown area where the coordinates are programmed into the computer software. Each grid area is tapped and the percent difference in stiffness or range in contact time is recorded in a color coded map of the area. This method provides the user with a map of quantitative information of the structure being inspected.

The previous section summarized three automated tap testing equipment available on the market today. However, all three methods have limitations. The RD[3] and CATT equipment measure the impact duration and relate this value to the contact stiffness. However, as pointed out by Cawley and Adams, in many instances it is difficult to measure the impact duration accurately due to asymmetrical 'tails' formed at the end of the force/distance curve[37]. As the curve becomes more asymmetrical and forms a 'tail", the finish time of the impact event becomes harder to determine. Also, what happens when

there is more than one peak? Measuring the impact duration will not provide any new information about the cause of the second peak and how it relates to the structural damage of the composite.   Furthermore, the Woodpecker equipment only focuses on evaluating the first peak and treats the second peak (when it occurs) as part of the first peak in the data analysis. A more sensitive percussion device is needed that will yield a greater amount of quantitative data about the inspected damaged composite part.

1.4 Quantitative Percussion Diagnostics (QPD) for Bonded Composite Structures

To overcome current limitations associated with state of the art and low TRL NDT methods when inspecting bonded structures, University of California, Irvine (UCI) and Perimetrics, LLC™ developed a new technology based on a technique using percussion diagnostics to better quantify bond quality in fiber reinforced composite materials. An example of the percussion technique the team will be using in this effort is quantitative instrumentation (Periometer®, see Figure 10) designed at UCI that was originally used to investigate and compare the damping capacity of human teeth and dental implants[52–58]. As shown in Figure 11, a stainless steel rod containing a force sensor is accelerated by an electromagnetic coil to a pre-determined velocity just prior to impact. While the percussion rod is in contact with the specimen, the electromagnetic coil is inactive so that only the kinetic energy of the rod is administered to the specimen. The low level impact of the percussion rod generates a nondestructive stress wave that propagates through the specimen. Inelastic deformation or damping of strain energy during impact is characterized by the loss coefficient, η, a commonly used damping capacity parameter. Custom software on a computer interfaced to the percussion rod determines the mechanical energy returned to the rod from the force measured versus time for 10 of the 16 impacts. The energy

dissipated by the specimen, *D*, is determined from $D = U - E_R - D_p$ (1) where *U* is the total

strain energy, E_R is the mechanical energy returned to the sensor in the percussion rod and

D_p is energy dissipated by sources external to the specimen[52]. The loss coefficient is given

by $h = \dfrac{D}{2\rho U}$ (2) where the total strain energy, *U*, for the present percussion testing is

approximately equal to the total kinetic energy prior to impact from the rod (1/2 mv^2). In

addition to displaying the loss coefficient, the output provided by the custom software is a

plot of the probe force measured during each impact event as well as the transmitted force

measured by a load cell on the opposing surface of the specimen plotted versus time. The

average maximum values of probe force and transmitted force are also displayed.

Figure 10 Periometer® instrumentation developed by Perimetrics, LLC (Image reproduced with permission from photographer).
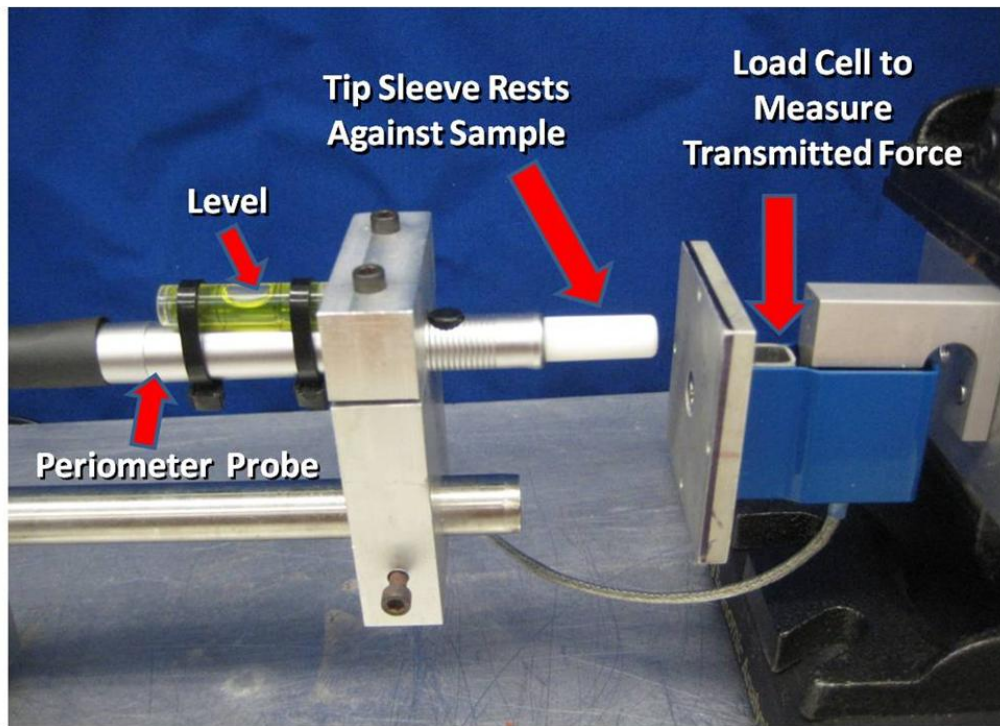
Figure 11 Photograph of the percussion probe and load cell used in the present work.

Data compiled using the Periometer has been found to be useful for analyzing damaged composite laminates. For example, Stanley et al. previously used this device to interrogate damage in a carbon fiber/epoxy laminate due to an impact event[53]. The authors discovered that the loss coefficient increased as the impact energy increased and as the measurement distance to the impact site decreased (see Figure 12). The rationale behind this trend is that there are considerably more sources of internal friction after an impact event caused by the movement of crack and delamination surfaces. Also, the breaking of fibers results in more stress being supported by the matrix that generally results in greater inelastic deformation and thus more energy dissipated. Fiber sliding also can occur, which increases internal friction and the amount of energy dissipated as heat.

Hence, a relationship between internal delamination/micro-cracking and local changes in damping capacity can be exploited to investigate internal damage in composites.
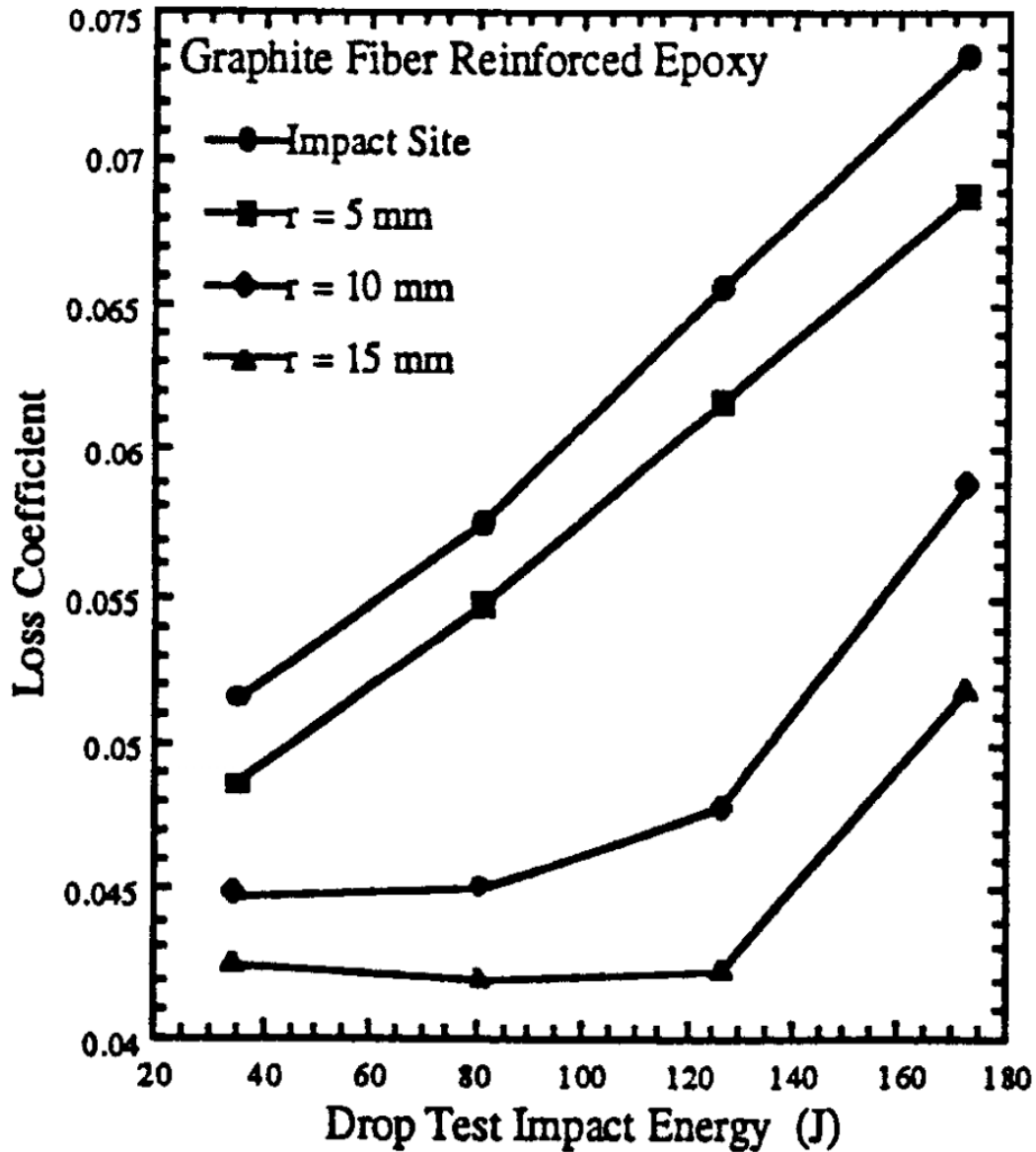
Figure 12 Loss coefficient vs drop test impact energy for fiber reinforced composite. From B.D. Stanley, L. Bustemante, and J.C. Earthman, "Novel Instrumentation for Rapid Assessment of Internal Damage in Composite Materials," in Nondestructive Evaluation and Material Properties III (1996), P.K. Liaw, O. Buck, R.J. Arsenault, and R.E. Green, Jr., eds., p. 99, Figure 3. Copyright (c) 1996 by The Minerals, Metals & Materials Society. Reprinted with permission[53].

In summary, quantitative percussion diagnostics (QPD) offers the following advantages:

- The Periometer measures the response of a material based on a known input of kinetic energy. Any type of defect that further depletes the kinetic energy applied to the material can be measured and evaluated.

- This percussion technique is rapid (4-5 seconds per measurement), portable, low cost, and easy to operate which lends itself to be used over large components in service.

- QPD can be used to characterize all types of composite materials and components.

- Data are taken from a single location and can be acquired in difficult to access areas that are common in composite structures.

The use of a percussion probe to measure the loss coefficient has the potential to provide more quantitative data about the structure of the composite than the current automated tap testing methods. Furthermore, these technical advantages directly address and meet the needs of the Department of Energy, Navy, Air Force, Army, and NASA for a nondestructive inspection tool that can be used during both manufacturing and service to detect defects in localized areas within composite structures used in various applications.

1.5 Objective

The overall goal of this project is to demonstrate for the first time the feasibility of using percussion diagnostics to detect 'kiss' bonds and low shear strength adhesive bonds in composite structures. The following specific objectives have been established as steps to reach this goal.

- Develop a consistent method for creating 'kiss' bonds and low shear strength adhesive bond 'standards'.

- Adapt the present percussion technique and establish test procedures to accurately measure damping capacity and probe force within composite bonded structures with and without release agent applied on the bonding surfaces.

- Compare experimental results to a finite element analysis (FEA) using MSC PATRAN/NASTRAN to understand the visco-elastic behavior of bonded composite laminates during QPD testing.

- Correlate QPD measurements to lap shear strength measurements taken of mechanical test specimens where the adhesive was cured at different conditions.

CHAPTER 2: FABRICATION OF REPRESENTATIVE 'KISS' BOND PANELS

2.1 Review of 'Kiss' Bond Fabrication Techniques in the Literature

Before a NDT technique can be developed to characterize bond integrity, kiss bond standards need to be fabricated. One common method used is to apply fluoropolymer films within the bond line to cause the adhesive not to stick to one or both adherends. For example, Kumar et al. characterized E-glass fiber/epoxy single lap shear joints that were bonded together with a two-part epoxy adhesive using digital image correlation[39]. Kiss bonds were introduced into these specimens using fluoropolymer films of different sizes and placed in the 25.4 mm (1 in.) overlap bond area. Teflon tape is also commonly used to create defect standards within composite laminates for conventional NDT methods. While these methods produce low shear strength values, they are not representative of a kiss bond. This is because the film or tape will create a change in acoustic impedance within the structure that will be detectable by ultrasound. A true kiss bond is not an observable defect when using standard NDT methods such as ultrasound and as a result cannot be fabricated using this approach.

Another more effective method to create a kiss bond is to apply contamination over the bonding surfaces using release agents, oils and greases[59–64]. Nagy bonded aluminum 2024 plates together with FM-300k epoxy film adhesive and used a thin coating of release agent to create 25 mm diameter kiss bond areas across the panel[4]. These circular areas could not be observed using conventional ultrasound techniques at 10MHz. Brotherhood et al. performed a study using petroleum jelly, Frekote release agent, and different greases to create kiss bonds within epoxy bonded aluminum structures[65]. For both room

temperature and elevated temperature curing epoxy bonded specimens, areas released

with a thin coating of Frekote could not be observed using conventional ultrasound at

10MHz. However, the greases and the petroleum jelly were detectable by ultrasound

within the room temperature curable epoxy bonded specimens as long as more than 1 mg

of contaminant was applied to the bonding surface. For the elevated temperature cure

adhesives, many of the greases absorbed into the adhesive during cure and could not be

observed by ultrasound even for large amounts of contaminant. Jeenjitkaew et al., also

successfully created kiss bonds using Frekote release agent in between aluminum plates

bonded together with epoxy film and paste adhesives[64]. Specimens were mechanically

tested and observed to fail at the release agent interface. Based on SEM and FTIR

characterization, migration of the release agent was limited to a few micrometers into the

adhesive (interphase area). The authors also tried using sweat and cutting oil as

contaminants to create kiss bonds, but both of these contaminants diffused into the bulk

adhesive and only caused a small reduction in the joint strength.

Another method used to create kiss bonds is not to add contaminants but to change

the surface preparation of the bonding surfaces to decrease the adhesive shear strength.

For example, Yang et al. created shear strength reductions in structural reaction injection

molded (SRIM) double lap shear joints bonded together with polyurethane adhesive by

varying the percent bond area that was sanded[2]. The authors discovered as the percent

bond area that was sanded decreased, the shear strength of the adhesive decreased. Also,

an extensive effort was completed by Bossi et al. where different peel ply and mechanical

surface treatments were used to prepare the surface for paste and film adhesive bonded

specimens[38]. It was discovered for EA 9394 epoxy paste adhesive that a 220 grit blast

surface preparation produced the highest strength while a solvent wipe, no sanding surface

preparation produced the lowest strength. For bonded specimens using epoxy film

adhesives, different peel ply treatments were used to vary the strength of the bond. The

highest strength bond resulted from using a polyester peel ply while the lowest strength

resulted from using a silicon peel ply. The specimens bonded in this study were all carbon

fiber-epoxy laminates; however the paper does not identify the exact fiber/resin type.

Finally, changing the bulk properties of the adhesive is another method to produce kiss

bonds. Adams et al, created weak bonds by using different shear strength adhesives in

different sections of a bonded panel[66]. Specifically, the authors fabricated 203.2 mm x

203.2 mm (8 in x 8 in) bonded laminates using a 5000 psi shear strength epoxy adhesive

while a 2000 psi shear strength adhesive was applied to a 50.8 mm x 50.8 mm (2 in x 2 in)

section of the bonded area. The potential issue with this approach is to make sure there

are no gaps in the bondline between the two adhesives and to ensure the two adhesives are

compatible with one another. Shiloh et al. also changed the properties of the adhesive by

thermally aging aluminum lap shear specimens bonded together with polyurethane paste

adhesive[33]. The shear strength was measured for specimens naturally aged for 42 days,

aged at 65°C for 4 hours and aged at 65°C for 48 hours followed by -10°C for another 48

hours. As expected, the last aging condition produced specimens with the lowest shear

strength that were 2.6 times less than the pristine value. Theoretically, if the specimen has

been thermally aged at a high enough temperature and long enough time a kiss bond

should also be created, but this method will take several trials and may result in damage of

the adherend material instead of only reducing the strength of the adhesive.

Based on the literature review the simplest approach to creating a kiss bond is to use a release agent as a contaminant on the adherend surfaces. This method was observed to work well for metal bonded structures using both epoxy paste and film adhesives. The other approach that will be used to create a kiss bond is to produce an amine blush surface layer which was not mentioned in the literature. This type of kiss bond is created by using epoxy paste adhesives where the curing agent is a low molecular weight amine[67]. Amines have a propensity to react with water and carbon dioxide to form a milky, waxy compound on the surface that does not stick to adherends. Also, the amine curing agent reacts to form this blush compound instead of reacting with the base epoxy. As a result, the epoxy adhesive will be under cured and thus have a lower shear strength. Environments that will promote amine blush formation are at cold temperatures where the reaction rate of the epoxy adhesive will be lower, high humidity environments where the water level in the air is high or in an industrial environment where a large amount of CO_2 is emitted in the air from forklifts or other gas powered equipment.

2.2 Experimental Procedures

2.2.1 Film Adhesive Panel Fabrication

Two composite laminates were fabricated; one bonded using release agent as a contaminant (kiss bonded panel #1, KBP), while the other was bonded per standard 'best' practices (well bonded panel, WBP). Two pre-cured carbon fiber/epoxy matrix laminates 305 mm x 305 mm x 1.59 mm (12 in. x 12 in. x 0.0625 in.) were bonded together with a 121°C (250°F) cure supported epoxy film adhesive. One specimen had Frekote 700NC release agent applied in a 152 mm x 152 mm (6 in. x 6 in.) area in the center of both laminates, which simulated a 'kiss' bond (KBP #1) while the other bonded laminate had no

release agent applied (WBP). To ensure the release agent created a poor bond, the released laminates were heat treated to 121°C (250°F) for 2 hours prior to adhesive bonding. Typically NDT standards are created using defects that are small (<25 mm) but these standards are based on physical defects such as delaminations, voids, and cracks. Kiss bonds can be almost any size depending on the extent of poor surface preparation and/or level of contaminants left on the bonding surfaces. A large area was chosen for this study to represent a severe case contamination scenario.

To determine if the kiss bond condition created was repeatable, another composite panel (KBP #2) was fabricated following similar manufacturing procedures described above. Two pre-cured carbon fiber/epoxy matrix laminates 266.7 mm x 190.5 mm x 1.59 mm (10.5 in. x 7.5 in. x 0.0625 in.) were bonded together with a 121°C (250°F) cure supported epoxy film adhesive. This kiss bond specimen had 5 coats of Frekote 700NC release agent applied in a 114.3 mm x 190.5 mm (4.5 in. x 7.5 in.) area in the center of both laminates as illustrated in Figure 13. Released laminates were again heat treated to 121°C (250°F) for 2 hours prior to adhesive bonding. A summary of all three secondary film adhesive bonded laminates is illustrated in Table 1.
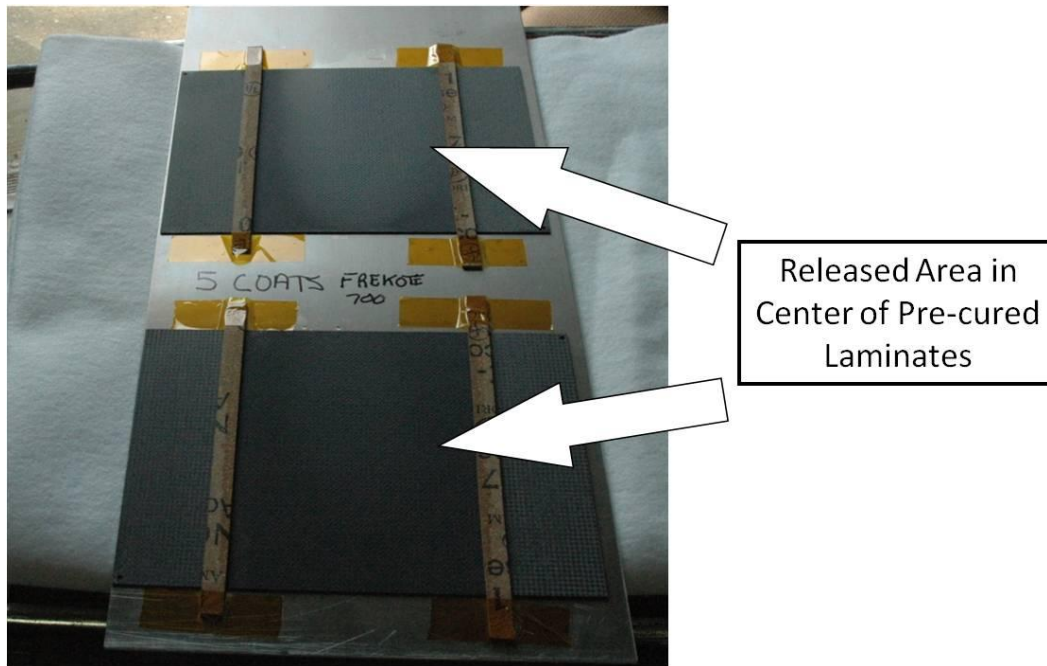
Figure 13 Illustration of released area on both pre-cured laminates for Kiss Bonded Panel #2.

Table 1 Summary of Film Adhesive Bonded Composite Laminates

Sample ID	Laminate Material Description	Adhesive Description	Surface Preparation
Well Bonded Panel (WBP)	AS4/Epoxy Plain weave carbon fabric 0/90 Lay-up	FM-300-2K - 0.06 psf	Remove peel ply
Kiss Bonded Panel #1 (KBP #1)	AS4/Epoxy Plain weave carbon fabric 0/90 Lay-up	FM-300-2K - 0.06 psf	Remove peel ply **Kiss bond area:** Apply 5 coats of release agent to both laminates **Perimeter Areas**: 80 grit wet sand, solvent clean with acetone followed by isopropyl alcohol
Kiss Bonded Panel #2 (KBP #2)	T300/Epoxy Plain weave carbon fabric Quasi-Isotropic Lay-up	FM-300-2K - 0.06 psf	Remove peel ply **Kiss bond area:** Apply 5 coats of release agent to both laminates **Perimeter Areas**: 150 grit wet sand, solvent clean with acetone followed by isopropyl alcohol

2.2.2 Paste Adhesive Panel Fabrication

Three 203.2 mm x 203.2 mm (8 in. x 8 in.) panels were fabricated to create 'kiss' bonds using a room temperature curable epoxy paste adhesive (see Figure 14). 20 ply base and 12 ply cover laminates were pre-cured using carbon fiber-epoxy pre-preg. Panel A represents a good bond where standard 'best' practices were followed throughout the bonding process. Panel B represents a 'kiss' bond created by an amine blush layer formed on the outside skin of the epoxy. This blush layer was not disturbed during bonding and created a non-stick surface. Panel C was bonded with 1 coat of release agent applied to a 152.4 mm x 152.4 mm (6 in. x 6 in.) area in the center of the top laminate (thick skin). No heat treating was performed prior to bonding of the released surface. The perimeter areas on this panel were considered good bonds. The epoxy coating near the edge of the panels was applied to the surface (non-bonding area) for another test and can be ignored for our test purposes. A summary of all three secondary bonded laminates with paste adhesive is illustrated in Table 2.

20 ply bases

← Adhesive layer

12 ply covers
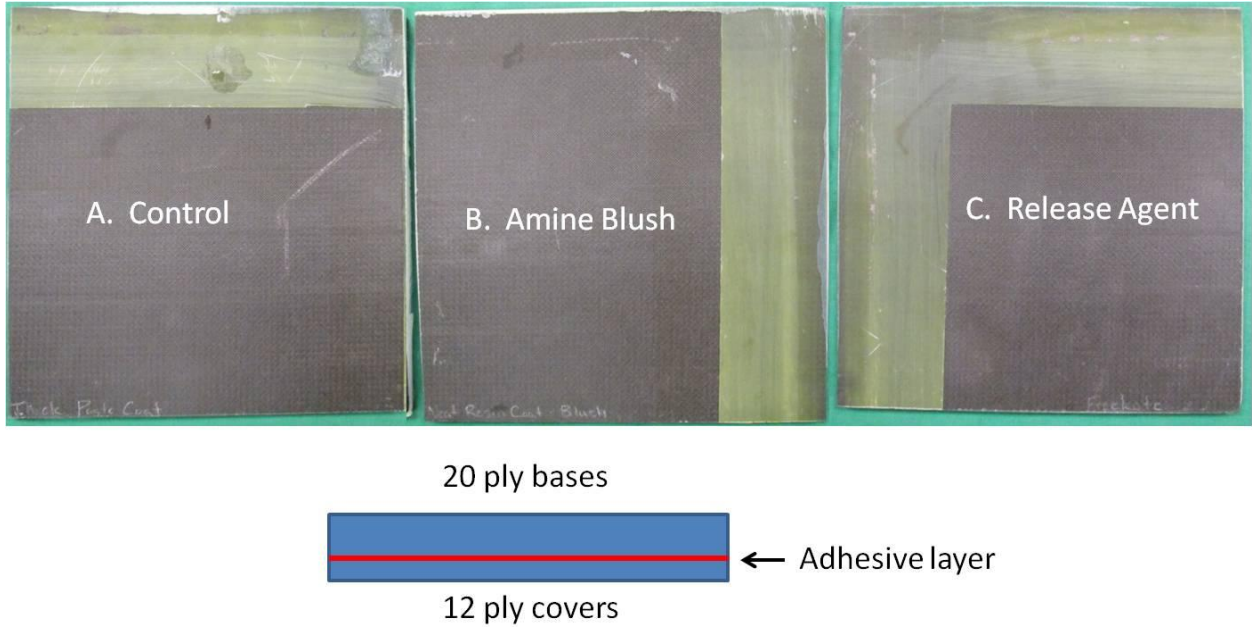
Figure 14 Top view and cross section of three 203.2 mm x 203.2 mm (8 in x 8 in) composite panels bonded together with a room temperature curable epoxy paste adhesive.

Table 2 Summary of Paste Adhesive Bonded Composite Laminates.

Sample ID	Laminate Material Description	Adhesive Description	Surface Preparation
Panel A: Control	AS4/Epoxy Plain weave carbon fabric Lay-up: $[45/0]_{3s}$ = 12ply $[45/0]_{5s}$ = 20ply	RT curing epoxy paste adhesive	Remove peel ply
Panel B: Amine Blush	AS4/Epoxy Plain weave carbon fabric Lay-up: $[45/0]_{3s}$ = 12ply $[45/0]_{5s}$ = 20ply	RT curing epoxy paste adhesive	Remove peel ply
Panel C: Release Agent	AS4/Epoxy Plain weave carbon fabric Lay-up: $[45/0]_{3s}$ = 12ply $[45/0]_{5s}$ = 20ply	RT curing epoxy paste adhesive	Remove peel ply Apply 1 coat of release agent to surface of thick skin laminate

2.2.3 Ultrasound Testing

All fabricated panels were examined using a 5-axis ultrasonic immersion system at Northrop Grumman. A C-scan of each panel was taken in pulse-echo (PE) mode at 5 MHz using a 5.1 cm (2 in) focused transducer. An illustration of kiss bonded panel #2 being inspected is shown in Figure 15. The C-scan data measured represents changes in amplitude of the reflected sound waves and was plotted as a function of distance across the length and width of the panels fabricated. For the paste adhesive panels, C-scan images created were based on PE measurements taken through the 20 ply thick skin laminate (front surface). A-scan measurements were measured at specific locations for the film adhesive bonded panels to highlight changes in ultrasonic energy as a function of time. Finally, bondline thickness variation for each panel was determined based on subtracting time of flight (TOF) measurements between the front surface and the back surface of the bondlines.
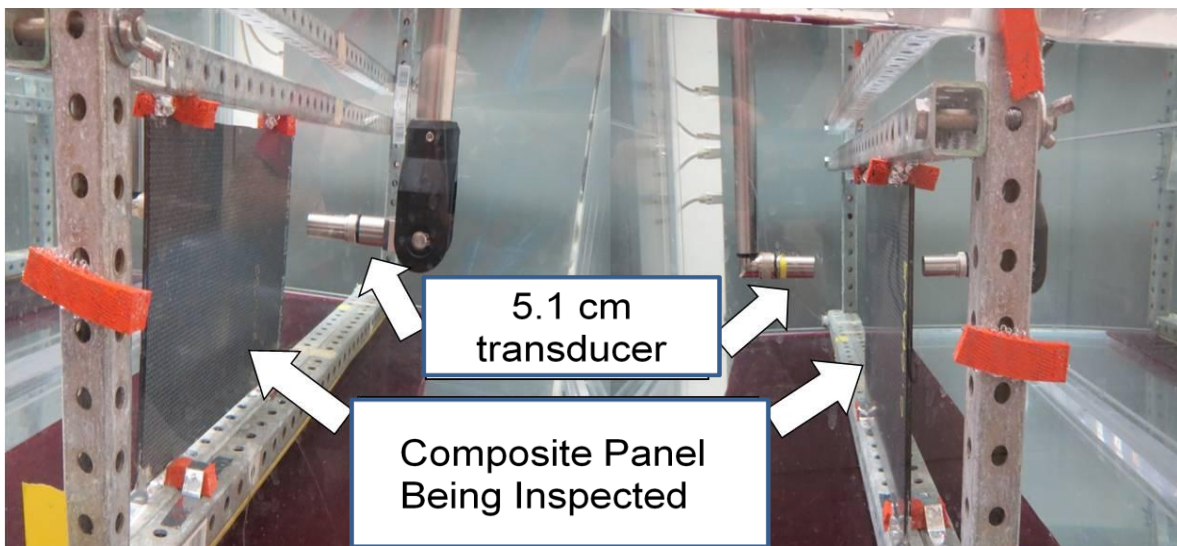
Figure 15 Illustration of ultrasonic tank set-up in pulse-echo mode.

2.3 Ultrasound Test Results

2.3.1 Film Adhesive Characterization

The results from the ultrasonic testing performed on both the well bonded panel and kiss bonded panel #1 are summarized in Figures 16 and 17.   Three gates were set-up when analyzing the data to help characterize the bonded panels. Gate 1 represents the front of the bondline, Gate 2 represents the back of the bondline and Gate 3 represents an image of the internal skin. Very little change in % amplitude was observed for the well bonded panel in all three Gate areas. A typical A-scan showed a very small change in amplitude within the bondline area (between gates 1 and 2). Also, a histogram of the time of flight measurements (difference between Gates 1 and 2) verified the film thickness to be centered around 0.229 mm (0.009 in.). Kiss bonded panel #1 illustrated an observable change in percent amplitude over the released area. The images of the front and back bondline show significant light areas in the center of the panel signifying the panel had disbonded. Typical A-scans show a large change in amplitude over the disbonded area compared to the well bonded area between Gates 1 and 2 (bondline).

The disbond observed in Figure 17 may have resulted from a trimming operation performed prior to inspection. The panels were trimmed ~25 mm (1 in) across the length using a cut-off saw which would create an air gap around the released area that ultrasound would detect. Another reason why ultrasound most likely was able to pick-up the poorly bonded area is due to the differences in thermal expansion (CTE) between the epoxy film adhesive and cured carbon fiber/epoxy laminates in the lateral directions. When the laminate is heated to 121°C (250°F) during the cure of the adhesive, the film adhesive will expand while the laminates will remain relatively stationary. Upon cool down the change

in strain of the film adhesive could cause the adhesive to disbond from the released area on
the laminate.
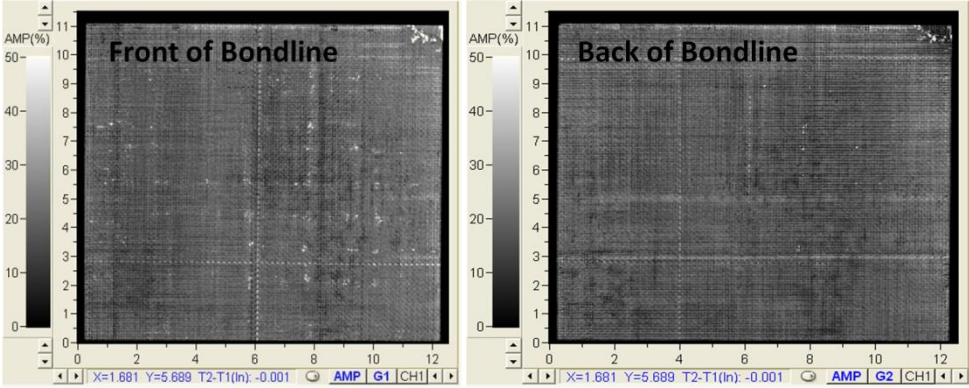
(a)

(b)
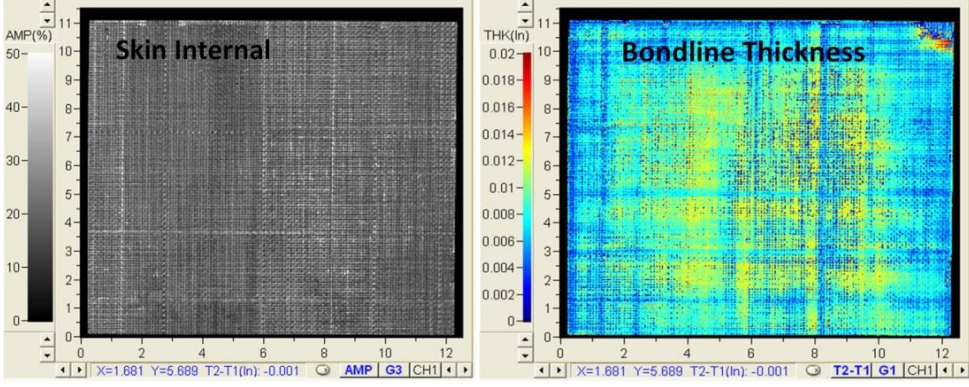
(c)

(d)
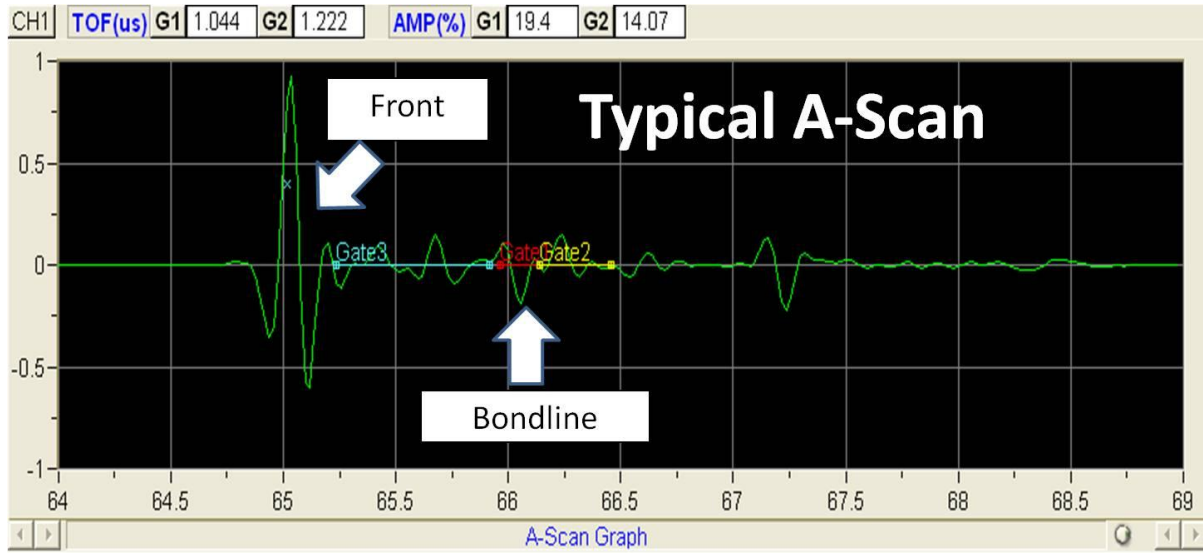
(e)

Figure 16 C-scans and A-scans of the well bonded panel. The C-scan data illustrates % wave amplitude plotted vs length (y-axis) and width (x-axis) of the well bonded panel. A-scan data shows voltage response vs time of flight in microseconds. (a) C-scan of top skin/bondline interface; (b) C-scan of bottom skin/bondline interface; (c) Percent amplitude change within laminate; (d) TOF through bondline thickness; and (e) Typical A-scan for the well bonded panel.
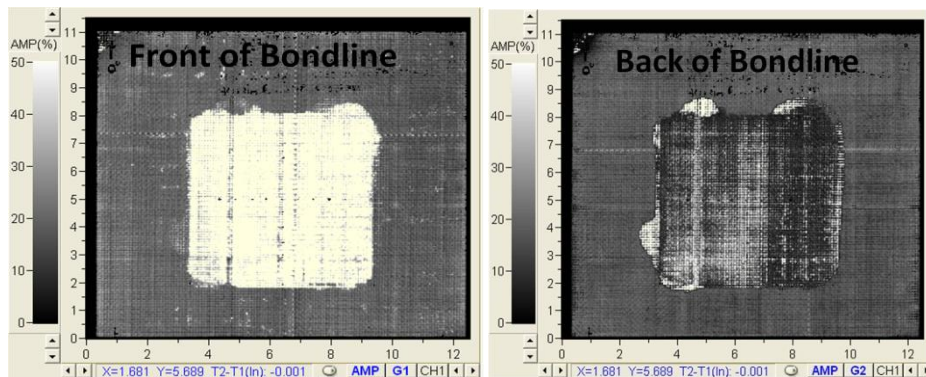
(a)

(b)
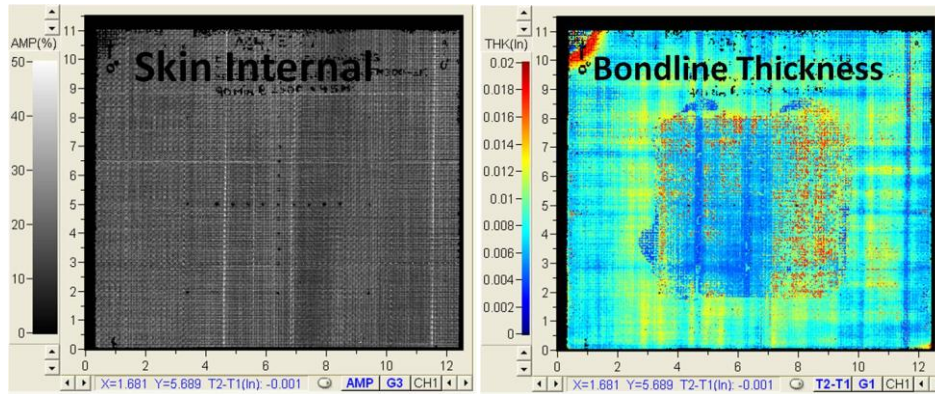
(c)   (d)
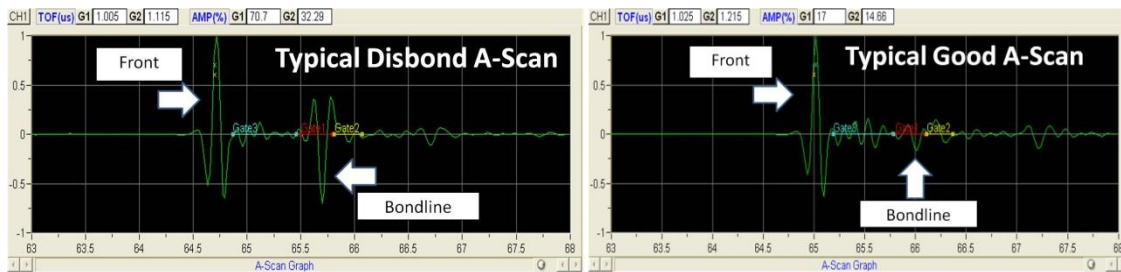
(e)   (f)

Figure 17 C- scans and A-scans of 'kiss' bonded panel #1. The C-scan data represents % wave amplitude plotted vs length (y-axis) and width (x-axis) of kiss bonded panel #1. A-scan data shows voltage response vs time of flight in microseconds. (a) C-scan of top skin/bondline interface; (b) C-scan of bottom skin/bondline interface; (c) Percent amplitude change within laminate; (d) TOF through bondline thickness; (e) Typical A-scan for the released area; and (f) Typical A-scan for the well bonded perimeter area.

The results from the ultrasonic testing performed for kiss bonded panel #2 are shown in Figure 18. A significant change in percent amplitude over the released area on kiss bonded panel #2 was observed. The large center area in the C-scan shown in Figure 18a illustrates a disbond over the entire released area of the panel. The speckled pattern observed over the released area may be due to the surface roughness of the peel ply surface that the release agent was applied to. The release agent may not have covered the bonding surface completely causing the speckled pattern C-scan image.
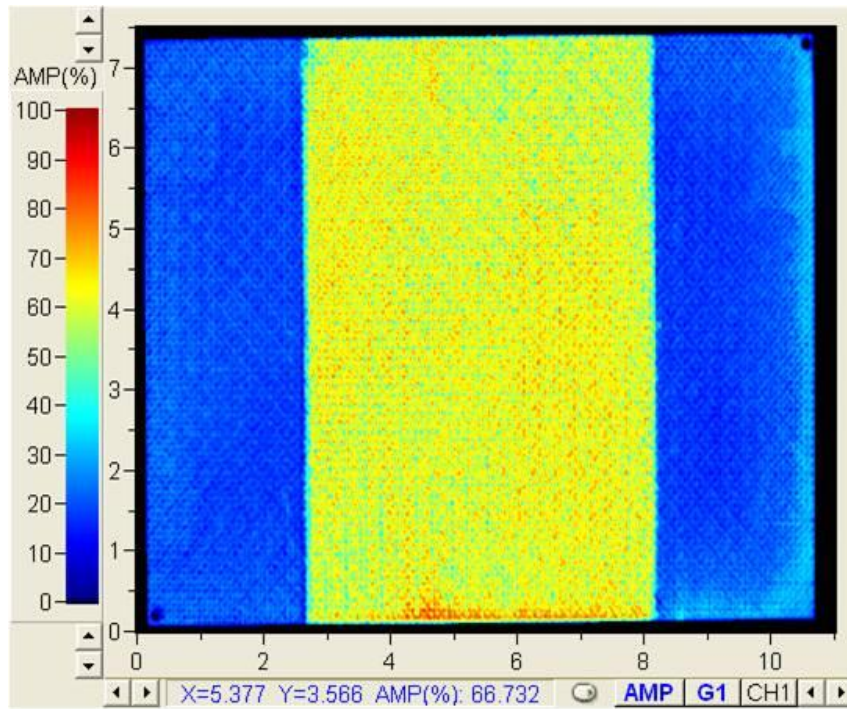
(a)
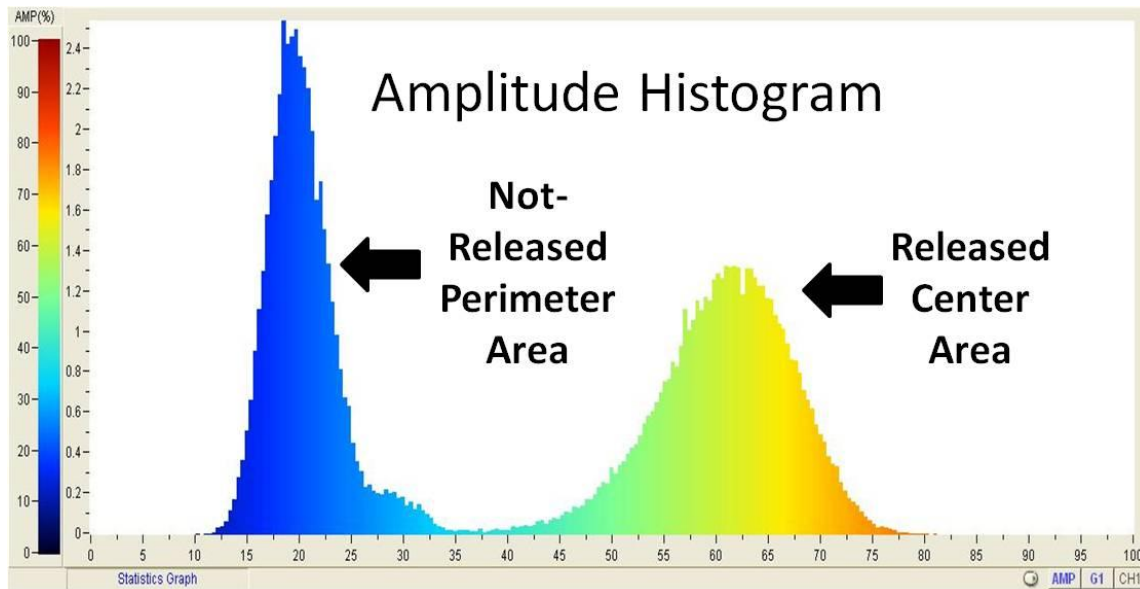
(b)

Figure 18 (a) C-scan of top skin/bondline interface of 'kiss' bonded panel #2. The C-scan data represents % wave amplitude plotted vs length (y-axis) and width (x-axis) of kiss bonded panel #2. (b) Amplitude histogram for released and not released areas of 'kiss' bonded panel #2.

2.3.2 Paste Adhesive Characterization

The results from the ultrasonic testing performed on the paste adhesive bonded panels are summarized in Figures 19-21. TOF measurements showed significant variations in paste adhesive bond thickness near the edges (see Figure 19c, 19f and 19i).   In the center of the panel the bondline thicknesses were relatively consistent and estimated based on the histograms plotted from the TOF images. The thickness results are tabulated in Table 3.

Table 3 Thickness measurements based on histogram plots of TOF measurements.

Panel Type	Thickness mm (in.)
Panel A (Control-Good Bond)	1.32 (0.052)
Panel B (Amine Blush)	1.55 (0.061)
Panel C (Released Agent)	1.4 (0.055)

Panel A and Panel B show no significant difference in percent amplitude as illustrated in Figure 19. No disbond areas were observed for the amine blush panel. Panel C (Release Agent) showed a significant change in percent amplitude around the border of the released area (white border). This area appears to be the result of release agent thickness build-up at the border caused by the masking tape used to protect the perimeter from being contaminated. The center section of the released area is observed to have a similar response as the perimeter areas.

In order to obtain a clearer understanding of the difference between both the released and un-released areas for Panel C, another C-scan was taken with the thin ply laminate as the front surface. A C-Scan image of the adhesive bondline-thick skin interface showing changes in % amplitude is shown in Figure 20. To interpret amplitude changes

illustrated in Figure 20, a histogram of four different regions was plotted and the results

are shown in Figure 21.   From left to right, the first curve represents the well bonded

perimeter area around the panel, and the second curve represents the area that was

released with release agent except the border area indicated in Figure 20. The amplitude

between both of these areas was small (≤ 5 dB) as expected and would be difficult to

distinguish if inspecting a large composite component. The third curve represents a

section of the released border area on the right side of Figure 20. The amplitude difference

between the border area and good area was 10 dB but the panel has not disbonded in this

border area. Lastly, the amplitude change for a void area (dots indicated in Figure 20) at

the adhesive/laminate interface displayed a ≥ 15 dB difference when compared to the good

area. The amplitude responses of voids are typically thresholds used when inspecting

composite parts. Amplitude differences below this threshold, as observed within the

released area, will be difficult to observe.
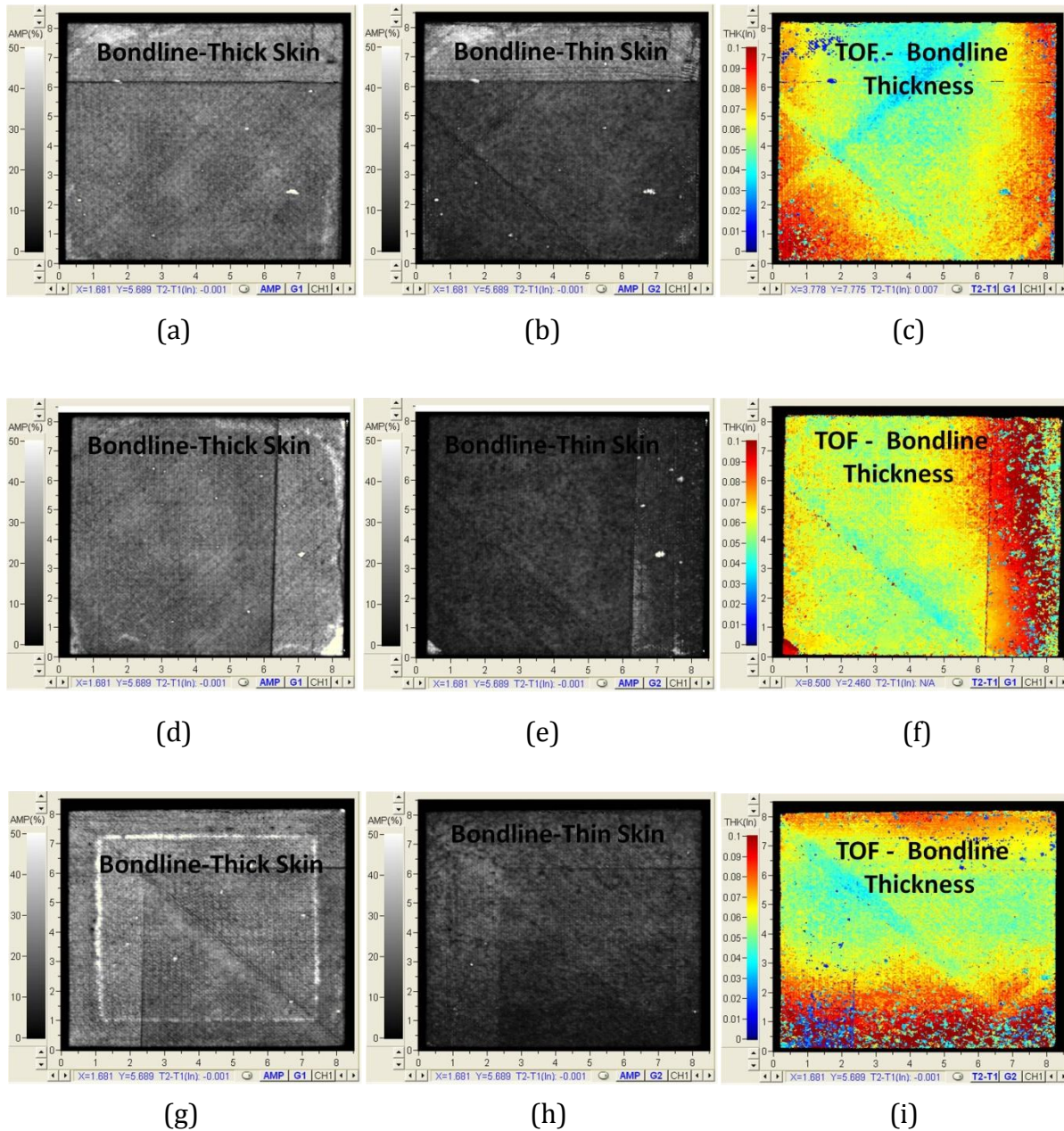
Figure 19 Pulse Echo C-scan results at 5 MHz for Panel A (a) bondline/thick skin interface; (b) bondline/thin skin interface; (c) TOF through bondline thickness; Panel B (d) bondline/thick skin interface; (e) bondline/thin skin interface; (f) TOF through bondline thickness; and Panel C (g) bondline/thick skin interface; (h) bondline/thin skin interface; (i) TOF through bondline thickness. The C-scan data represents wave amplitude plotted vs length (y-axis) and width (x-axis) of the composite panel. Measurements were taken using the 20-ply thick skinned laminate as the front surface.
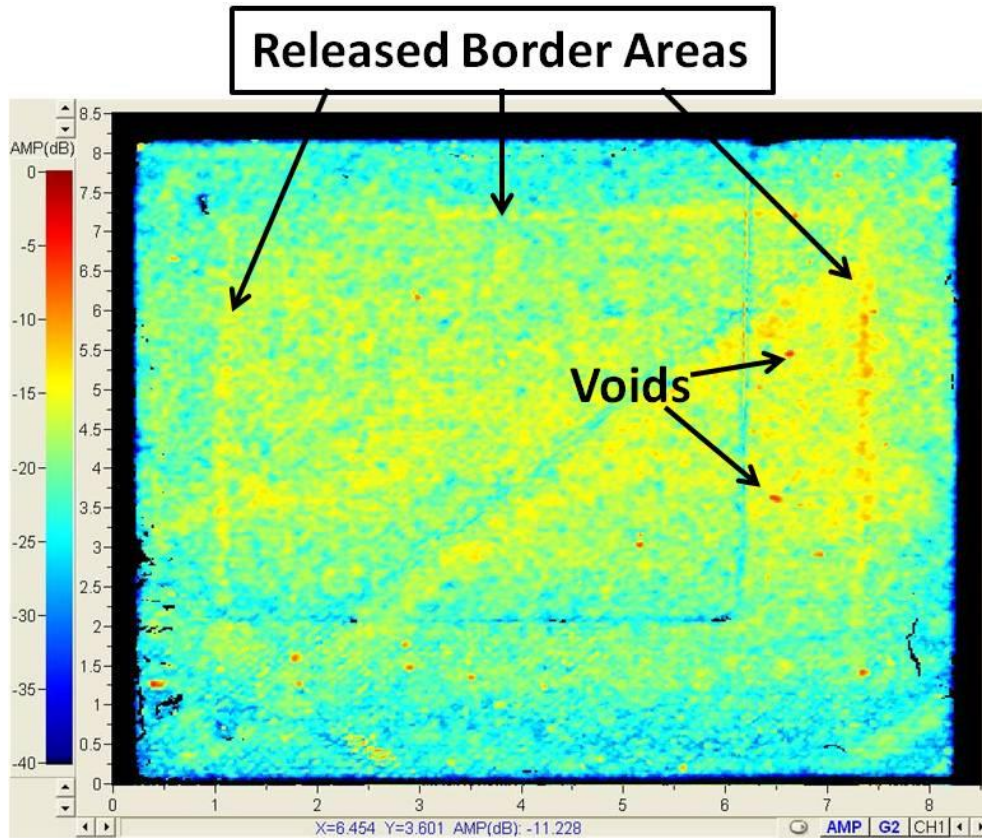
Figure 20 Pulse Echo C-scan results for Panel C at 5 MHz. The C-scan data represents wave amplitude plotted vs length (y-axis) and width (x-axis) of the composite panel. Measurements were taken using the 12-ply thin skinned laminate as the front surface.
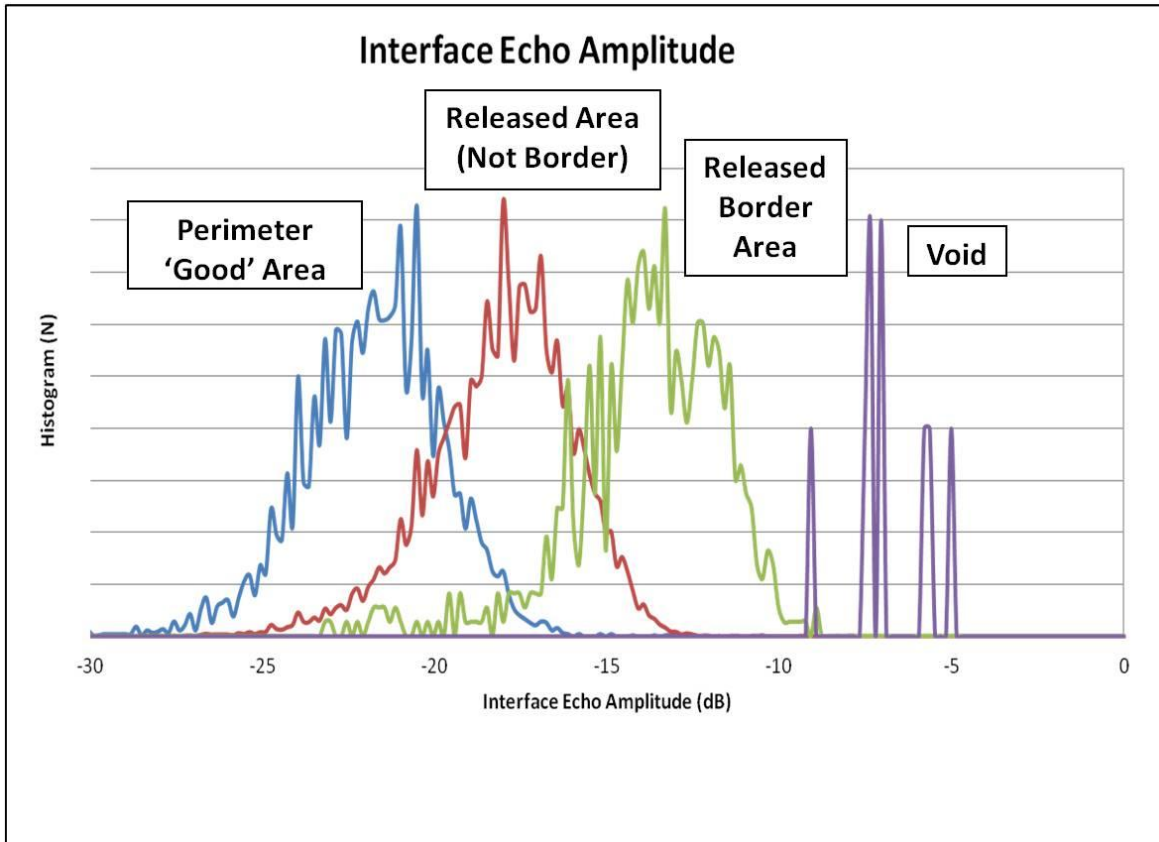
Figure 21 Comparison of interface echo amplitude in 'good' and 'released' areas for Panel C.

2.4 Conclusions

The objective of the present work was to create kiss bonds between film adhesive and paste adhesive bonded composite laminates. For film adhesive bonded laminates, disbonds were observed in C-scan images from ultrasonic testing in pulse-echo mode at 5 MHz in the areas where release agent was applied to the bonding surfaces. The disbond areas occur due to differences in CTE between the film adhesive and carbon fiber/epoxy laminates upon cool down from the adhesive cure temperature. Machining and/or excessive handling of laminates with kiss bonds may also cause the disbonds to form.

For the paste adhesive bonded laminates tested, C-scan images from ultrasonic testing in pulse-echo mode at 5 MHz showed no significant percent amplitude change for

all three panels fabricated; the good bond panel, the amine blush panel as well as the panel

contaminated with release agent. The paste adhesive bonded laminates were cured at

room temperature and were not machined after bonding. As a result, kiss bonds were

successfully created within these laminates.

CHAPTER 3: QUANTITATIVE PERCUSSION DIAGNOSTIC TESTING OF FILM AND PASTE ADHESIVES

3.1 Quantitative Percussion Diagnostic Testing Objectives

In chapter 2 film and paste adhesive bonded composite panels were fabricated to assess the validity of using quantitative percussion diagnostics to characterize the structural integrity. The design of the percussion diagnostic equipment has been developed. However, we shall focus on modifying the test set-up including the test fixtures used to secure the panels to be inspected as well as develop a test procedure to minimize standard deviation. The following chapter will describe the procedures followed in taking measurements of both the film and paste adhesive bonded panels.   The results from this testing shall then be summarized and discussed.

3.2 Quantitative Percussion Diagnostic Procedures

3.2.1 Film Adhesive Bonded Panels

The Well Bonded Panel (WBP) and Kiss Bonded Panel #1 (KBP) identified in Table 1 shall be characterized by QPD testing. A description of the Periometer® and quantitative percussion analysis is included in Appendix I for reference. Before testing, the Periometer® was powered on and left idling for 15-30 minutes to eliminate the possibility of electronic drift effects during testing. Next, the Periometer® was calibrated using two different materials with known loss coefficient values; aluminum alloy 6061-T6 rod and polytetrafluoroethylene (PTFE). The loss coefficient was measured three separate times on each of these materials and the data were used to calculate the effective elastic modulus of the rod and the amount of energy dissipated by external sources (not the specimen) such

as the probe[53]. Once these values were computed, the system was calibrated and testing

could begin.

One of the key factors to ensure consistency in measurements is alignment of the

specimen with the percussion probe. The WBP and KBP specimens were both tested while

being held in a welded aluminum test fixture as shown in Figure 22.
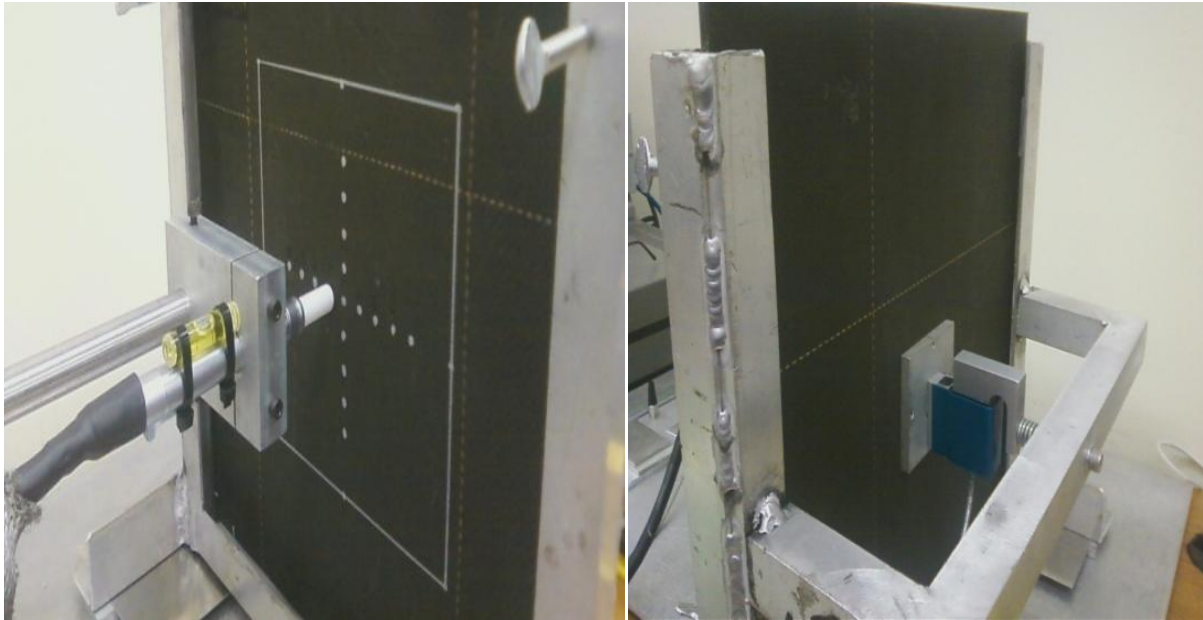
Figure 22 Photographs of fixture holding the 305 mm x 305 mm (12 in. x 12 in.) bonded
laminates tested using the present (a) percussion probe and (b) load cell. During
transmitted force measurements only the specimen was preloaded by pressing it against
the backing plate on the load cell by the probe and positioning bolts shown.

The fixture was designed to hold a 305 mm x 305 mm (12 in. x 12 in.) specimen in place

using four hand screws at the corners. Silicone rubber pads were placed behind the

composite specimen at these four corner locations and at the bottom of the test fixture to

separate the panel from the aluminum frame. The pads will help prevent excess vibration

caused by the metal frame during testing through the specimen. The hand screws were

tightened until the panel made contact with the silicone pad. The screws were not over-

tightened to avoid damping effects caused by an increase in torque. The thickness of the

silicone pad was the same at each corner allowing the specimen to be aligned after securing

all four hand screws. Also shown in Figure 22 are the aluminum angle bars used at the

base to keep the fixture upright. Aluminum shims were placed underneath the base to

keep the fixture level. C-clamps were then clamped onto each side of the base of the test

fixture to lock in place and prevent the fixture from moving during percussion testing.

Once the fixture was level, aligned, and locked in place the percussion probe was

added into its own aluminum fixture as shown in Figures 23 and 24.
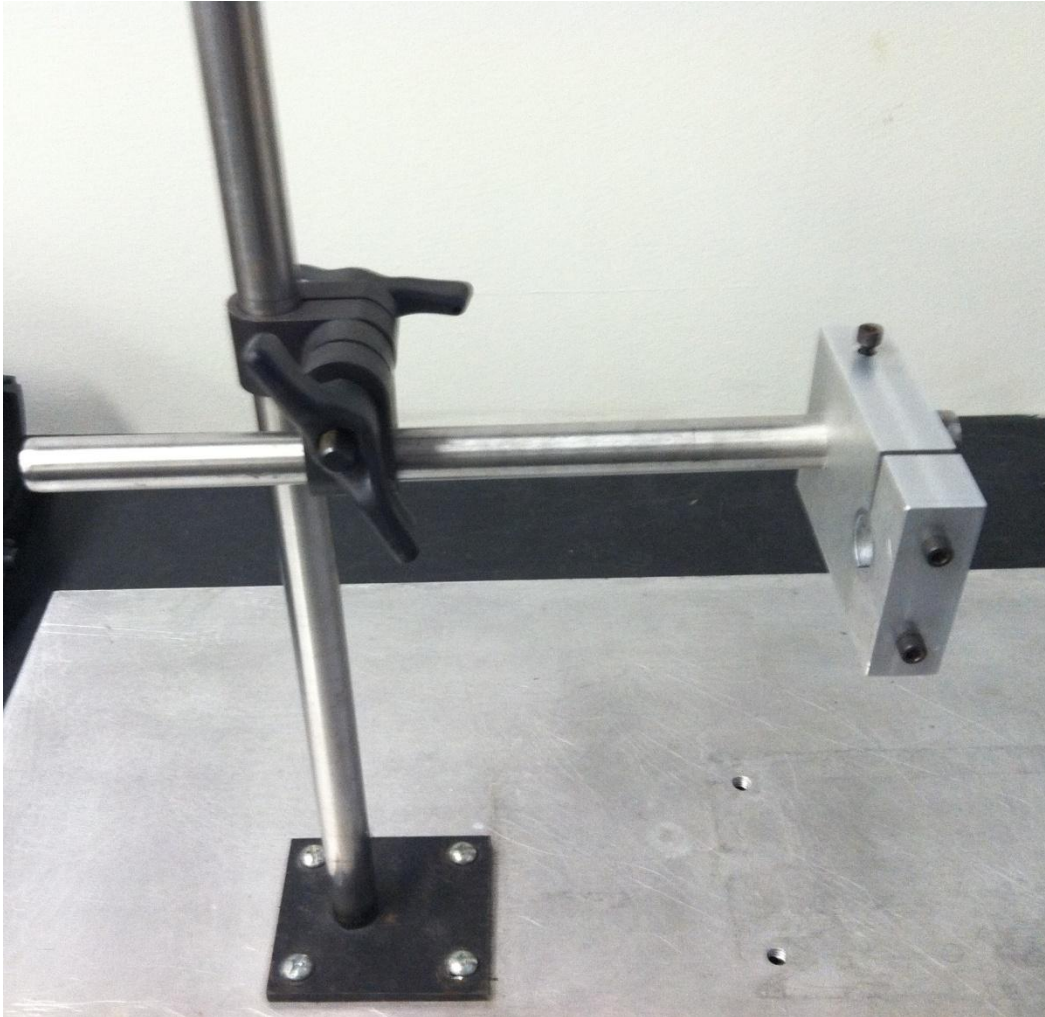
Figure 23 Illustration of Percussion Probe Fixture.
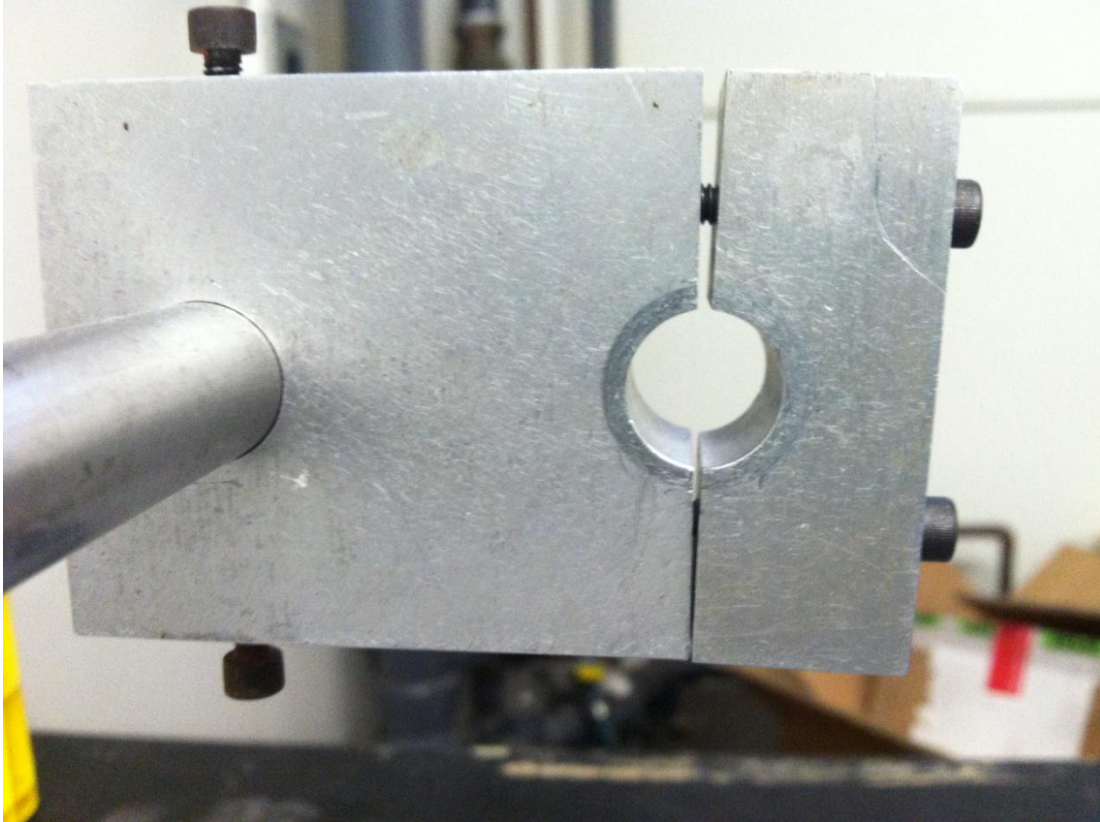
Figure 24 Close-up view of aluminum blocks used to hold percussion probe in place.

The aluminum casing protecting the probe was slid into a hole created between two aluminum blocks (see Figure 24). The blocks were tightened with screws until the probe was secure and would not move during percussion testing. The probe fixture was fastened to a steel rod which could be tilted until the probe was level (parallel to the table top) based on the level indicator attached to the aluminum casing. The laboratory stand holding the steel rod was then moved toward the test fixture until the probe was in contact with the specimen. The nozzle (shown in Figures 22 and 25) covering the end of the percussion rod has two important functions during testing. First, the nozzle is designed to help guide the percussion rod, when it is actuated by the electromagnetic coil, to impact the specimen from a fixed distance away from the specimen surface. This increases the

repeatability and consistency of test data. Second, the nozzle ensures that the entire

percussion tip area will make contact with the inspection area during testing as long as it

rests flat against the surface of the specimen to be inspected. To ensure this occurs, a

Teflon nozzle was used instead of the standard black plastic tip (shown in Figure 26)

because of the contrast in color between the black composite test specimen and white

nozzle. The Teflon nozzle also is larger than the black plastic tip and was easier to verify

that the nozzle was flush against the specimen surface before each measurement.

Figure 25 Illustration of black plastic and white Teflon nozzles used to direct the percussion rod onto the test specimen surface.

Once both the probe and specimen are aligned, the percussion rod is calibrated and the nozzle is in contact with the test specimen, QPD testing was performed. The Labview software controlling the Periometer® asks the user to actuate the percussion rod when ready. This was done by pressing the black button found on the aluminum casing behind the nozzle. Once actuated, the percussion rod impacted the specimen 16 times and the lab view software captured data from 10 of the 16 impacts. The average loss modulus, standard deviation, average maximum probe (impact) force and average maximum transmitted force were calculated based on the equations summarized in the background section and recorded. An example of the output from Lab View after each measurement is shown in Figure 26. Also, the raw probe force and transmitted force data were recorded for each of the 10 impacts and saved in a spreadsheet to enable the user to plot the impact/time curves for both.
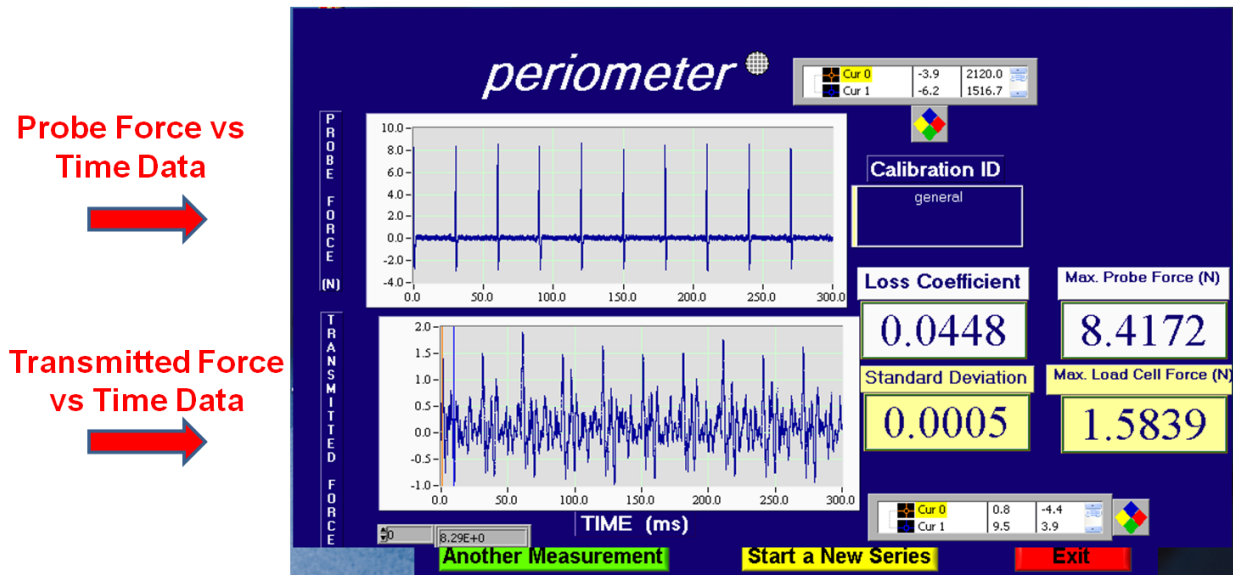
Figure 26 Illustration of output from Lab view once the Periometer has completed one set of measurements (10 impacts on the surface). The averages from these 10 impacts of the loss coefficient, maximum probe force and maximum transmitted force are recorded.

The probe force was measured based on data received by the piezoelectric sensor (accelerometer) attached to the percussion rod during impact. The transmitted force was measured using a 44.5 N (10 lbf) load cell on the side of the specimen opposite to where the percussion was performed. The load cell was attached to a 50.8 mm x 50.8 mm (2 in. x 2 in.) backing plate. The backing plate maintained uniform contact with the specimen and facilitated the measurement of a representative transmitted force by the load cell. An illustration of where the backing plate was located relative to the impact locations is illustrated in Figure 27. The backing plate was only in contact with the specimen when transmitted force was being recorded. For probe force measurements the backing plate was not in contact with the specimen.
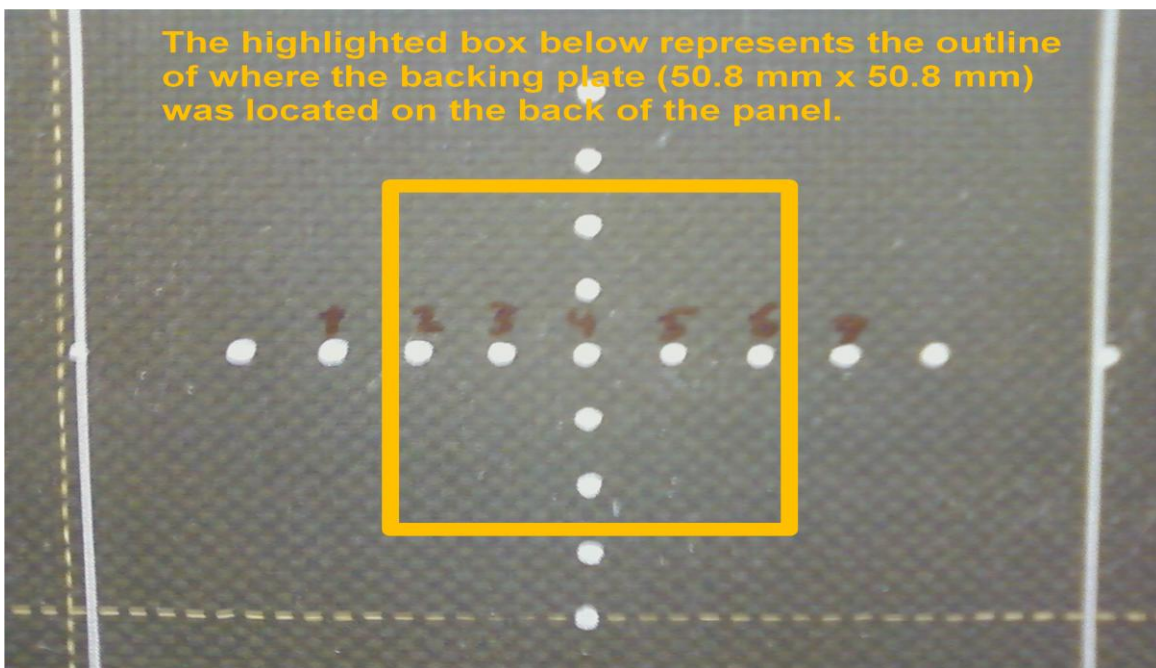
Figure 27 Illustration of location of load cell backing plate (orange outline) relative to the impact locations.

3.2.2 Paste Adhesive Bonded Panels

Changes were made to the equipment and test procedures for the QPD testing of the paste adhesive bonded panels. A new Periometer®, in which the electronics were updated causing the piezoelectric sensor to be more sensitive to defects, was purchased and used to characterize these specimens. The new equipment was operated by a similar Lab-view software program as the previous equipment used at UCI except the new program allowed the user to take multiple measurements at a time (up to 20 measurements) and provided the statistical data in a spreadsheet. Also, a defect factor was calculated which determined how asymmetric the impact/time curves were after each measurement. Asymmetry usually occurs due to cracks in the test specimen and can be observed by the formation of shoulders on the main impact/time peak or the existing second and third peaks.

As discussed in the film adhesive procedure section, one of the key factors to ensure consistency in measurements is alignment of the specimen with the percussion probe. For the paste adhesive specimens a new test fixture design was implemented illustrated in Figures 28 and 29. In this design, flat panels ranging from 152.5 mm (6 in.) to 609.6 mm (24 in.) high can be tested. Two pairs of aluminum bars were used to hold the specimen in place on the top and bottom. The bottom set of bars remain fixed while the top set can be moved up and down depending on the height of the test panel. The test panels were secured using rubber pads in a three point configuration to avoid bending moments during percussion testing; one pair on the top bars and two pairs near the edges of the bottom bars. The rubber pads were hemispherical in shape to help self align the test specimen when the fixture was tightened.
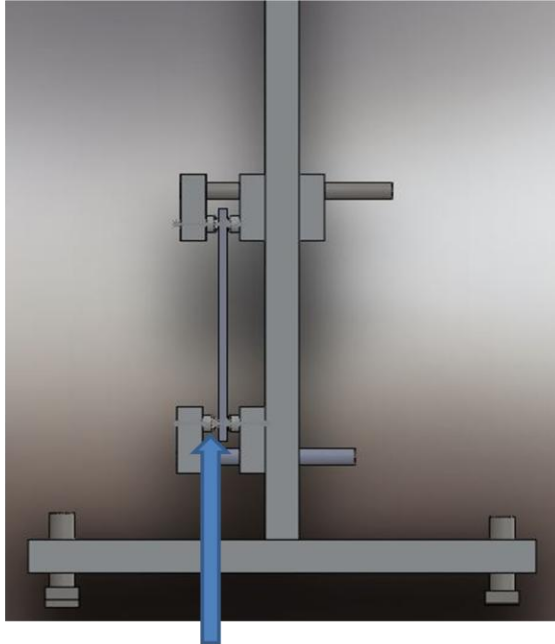
Side View
Panel Connecting Points on
Hemispherical Pads.

Front View
Minimum panel size 6 in.
Maximum panel size 24 in.

Figure 28 Side view and front view drawings of new specimen test fixture for paste adhesive bonded panels.

Figure 29 Photo of fabricated percussion test fixture.

Fine threaded screws were used to adjust the top and bottom pairs of aluminum bars. The fine adjustment allows the user to precisely control the amount of torque applied to the test panel. The final alignment of the test panel was verified by several measurements between the fixture and specimen. An example of this is shown in Appendix II. The most crucial measurement was the distance between the top pair of bars and bottom pair of bars which determined the amount of torque applied to the panel. Finally, rubber coated metal 'feet' were screwed into the aluminum base of the fixture which helped level the test fixture. The base was also made thick enough to prevent it from moving during the percussion testing and as a result did not need to be clamped down.

One of the advantages of QPD is the ability to take manual measurements at local areas that are difficult to access. As a result going forward percussion measurements will be conducted by hand holding the percussion probe during testing. A larger 1 inch diameter Teflon nozzle (see Figure 30) shall be used to help ensure the nozzle is flush onto the specimen's surface for each hand held measurement. Also, care was taken to apply only a small force onto the test specimen when taking the hand held measurement. This was done to avoid potential energy dissipation due to the force applied by the nozzle itself.

Figure 30 Photo of the one inch diameter Teflon nozzle.

3.3 QPD Results and Discussion

3.3.1 Loss Coefficient and Impact Force Measurements-Film Adhesive

Impact measurements were taken at seven different locations horizontally across the middle of the two composite laminates as shown in Figure 27. A summary of the results for this testing is illustrated in Figures 31, 32, and 33. The loss coefficient was found to be higher at every location tested for the released ('kiss' bond) panel when compared to the not-released (well bonded) panel. The maximum probe force (shown in Figures 32 and 33) is also lower for all locations located on the released panel. A single factor analysis of variance (ANOVA) was completed for the loss coefficient and maximum probe force between data collected for released versus the well bonded specimens. The p values obtained for loss coefficient and probe force data were between 6 to 8 x 10^{-5} (< 0.02) indicating significant difference between the results for the released and not-released panels. The significantly greater loss coefficient and corresponding lower decrease in probe force can be explained by greater internal friction within the poorly bonded specimens. This explanation is consistent with damping capacity data generated for metal adherends[33,34].   Finally, the probe force vs time curves in Figure 34 shows similar behavior for both well bonded and kiss bonded panels. The significant difference is between the peak values of the curves which are captured in Figure 32. No secondary peaks or shoulders were observed for either panel which can be attributed to no cracking within the laminates.
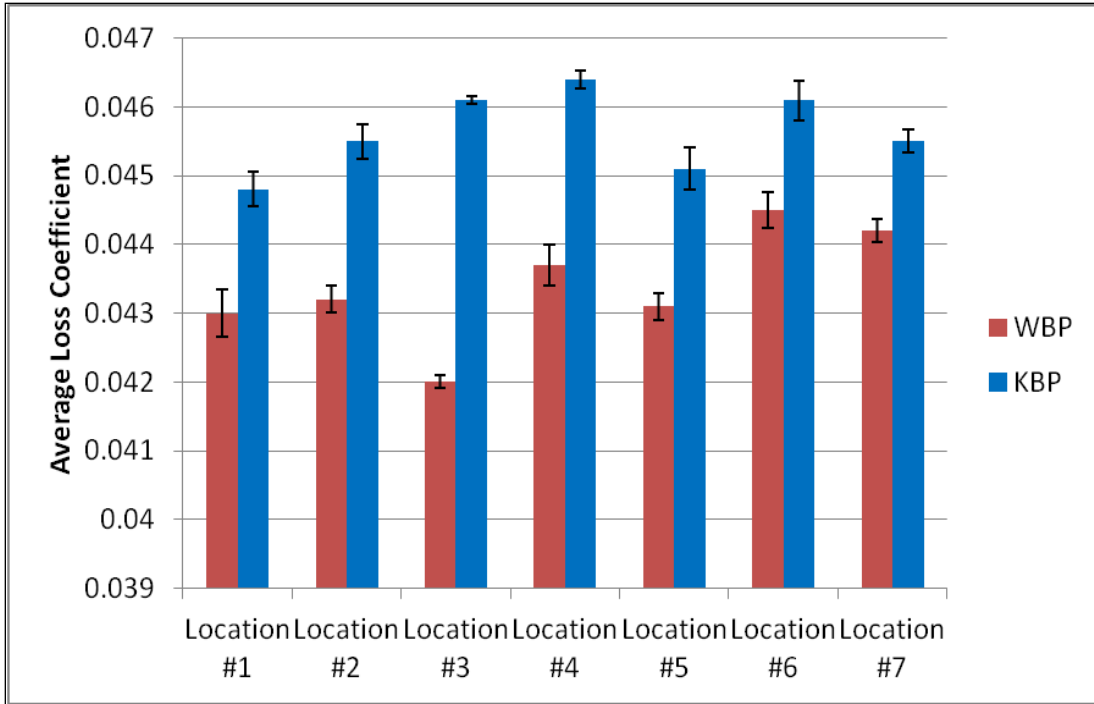
Figure 31 Loss coefficient measured at different locations for the well bonded-not-released panel (WBP) and the released 'kiss' bond panel (KBP).
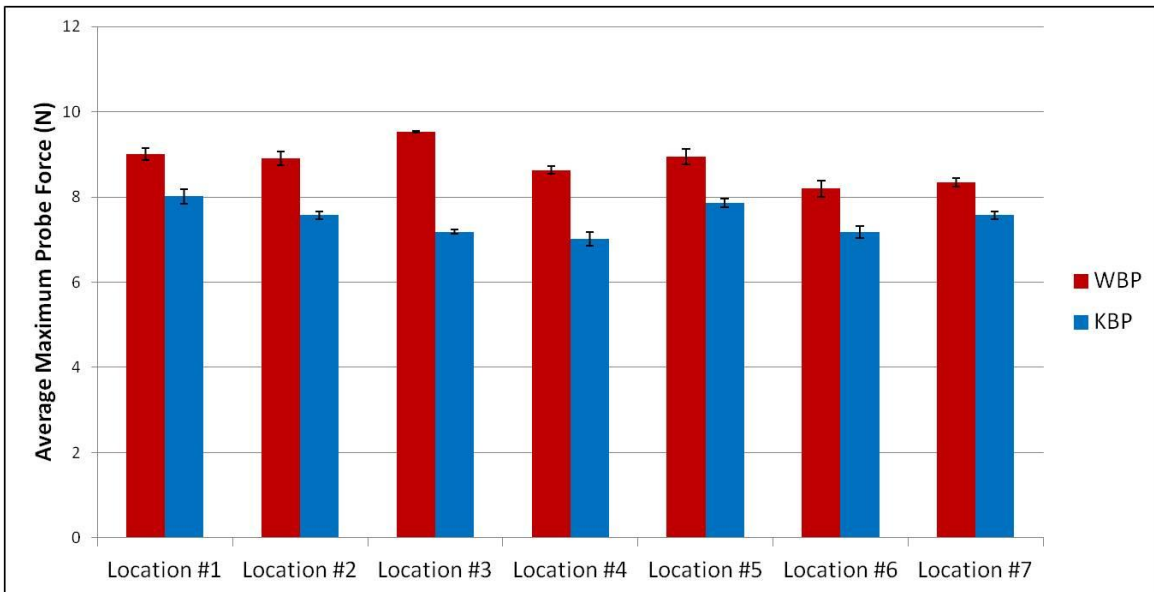
Figure 32 Average maximum probe force (impact force) measured at different locations for the well bonded-not-released panel (WBP) and the released 'kiss' bond panel (KBP).
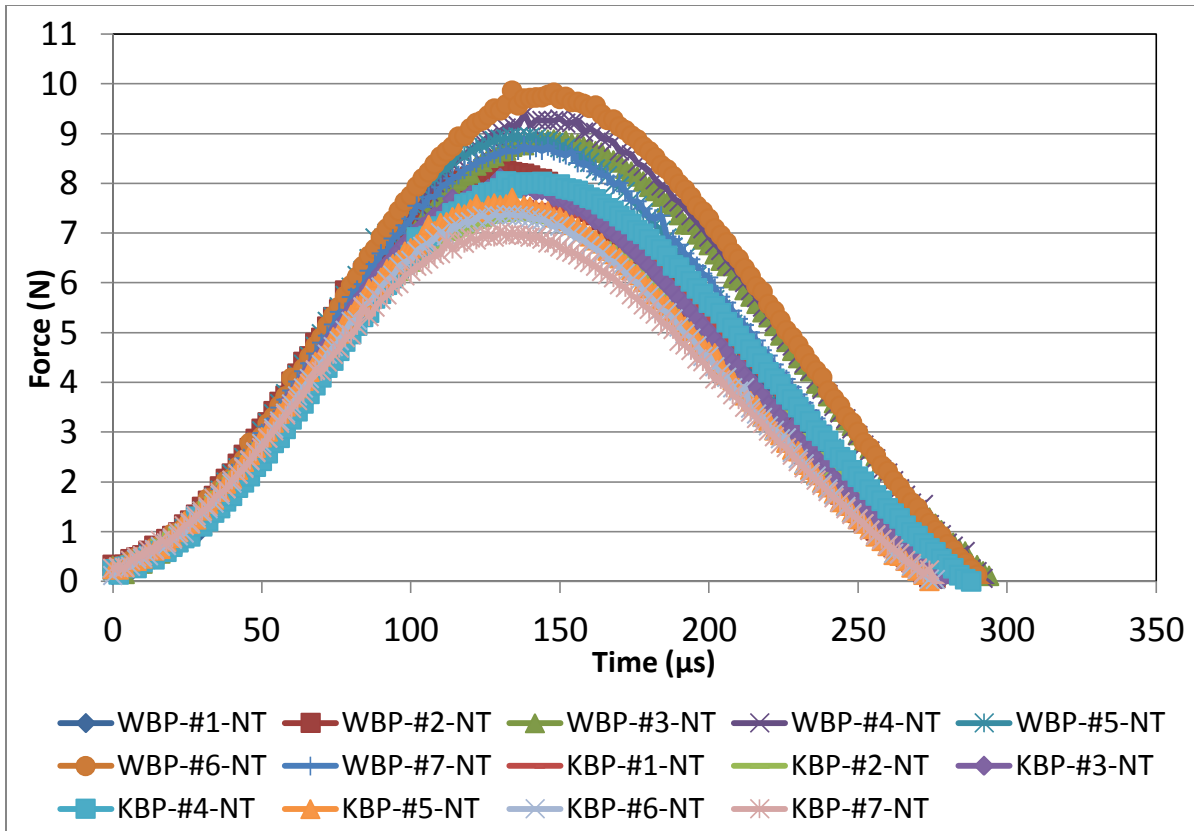
Figure 33 Probe force vs time measured at 7 different locations for the well bonded not-released panel (WBP) and the released 'kiss' bond panel (KBP).

3.3.2 Transmitted Force Measurements-Film Adhesive

For transmitted force measurements, a pre-load was needed to ensure good intimate contact between the backing plate and sample. However, the pre-load was found to have an effect on the transmitted force measurement as well as the loss coefficient and probe force measurements. A low pre-load of 3 to 4 N was used to create contact between the backing plate and sample but not too high to change the alignment of the sample during testing. The results of the transmitted force measurements are shown in Figure 34. Most of the maximum transmitted force measurements were higher on the not released (well bonded) panel compared to the released ('kiss' bonded) panel. This was especially true for

the three central locations where the well bonded panel recorded significantly higher

transmitted force values. The explanation for this trend could be that the impact energy

will have a harder time propagating through the thickness of two laminates that are poorly

bonded at the interface. The well bonded laminates should be able to transmit force easier

from the front to back surface. The p-value calculated in a completed analysis of variance

for the three central locations was 0.0013 (< 0.02).
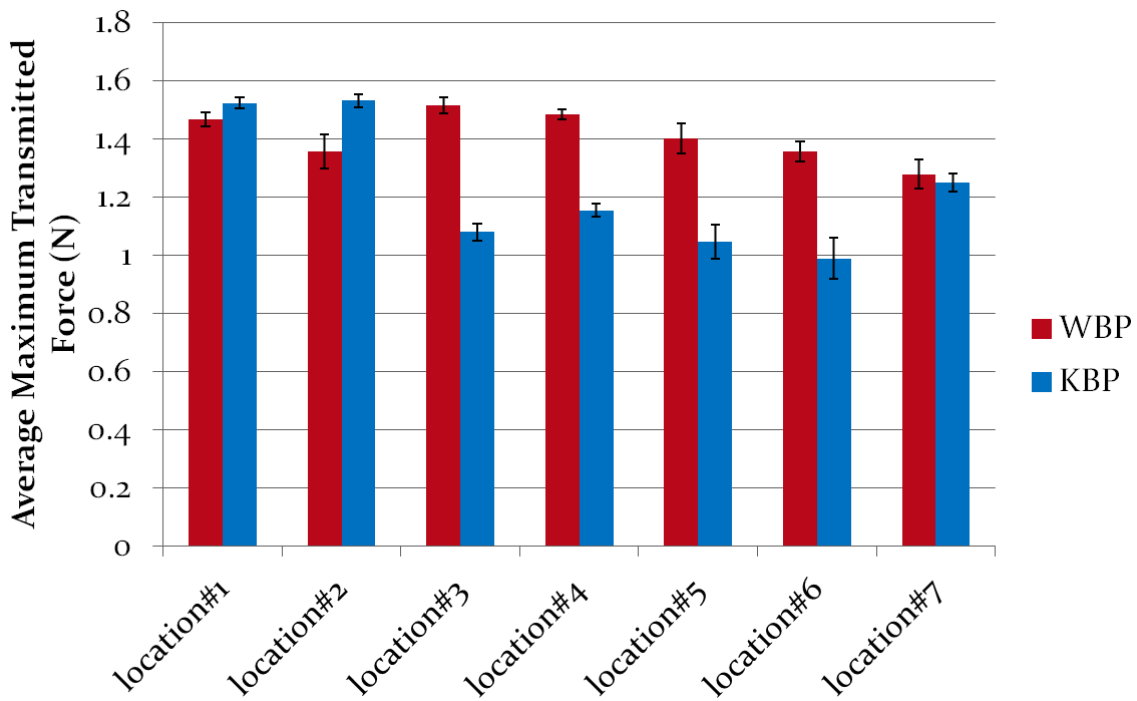
Figure 34 Average maximum transmitted force measured at 7 different locations using a low pre-load (3 to 4 N) for the well bonded-not-released panel (WBP) and the released 'kiss' bond panel (KBP). A significant difference (p = 0.0013) in transmitted force was determined for the three central locations (3 through 5).

The maximum transmitted force also varied as a function of percussion location on the

specimen as shown in Figure 34. The transmitted force was higher at locations #1 and #2

for the KBP when compared to the middle locations (#3, #4, and #5). This trend was not

observed for the WBP. It appears that locations 1, 2, and 7 were sufficiently close to the edge of the released area so that greater forces can still be transmitted to the load cell. The probe force and loss coefficient were also measured with the backing plate in contact with the WBP and KBP samples at a pre-load of 3 to 4 N. Table 4 shown below summarizes the average maximum probe force and average loss coefficient measured with corresponding p-values. The average probe force and loss coefficient were similar in value for WBP and KBP samples.

Table 4 Average loss coefficient and probe force measurements for WBP and KBP tested at low pre-load conditions. Average values reported are the overall average of the measurements taken at each of the seven locations across the sample.

Specimen	Pre-load	Avg. Loss Coefficient	Single Factor ANOVA P-value	Avg. Max Probe Force (N)	Single Factor ANOVA P-value
WBP	Low	0.0338	0.667	9.07	0.780
KBP	Low	0.0351		9.16	

3.3.3 *Comparison of Transmitted and Impact Force Measurements-Film* Adhesive

Transmitted force and probe force data for both a WBP and a KBP at location #4 are shown in Figure 35. No difference was observed in the probe force plots. However a difference in the behavior of the transmitted force curves was observed after 0.001 seconds. The transmitted force for the WBP was slightly higher than for the KBP after 0.001 seconds until both force curves attenuated at about 0.003 seconds. A difference in transmitted force between these panels was expected as the WBP should record a higher transmitted force.
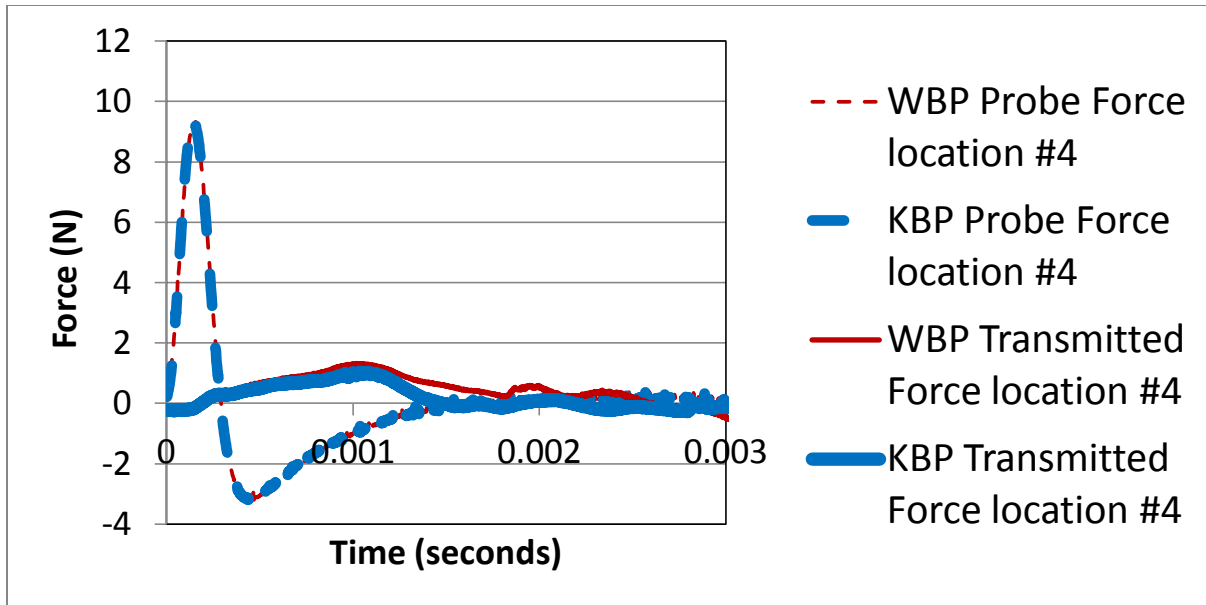
Figure 35 Probe and transmitted force vs time measured at location #4 using a low pre-load (3 to 4 N) for the well bonded panel (WBP) and the released 'kiss' bond panel (KBP).

3.3.4 Loss Coefficient and Impact Force Measurements-Paste Adhesive

Three paste adhesive non destructive inspection (NDI) standards described in Chapter 2 (Panels A, B and C) were characterized using quantitative percussion diagnostics. Several percussion measurements were taken at four different locations near the center of the panels as shown in Figure 36.   An average of the loss coefficient values vs locations are shown in Figure 37. An average of the maximum probe force values vs locations are also shown in Figure 38. Although the standard deviation in measurements for the paste adhesive panels was high for many of the measurements, the green bars show the clear difference between the released panel vs the control panel (blue bars). This increase in damping capacity (and subsequently decrease in probe force) was expected due to the increase in energy dissipation caused by the thin contamination layer between bonded laminates.   A single factor analysis of variance (ANOVA) was completed for the loss coefficient and maximum probe force between data collected for released versus the

control specimen. The p values obtained for loss coefficient and probe force data were 0.007 and 0.01 (< 0.02) indicating a significant difference between the panels. The higher standard deviation obtained during this testing was attributed to the weave style and surface roughness of the laminate. The metal rod is only 2mm in diameter and may not be impacting the surface squarely for each measurement. A larger diameter may be needed to lower the standard deviation when taking measurements on irregular surfaces. Also, paste adhesive bonded panels tend to have higher bondline thickness variation (as shown in Chapter 2) and more porosity compared to film adhesive bonded specimens which have the potential to increase the scatter observed in the QPD measurements.

The red bars in Figures 37 and 38 show an alternating pattern of damping capacity and probe force measurements for the amine blush panel. This pattern in the data suggests the amine blush layer is not consistent across the bondline; some areas within the bondline the amine blush occurred while in other areas the amine blush did not occur.   As a result, this variation in the amine blush layer will cause a variation in stiffness of the epoxy adhesive. Assessing the bond integrity will require localized shear testing to be performed at the different percussion measurement areas and compared to the QPD results.
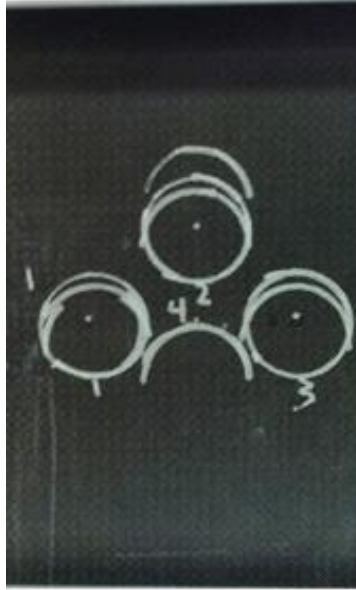
Figure 36 Four locations where QPD measurements were taken for each Paste Adhesive Bonded Panel (A-C).
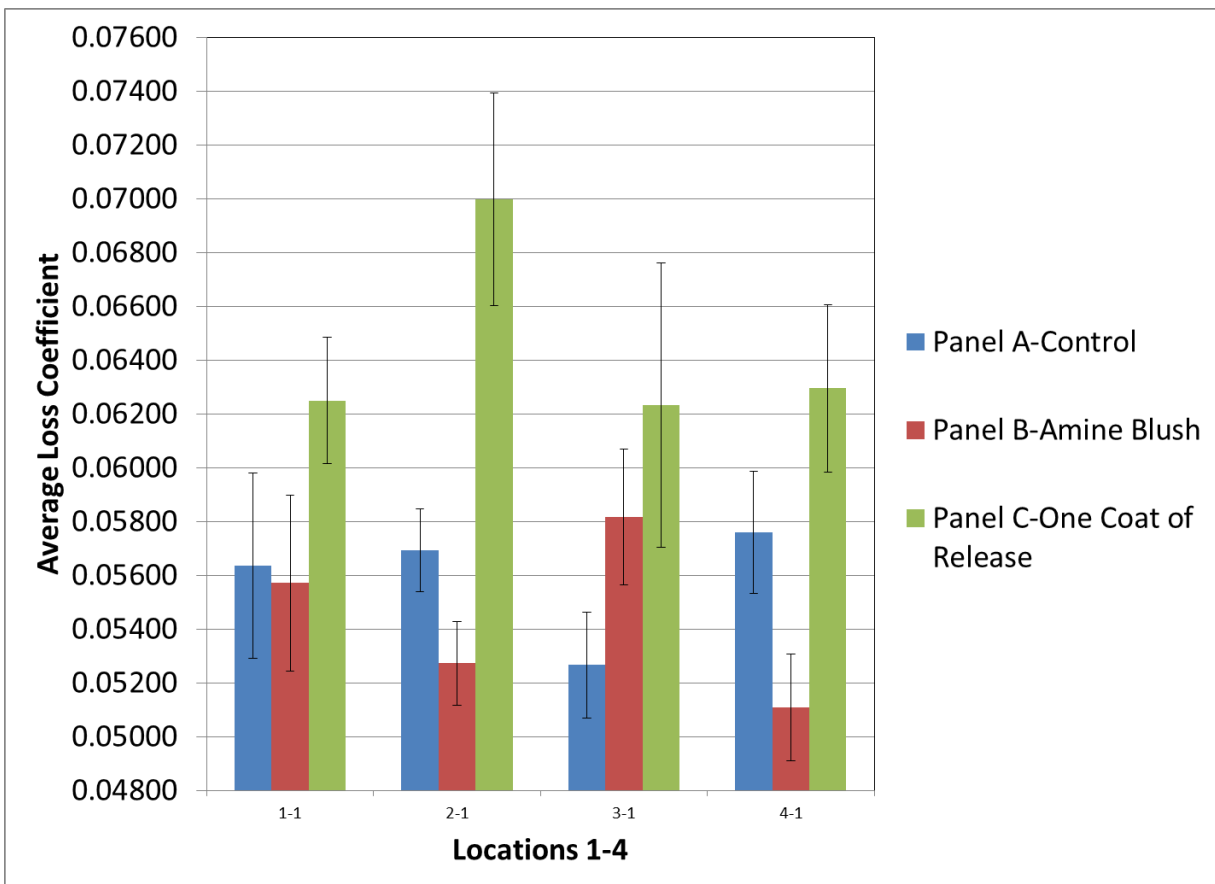
Figure 37 Average Loss Coefficient vs Locations 1-4 for Paste Adhesive Panels A-C.
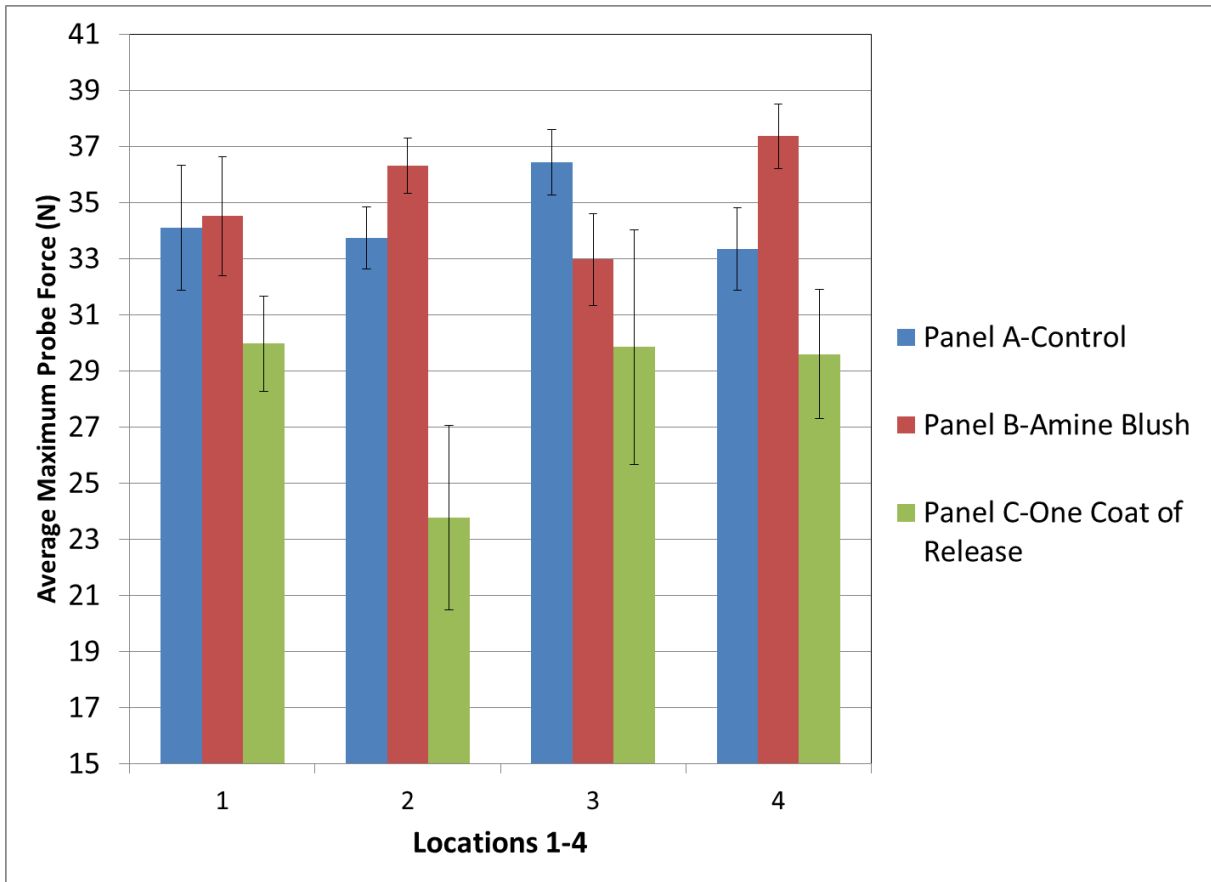
Figure 38 Average Maximum Probe Force vs Locations 1-4 for Paste Adhesive Panels A-C.

3.4 Conclusions

3.4.1 Film Adhesive

A significantly greater loss coefficient determined from percussion testing was observed for the release coated 'kiss' bonded panel compared to that for the not release coated well bonded panel. Also, a significantly lower maximum probe force was observed for the release coated 'kiss' bonded panel compared to that for the well bonded panel. The increase in loss coefficient and decrease in probe force are thought to be due to greater internal friction during the percussion for poorly bonded specimens when not using the load cell backing plate on the backside of the test specimen.

Using a low pre-load force (load cell backing plate in contact with the test specimen), a significantly greater maximum transmitted force was observed for the not release coated well bonded panel compared to that for a release coated 'kiss' bonded panel. The maximum transmitted force was higher for locations closer to the edge of the release coated area when compared to locations near the center of the release coated region. The greater transmitted force for the well bonded panel under a low pre-load appears to be the result of the two bonded substrates having a greater ability to transmit load across the interface when compared to the release coated 'kiss' bonded panel.

3.4.2 Paste Adhesive

A significantly higher average loss coefficient and significantly lower average maximum probe force across four different locations for Panel C (one coating of release agent) was observed when compared to Panel A (control). The increase in loss coefficient and decrease in probe force are thought to be due to greater internal friction during the percussion response. A change in loss coefficient or probe force between Panel A (control) and Panel B (amine blush) was not evident due to the variation in the amine blush layer. A localized shear test must be performed at the individual percussion measurement locations to assess the integrity of the bond and compare to QPD measurements.

CHAPTER 4: FINITE ELEMENT ANALYSIS OF QUANTITATIVE PERCUSSION DIAGNOSTICS FOR EVALUATING THE STRENGTH OF BONDS BETWEEN COMPOSITE LAMINATES

4.1 Finite Element Analysis Background

In chapter 3, quantitative percussion diagnostic testing results for both film and paste adhesive bonded panels were discussed. In order to understand why we are able to observe changes in bond integrity using QPD, a model of how the percussion rod interacts with the test specimens must be created. A common method used to analyze damage in composite bonded structures is through cohesive zone modeling[68–70]. Here cohesive elements are placed at the interface between two components to help estimate the amount of force it takes to separate these components. This modeling method assumes fracture takes place gradually across a cohesive zone where these elements are applied. Cohesive elements do not have any properties and are considered '0' thickness. Their primary role is to help estimate damage growth at the interface; crack initiation and crack propagation; as stress is applied to the composite material. However as explained previously, kiss bonds are not physical defects and cracking will not result from the creation of these low strength bonds. As a result, a different strategy must be followed in order to model kiss bonds. Also, we will be modeling the QPD technique which is non-destructive and will not result in damage growth of the composite. Therefore failure criterion and strength properties will not be needed in this analysis.

In the following chapter, experimental results from chapter 3 were compared to a finite element analysis (FEA) using MSC PATRAN/NASTRAN to understand the visco-elastic

behavior of film adhesive bonded laminates during percussion testing. Specifically, the dynamic FEA models will be used to directly predict changes in the probe force, as well as effective stress distributions across the bonded panels as a function of time. A summary of the details of the FEA model as well as the results from a model of a film adhesive bonded panel tested using QPD shall be discussed.

4.2 Finite Element Analysis Details

Finite element analysis using MSC PATRAN/NASTRAN software was completed in order to characterize low shear strength adhesive bonds within secondary bonded composite laminates. The bonded panel was modeled as three 101.6 mm x 101.6 mm (4 in. x 4 in.) rectangular solids where the top and bottom solids (facesheets) had high stiffness (68.9 GPa) and the middle solid (adhesive layer) had low stiffness (2.41 GPa). The model created represents two pre-cured standard modulus carbon fiber/epoxy matrix laminates, each 3.175 mm (0.125 in.) thick, that were bonded together with a 121 °C (250 °F) cure supported epoxy film adhesive that was 0.229 mm (0.009 in.) thick. The bonded panel was meshed using 3-dimensional hexagonal 8-node elements (6 faces and 8 nodes per element). Using an aspect ratio of 10 to 1, the fine mesh created in the model was 178 elements by 178 elements with four elements across the thickness of the adhesive layer and four elements across the thickness of the facesheets of the panel.   The number of elements across the bondline thickness was determined based on a preliminary linear analysis using a static load and discussed in more detail in the next section. Properties of the facesheets were modeled as 3d orthotropic and the film adhesive and steel percussion rod were modeled as isotropic. A summary of the properties can be found in Table 5. The low shear strength 'kiss' bond area was simulated by reducing the modulus of the film

adhesive layer from the ultimate value of 2.41 GPa. Displacement constraints were applied

in a three-point configuration from nodes on the back edge of the panel. To reduce the

number of elements to ~380,000, a symmetry plane was created at one of the panel edges

through the percussion rod as shown in Figure 39.

An implicit nonlinear analysis (SOL 400 in NASTRAN) was used to analyze the

impact event at duration of 0.32 ms for 10 µs time increments. The rod was moved to

within 0.00254 mm (0.0001 in.) of the panel to reduce model time and an initial velocity of

60 mm/s (2.36 in/sec) was applied. Also, the percussion rod was modeled as two contact

bodies; the percussion rod and percussion rod tip, which were glued in contact to one

another. The plane of nodes in contact with both bodies (contact surface) represents the

piezoelectric sensor used to measure the force of the impact as shown in Figure 40.

Table 5 Summary of material properties used in the finite element model.

Properties	AS4 carbon plain weave fabric/epoxy matrix (assuming ~0.62 F_v)	FM-300-2 epoxy film adhesive	Steel Percussion Rod
E_1 Gpa (psi)	68.9 $(10e^6)$	2.41 $(0.35e^6)$	206.8 $(30e^6)$
E_2 Gpa (psi)	68.9 $(10e^6)$	-	-
E_3 Gpa (psi)	9.65 $(1.4e^6)$ Assume = to E2 for AS4 Unidirectional Tape)	-	-
V_{12}	0.06	0.34	0.30
V_{23}	0.06	-	-
V_{31}	$0.007 = v_{13} \times (E_3/E_1)$	-	-
G_1 Gpa (psi)	6.89 $(1e^6)$	-	-
G_2 Gpa (psi)	6.89 $(1e^6)$	-	-
G_3 Gpa (psi)	6.89 $(1e^6)$	-	-
P g/cm^3 (lbs/in^3)	1.61 (0.058)	1.27 (0.046)	7.92 (0.286)
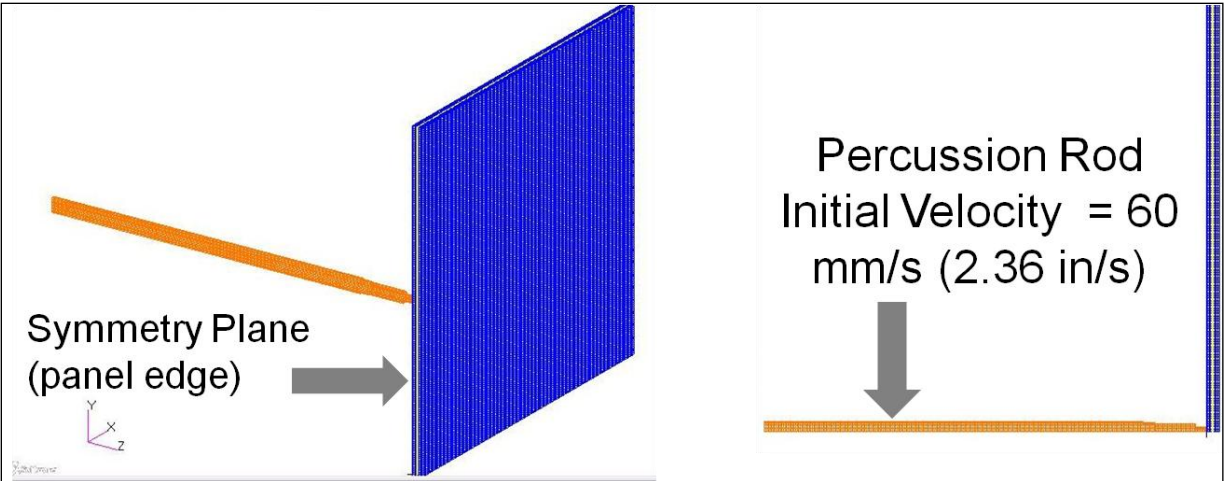
Figure 39 Illustration created in PATRAN of the half model showing the percussion rod and symmetry plane along the 101.6 mm x 101.6 mm (4 in. x 4 in.) composite panel edge.
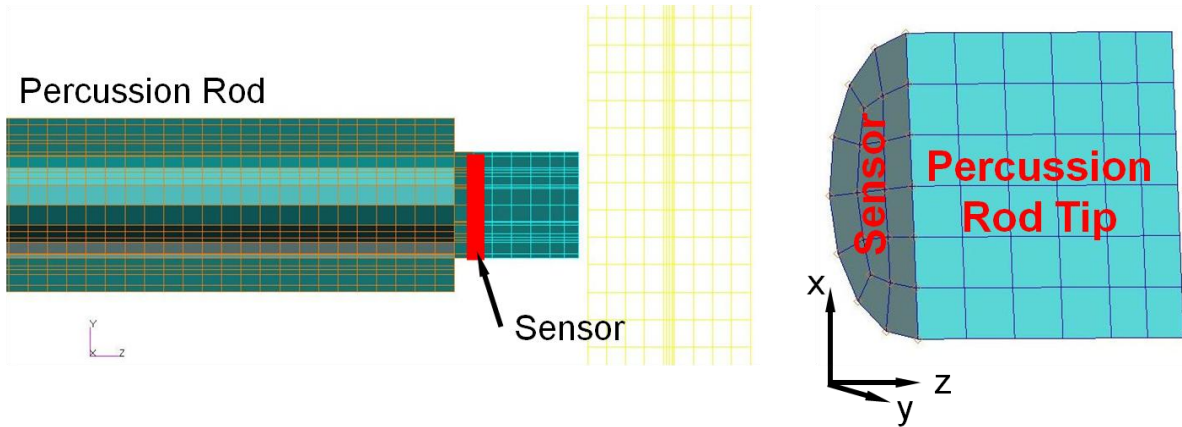
Figure 40 A detailed illustration of the percussion rod model and piezoelectric sensor used to measure force during the impact.

4.3 Summary of Static Linear Analysis Results

Before performing non-linear analysis of the QPD technique, a simple linear analysis using a static load was performed on the bonded composite laminates described in the previous section. There are two main questions the linear analysis conducted will address. First, what are the differences between modeling the composite laminate with 2 elements through the bondline thickness vs 4 elements through the bondline thickness? Secondly, how much do the maximum displacements change from a well bonded model compared to models where the stiffness was reduced to 1% and 10% of the ultimate value? A loading of 10N or 2.25 lb (5N or 1.13 lb because of the symmetry plane) was used as the static load which represented the weight of the steel percussion rod. The boundary conditions were set-up as displacement constraints in a three point configuration and a symmetry plane was defined across the right edge of the laminate (as shown in Figure 41) which allowed a reduction in the number of elements and a decreased run time.
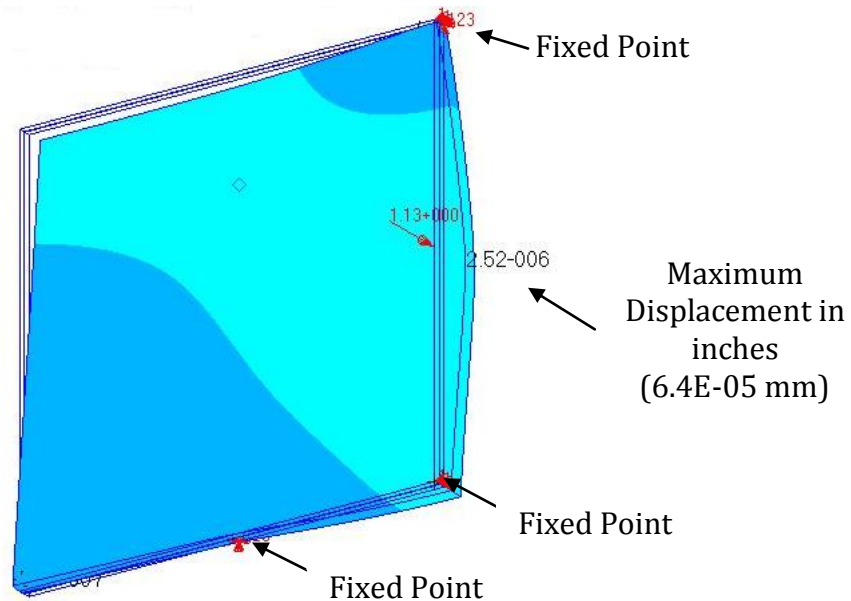
Figure 41 Illustration of boundary and loading conditions used in the static linear analysis performed.

Models with 2 elements and 4 elements across the 0.229 mm (0.009 in.) bondline thickness were analyzed. The elastic modulus of the film adhesive was also varied from its measured value of 2.4 GPa (well bonded condition) to 1% and 10% of that value. The results are summarized in Table 6 and Figure 42 below.

Table 6 Summary of maximum displacement data for 2 element and 4 element bondline conditions.

Type of Bond	Elastic Modulus Gpa (psi)	2 Element Max Displacement mm (in)	4 Element Max Displacement mm (in)
Well Bonded	2.4 (350000)	3.33E-05 (1.31E-06)	3.66E-05 (1.44E-06)
1%	0.024 (3500)	6.4E-05 (2.52E-06)	6.78E-05 (2.67E-06)
10%	0.24 (35000)	3.86E-05 (1.52E-06)	4.22E-05 (1.66E-06)
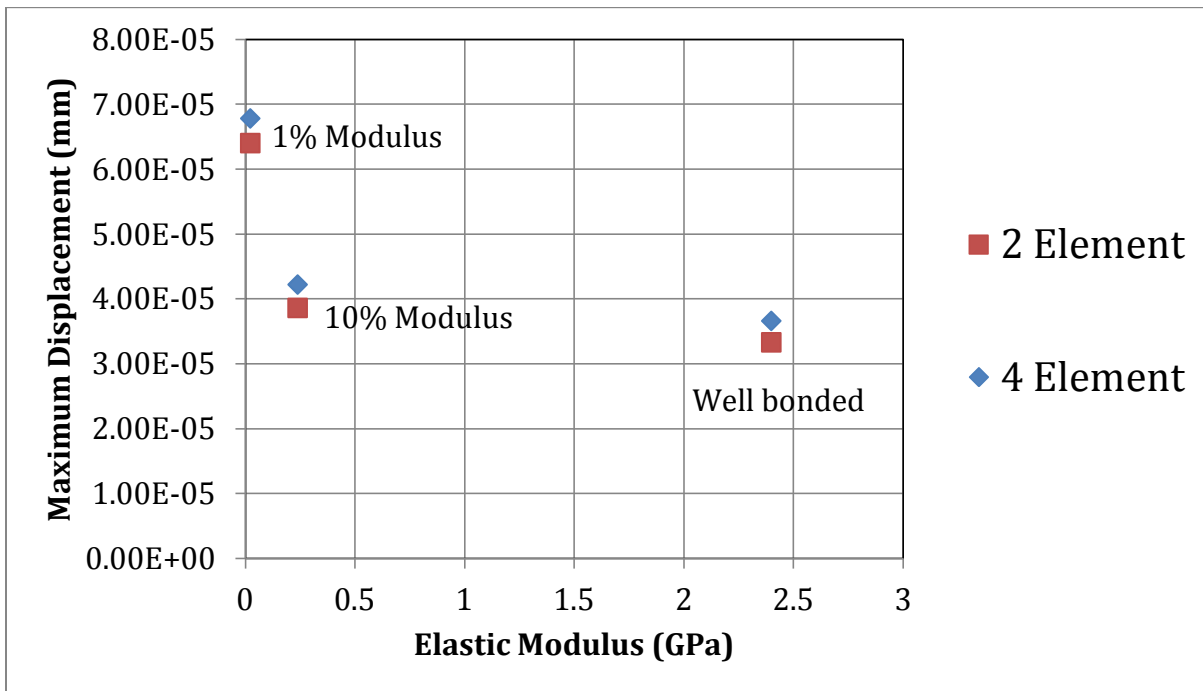
Figure 42 Plot of maximum displacement vs elastic modulus for the 2 element and 4 element models.

The differences in maximum displacement between the two and four element

models are similar as the elastic modulus is reduced. There also is not a large difference in

displacements between the two and four element models which indicates that an increase

in the number of elements through the bondline thickness greater than four is not needed.

Also, increasing the number of elements from four would significantly increase model run

time. As a result, 4 elements through the bondline thickness shall be used in the non-linear

analysis described in the next sections. Using 4 elements will allow changes in the adhesive

stiffness at only the interface areas which can be compared to changing the modulus

through the entire thickness of the adhesive.

Finally, a significant increase in maximum displacement is observed for the 1%

model when compared to the well bonded model. However, in the 10% elastic modulus

model there is a small increase in maximum displacement compared to the well bonded

model.   Any increase in elastic modulus from the 10% condition would likely produce

minimal difference in maximum displacement. The percent change in maximum

displacement compared to the well bonded maximum displacement is shown in Figure 43.

The 1% bond is almost double the maximum displacement compared to the well bonded

model, while the 10% bond is significantly lower in change. As a result, we will begin our

non-linear analysis study looking at using adhesive modulus values less than 10% of the

ultimate property value (2.4 GPa) when simulating a kiss bond.
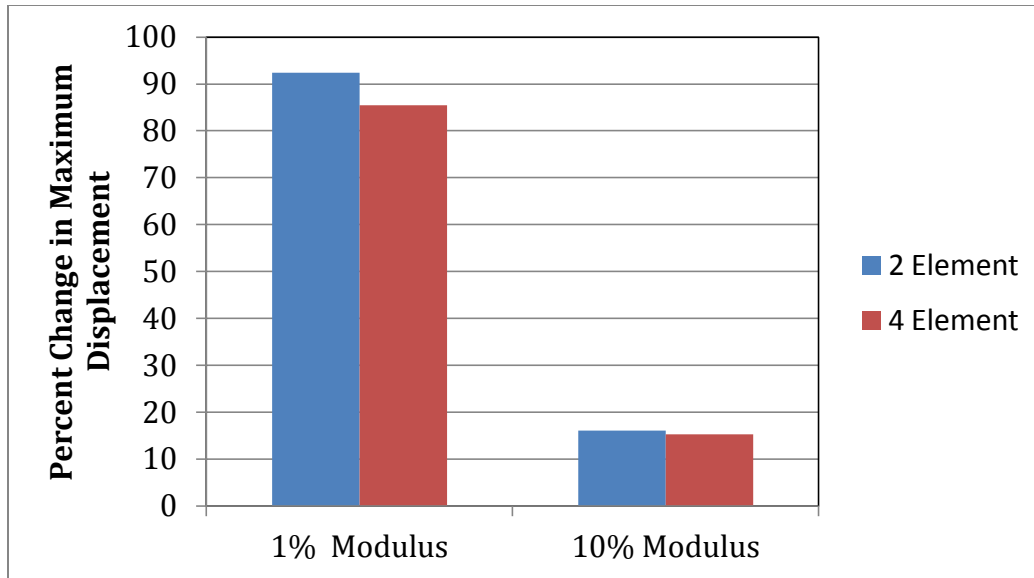
Figure 43 Percent change in maximum displacement for 1% and 10% modulus models for both 2 element and 4 element models.

4.4 Review of Impact Force Measurements for Film Adhesive Bonded Panels

As described in chapter 3, impact measurements were taken at seven different locations horizontally across the middle of the two bonded composite panels. A summary of the results for this testing is illustrated again in Figure 44. The maximum impact (probe) force was found to be lower at every location tested for the released ('kiss' bond) panel when compared to the not-released (well bonded) panel. The reduced percussion force for the released panel was observed to vary from 9%-25%. A single factor analysis of variance (ANOVA) was completed for the maximum probe force between data collected for released versus the well bonded specimens. The p value obtained for the probe force data was 6.84×10^{-5} indicating a significant difference between the results for the released and not-released panels. The data shown in Figure 44 will be compared against the results from FEA analysis described in the following sections.
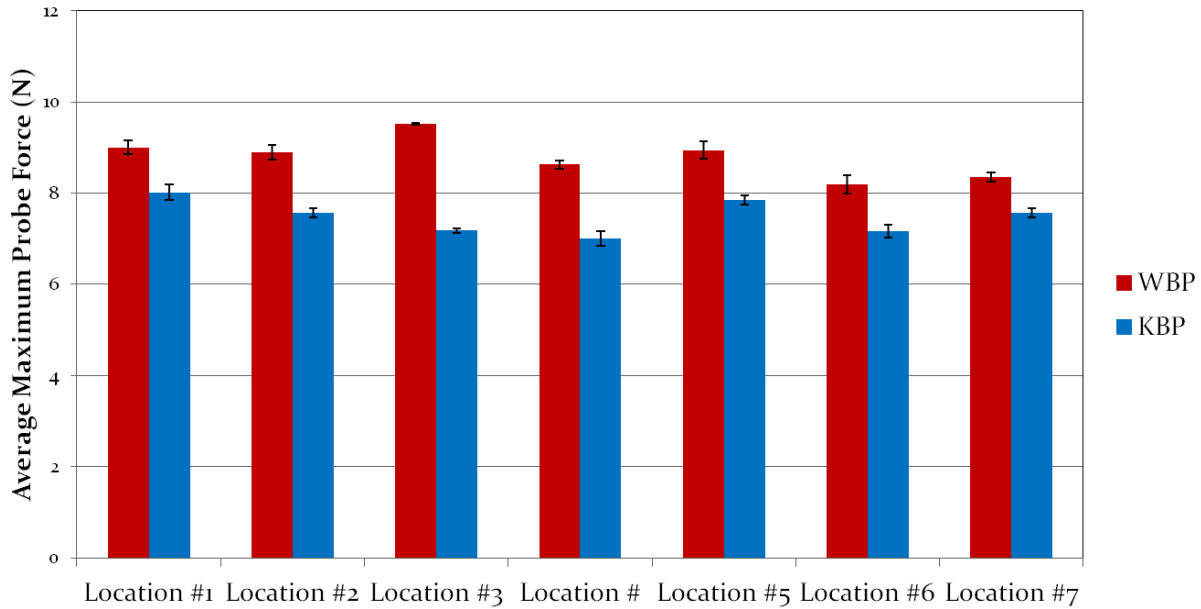
Figure 44 Probe force vs time measured at 7 different locations for the well bonded not-released panel (WBP) and the released 'kiss' bond panel (KBP).

4.5 Finite Element Analysis Results-Stiffness Changes of Bulk Adhesive

An implicit nonlinear analysis was run for seven different conditions using the

percussion rod/composite model described in section 4.2.

- Well Bonded Panel (Adhesive modulus = 2.4 GPa)

- Kiss Bonded Panel 50% (Adhesive modulus = 1.2 GPa)

- Kiss Bonded Panel 30% (Adhesive modulus = 0.72 GPa)

- Kiss Bonded Panel 20% (Adhesive modulus = 0.48 GPa)

- Kiss Bonded Panel 5% (Adhesive modulus = 0.12 GPa)

- Kiss Bonded Panel 1% (Adhesive modulus = 0.024 GPa)

- Kiss Bonded Panel 0.5% (Adhesive modulus = 0.012 GPa)

The von Mises, normal (Z-component) and transverse (Y-component) stresses were

calculated (psi) vs time and plotted as fringe plots over the percussion rod and composite

panel. It was observed that the percussion rod made contact with the composite panel at time 40μs and peak stresses occurred at time 60μs during the impact. Snapshots of all three stress types at 60μs are shown in Figures 45-50.

The von Mises stress for the well bonded panel is well distributed from the front to back laminate indicating good load transfer across the adhesive. However for the kiss bonded panel (1% modulus) the distribution of stress is mostly localized on the front laminate indicating lower load transfer across the adhesive. Also, the maximum stress is similar for the front and back laminates in the well bonded model. This is not the case for the kiss bonded panel where there is a large difference between the stresses measured for the front and back laminate. The normal stress at 60μs for the well bonded panel also showed good stress distribution from the front to back laminate through the adhesive as well as in the Y direction above and below the percussion rod in the front laminate. This was not the case for the kiss bonded panel (1% modulus) as the stresses were mostly observed in the front laminate adjacent to the adhesive. Finally, there is a large difference in stress on the back side of the back laminate when comparing the well bonded panel to the kiss bonded panel for the von Mises and normal stress fringe plots. These results indicate that a measurement of transmitted force through the panel should result in significantly different values for the well bonded and kiss bonded panels.

The change in von Mises and normal stress distribution across the thickness of the composite panel due to the impact event for the kiss bonded model can be attributed to the localized bending stress being applied on the front laminate. This can be observed in the transverse (Y-component) stress fringe plots (see Figures 49 and 50). As the rod makes impact with the kiss bonded panel (Figure 50), compressive stress is applied over the area

of impact on the front side of the front laminate. Tensile stresses (in red) are observed to be in a small local area on the back side of the front laminate across from the probe.   The areas above and below the localized tensile stress region (in the Y-direction) are large enough to support the laminate during the impact event even though the adhesive has very low stiffness. As a result, a localized bending moment is created which causes the change in probe force we see in the sensor and lower load transfer through the adhesive to the back laminate. The transverse (Y-component) stress for the well bonded panel on the front laminate is mostly in compression and is not in bending (Figure 49). A tensile stress is observed in the center on the back side of the back laminate (in red) for the well bonded model. This tensile stress area is much larger than observed for the kiss bonded model and spread across the center of the back laminate in the Y-direction indicating better load transfer through the adhesive.
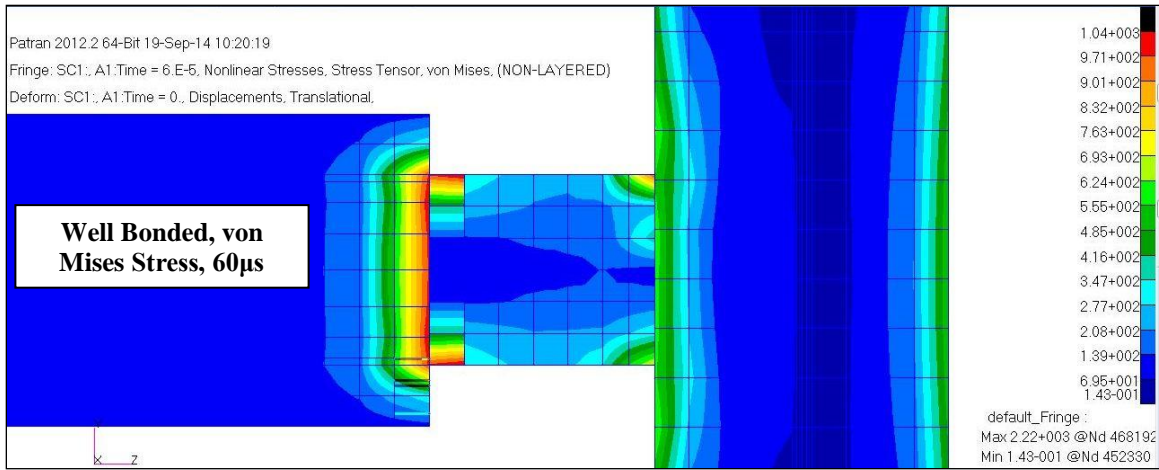
Figure 45 Fringe plot of von Mises Stresses (psi) at 60μs for the Well Bonded Laminate.
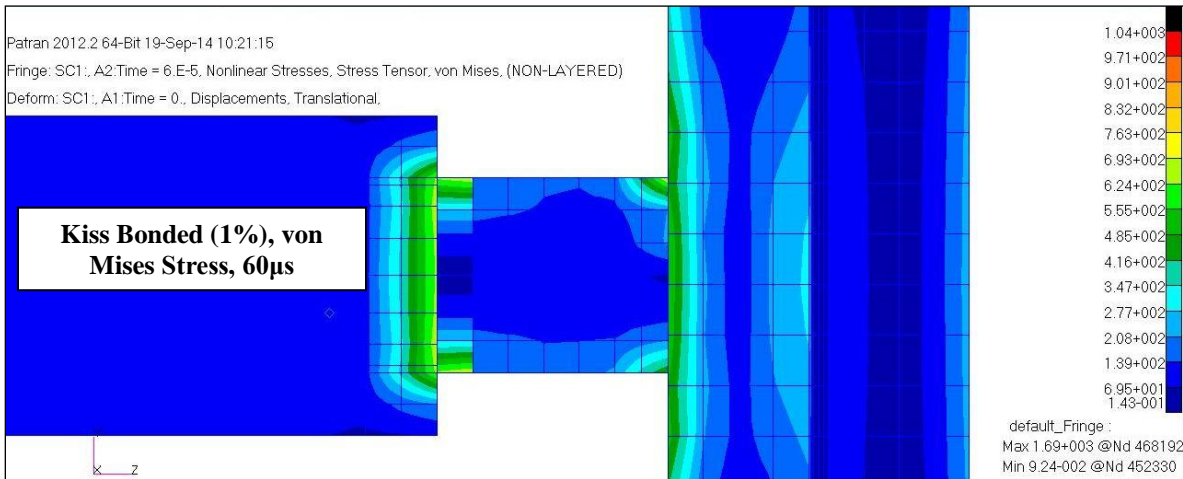
Figure 46 Fringe plot of von Mises Stresses (psi) at 60μs for the Kiss Bonded Laminate (1% modulus).
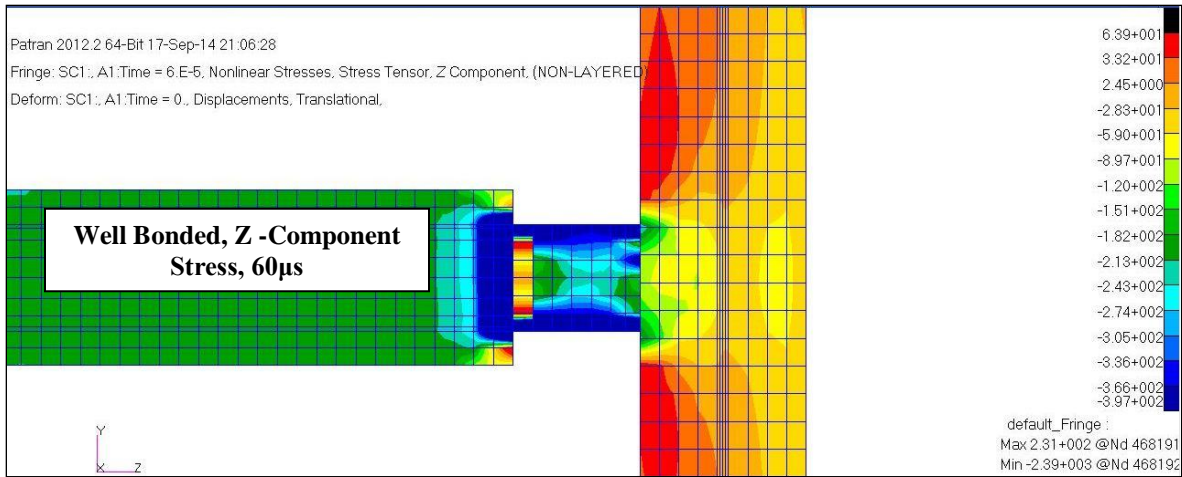
Figure 47 Fringe plot of Normal (Z-Component) Stresses (psi) at 60μs for the Well Bonded Laminate.
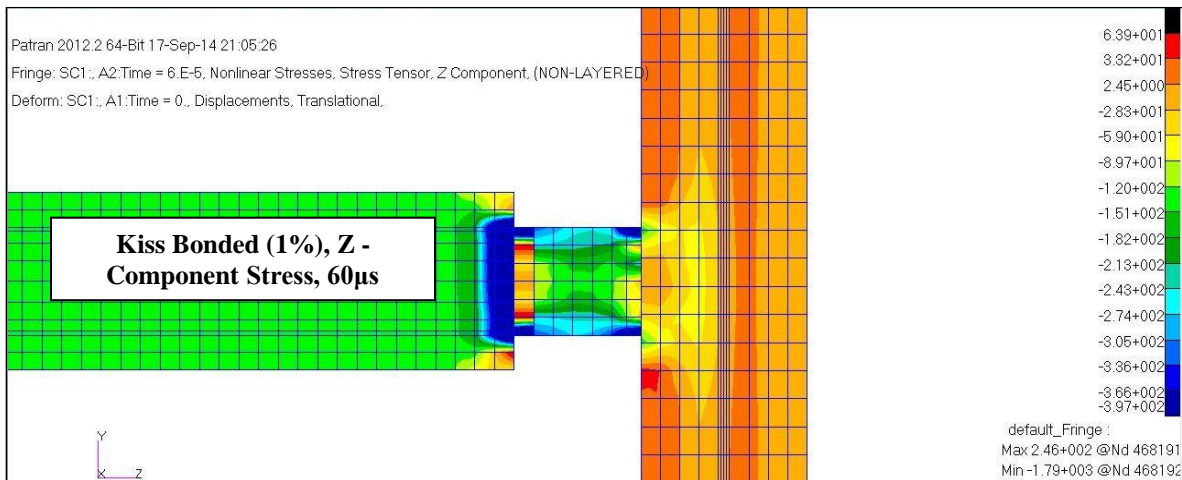
Figure 48 Fringe plot of Normal (Z-Component) Stresses (psi) at 60μs for the Kiss Bonded Laminate (1% modulus).
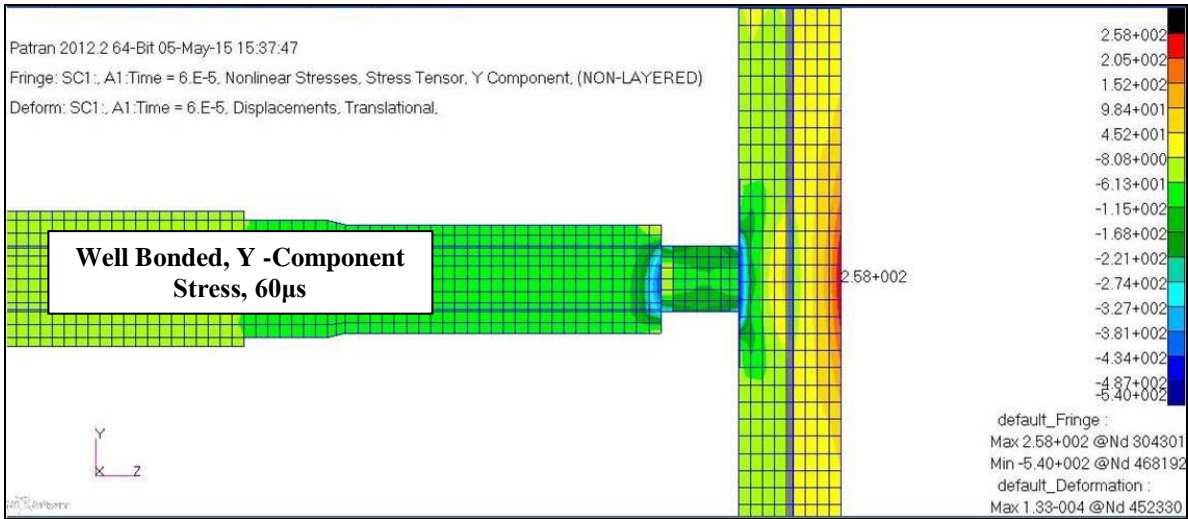
Figure 49 Fringe plot of Y-Component Stresses (psi) at 60μs for the Well Bonded Laminate.
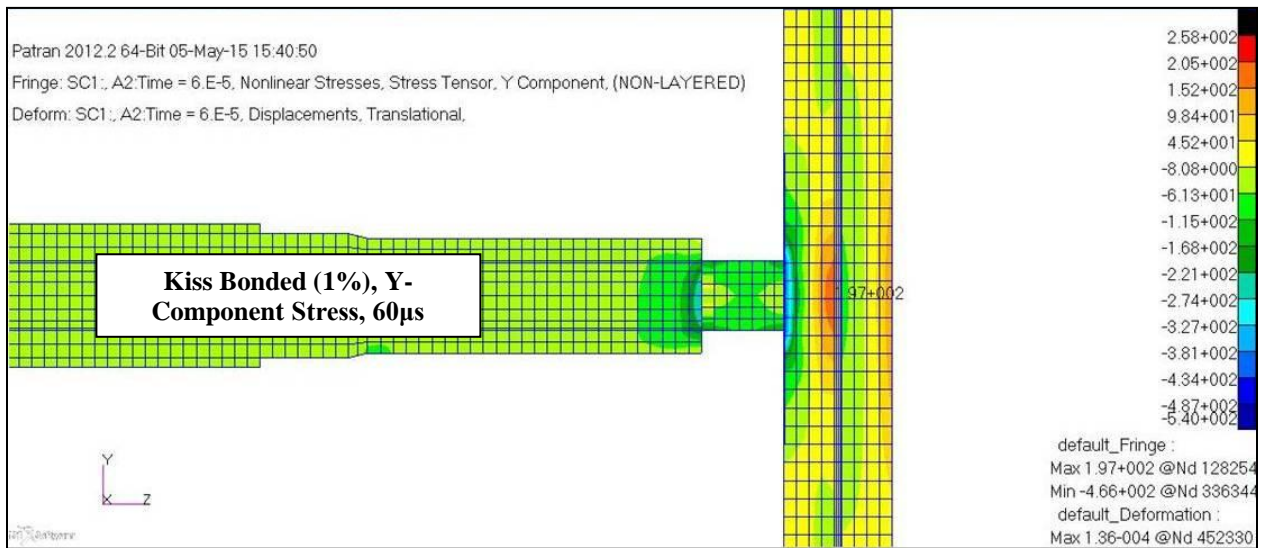
Figure 50 Fringe plot of Y-Component Stresses (psi) at 60μs for the Kiss Bonded Laminate (1% modulus).

The next output analyzed was the force measured at the sensor area in between the percussion rod body and tip. The force at the sensor area was calculated by first measuring the Z-component stress at all 24 nodes representing the piezoelectric sensor as illustrated in Figure 51. The total stress for each time increment was then divided by 24 to get an average stress and then multiplied by the area of the percussion rod tip which is ~2 mm in diameter. The resulting force/time data was then plotted and compared to the experimental data.
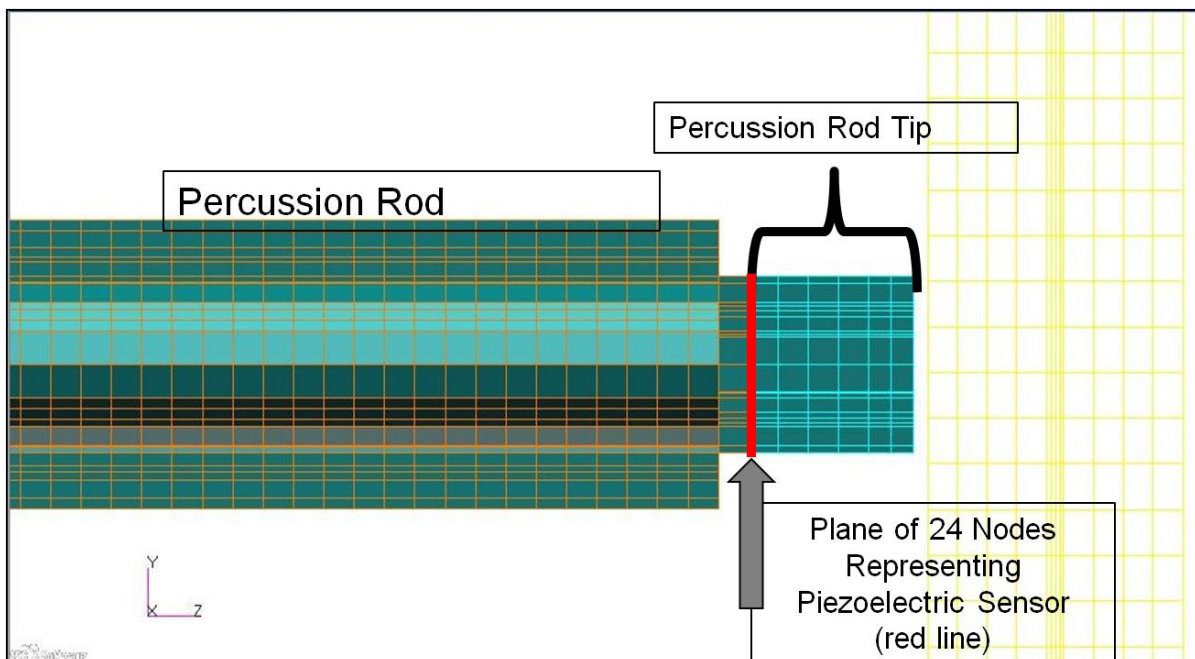
Figure 51 Illustration of percussion rod and piezoelectric sensor used to measure impact force.

The percussion force vs time curves predicted by the FEA models are shown in Figure 52. During the modeled impact event, the percussion rod makes contact with the composite panel at time step #4 (40 μs) and reaches a maximum peak at time step #6 (60 μs). After the peak force is reached, the percussion probe decelerates and the probe force decreases. For the well bonded panel model the probe force decreases to a slightly

negative value at 160 μs which is attributed to the change in momentum of the probe (compression to tension) when it comes off the composite panel. To verify that the probe came off the panel at this time, the displacement in the normal direction (Z-Component) was plotted vs time at a node on the percussion rod tip surface and at a node on the composite panel surface in the impact area. This plot is illustrated in Figure 53.

If the probe is in contact with the composite panel, the displacement values should be very similar. However, once the probe comes off the panel the displacement values should be different from one another. The displacement values begin to separate for the well bonded model at time increment 160 μs which indicates the probe is no longer in contact with the composite panel. Next, both normal displacement values for the rod surface and composite panel surface begin decreasing and returning to zero. However, starting at time increment 310 μs the displacement value for the composite panel surface begins to increase again as the model time ends. This change in displacement is caused by a stress wave from the impact event that has been reflected within the composite panel.

Next, a plot of normal displacement at the rod surface and composite panel surface for the kiss bond 1% model were compared. This plot is illustrated in Figure 54. The normal displacement values are right on top of each for both the rod and composite surface throughout the entire model run time indicating the rod does not come off the panel. This matches with the force vs time curve data for the kiss bond 1% model which shows the force never reaching zero before increasing again into a second smaller peak.
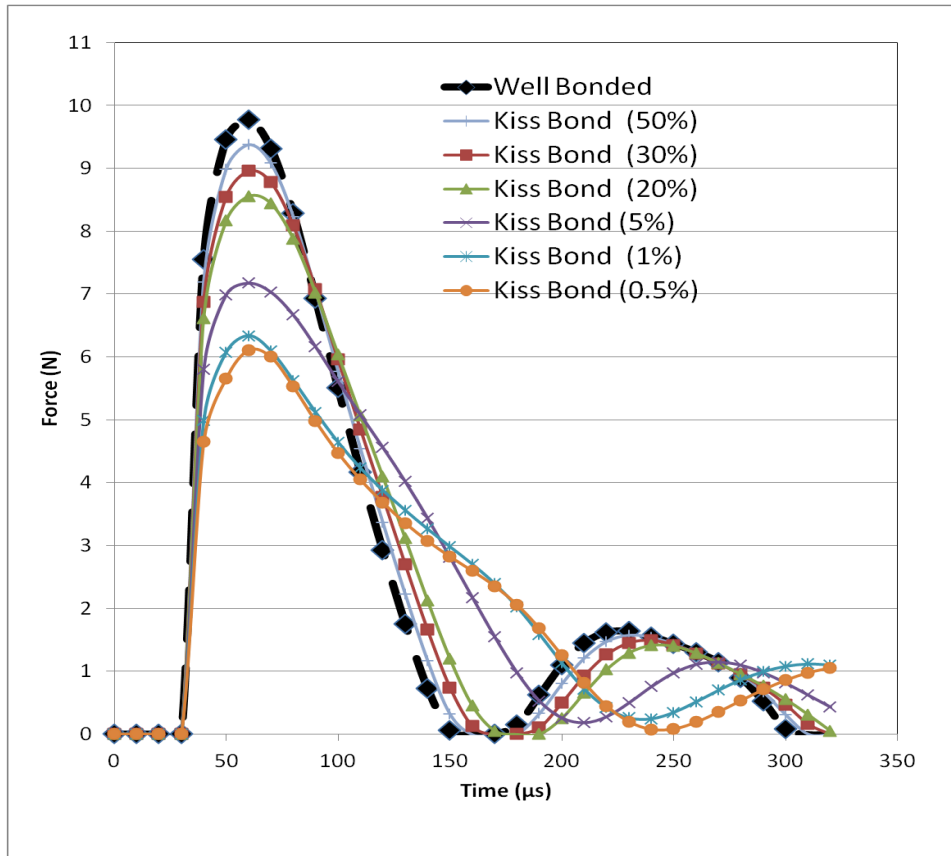
Figure 52 Predicted Force vs Time Curves for Well Bonded and Kiss Bonded Models.
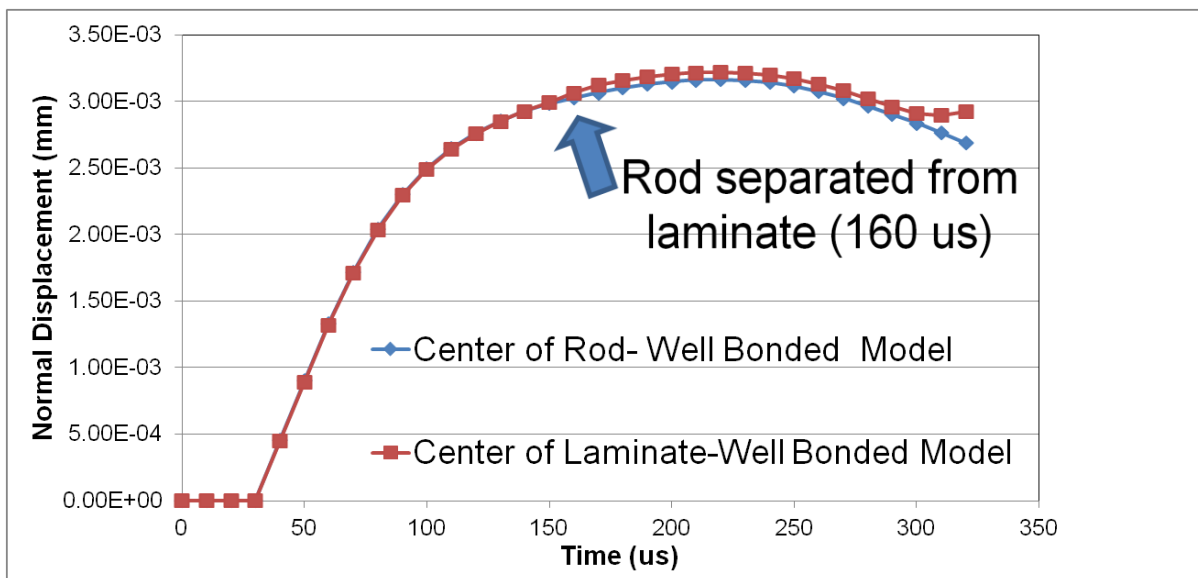
Figure 53 Normal (Z-Component) Displacement vs Time Curves for Well Bonded Model.

82
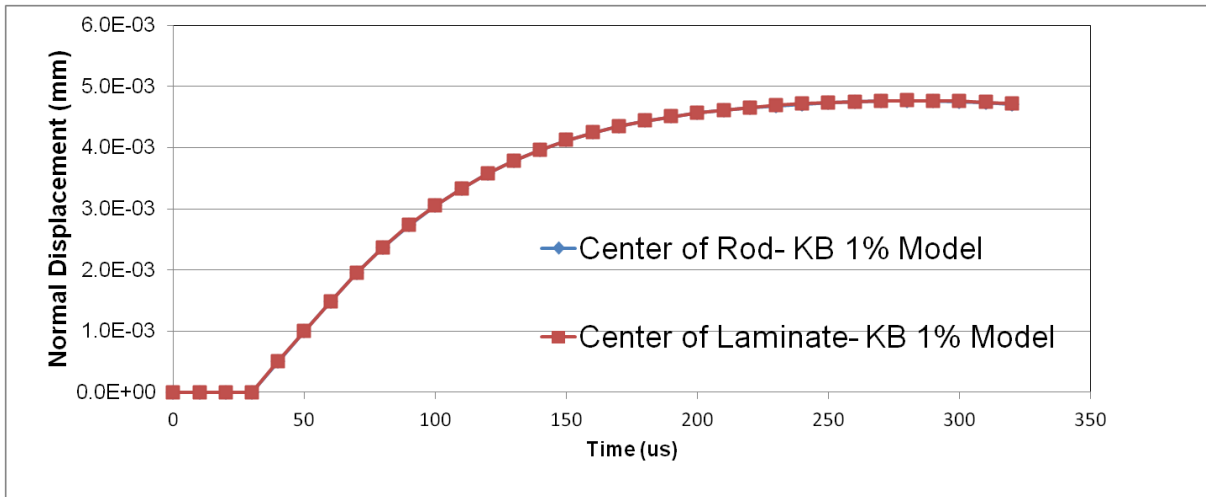
Figure 54 Normal (Z-Component) Displacement vs Time Curves for Kiss Bond (KB) 1% Model.

A comparison of the maximum force values predicted by the different models is summarized in Table 7. The force curve representing the well bonded panel displayed the highest peak percussion force at 9.77 N while the force curves representing the kiss bond models showed lower peak percussion forces. The peak force values for the well bonded model (9.77 N) and the 5% kiss bonded model (7.17 N) match very close to the experimental data. Based on the experimental measurements, a change in percussion force of ~10% should be observed using QPD. This corresponds to the results predicted in the 20% kiss bonded panel model highlighted in Table 7. As a result, QPD should have the resolution to detect adhesive stiffness degradation equal to or greater than ~80% of the well bonded value.

The predicted impact time response for the kiss bond models all are longer in time than the predicted well bonded model although this time increase was very small for the 20% , 30% and 50% kiss bonded models. As the modulus increased for the kiss bond models, the impact time duration decreased. This was not the case in the experimental

data which did not show a significant difference in the shape of the curves (illustrated in Figure 55). Also, the experimental impact time response was around 0.3ms whereas the models predicted time responses ranged from 0.15 ms to 0.25 ms. This discrepancy may be due to the fact that damping was not included in the model material properties. Also, a finer time step in the analysis may be introduced to capture the initial slope of the curve more accurately.

Table 7 Summary of maximum force values predicted by kiss bonded models and compared to well bonded model

Panel Description	Max Force (N) at 60μs	% Change from Well Bonded Panel
Well Bonded Panel	**9.77**	**NA**
Kiss Bond Panel (50%)	9.38	3.99
Kiss Bond Panel (30%)	8.96	8.29
Kiss Bond Panel (20%)	**8.56**	**12.38**
Kiss Bond Panel (5%)	7.17	26.58
Kiss Bond Panel (1%)	6.34	35.15
Kiss Bond Panel (0.1%)	6.11	37.48
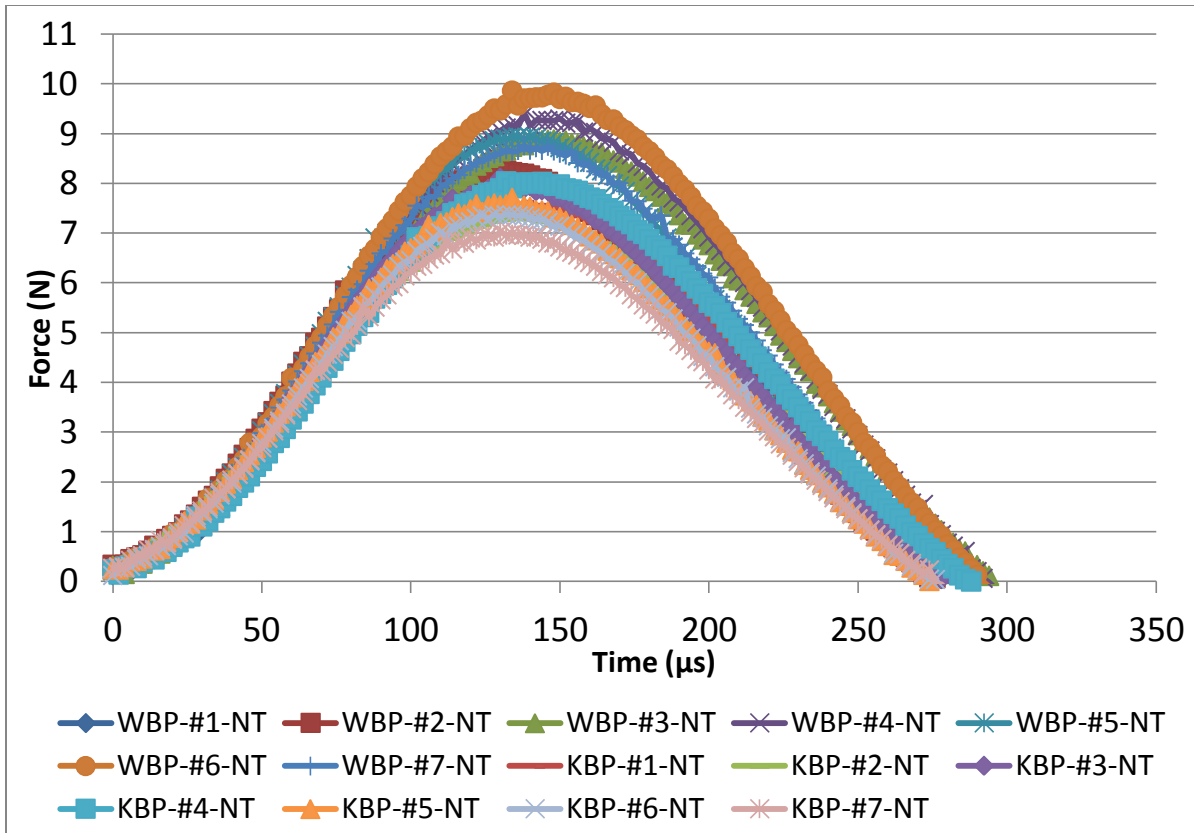
Figure 55 Experimental Force vs Time Curves for Well bonded and Kiss Bonded Panels.

4.6 Finite Element Analysis Results-Modeling Contamination

The previous kiss bond modeling conditions were based on making changes to the stiffness of the entire adhesive bondline thickness. This method represents a kiss bond where the bulk adhesive was cured improperly or was degraded due to an external stimulus. Another type of kiss bond is when contamination on the bonding surfaces causes a decrease in bond integrity. In order to model this type of kiss bond, the stiffness was reduced in only the adhesive elements that are in contact with the composite laminates. The properties of the middle adhesive elements were left unchanged simulating the effect of contamination focused on the interface between the adhesive and laminate. For this

study, an implicit nonlinear analysis was run for the following nine different conditions using the percussion rod/composite model described in section 4.2.

- Front Adhesive Layer 5% (Adhesive modulus = 0.12 GPa)
- Back Adhesive Layer 5% (Adhesive modulus = 0.12 GPa)
- Front/Back Adhesive Layer 5% (Adhesive modulus = 0.12 GPa)
- Front Adhesive Layer 3% (Adhesive modulus = 0.072 GPa)
- Back Adhesive Layer 3% (Adhesive modulus = 0.072 GPa)
- Front/Back Adhesive Layer 3% (Adhesive modulus = 0.072 GPa)
- Front Adhesive Layer 1% (Adhesive modulus = 0.024 GPa)
- Back Adhesive Layer 1% (Adhesive modulus = 0.024 GPa)
- Front/Back Adhesive Layer 1% (Adhesive modulus = 0.024 GPa)

First, the von Mises stresses were calculated (psi) vs time and plotted as fringe plots over the percussion rod and composite panel. It was observed that the percussion rod made contact with the composite panel at time increment 40μs and peak stresses occurred at time increment 60μs during the impact. Snapshots of the von Mises stresses at 60μs for all 9 conditions analyzed are shown in Figures 56-58, 60-62, and 64-66. The well bonded fringe plot is shown on Figure 45 for reference.

As described previously, the von Mises stress for the well bonded panel (Figure 45) is well distributed from the front to back laminate indicating good load transfer across the adhesive. For the contamination runs, the distribution of stress is mostly localized on the front laminate indicating lower load transfer across the adhesive (as illustrated in the kiss bonded panels). The stress distributions for the 1%, 3% and 5% front and back layer models were very similar to one another. It appears changing the stiffness of one layer of

elements within the bondline on either interface will cause the composite panel to respond the same during the percussion event. However, when the stiffness for both the front and back layer elements are decreased the stress along the interface areas between the laminate and film adhesive are usually larger and distributed over a larger area. This larger distribution of stress can be observed on both the front and back interface. Finally, all contamination models indicate that a measurement of transmitted force through the panel should result in significantly different values compared to the well bonded panels.

The percussion force vs time curves predicted by the FEA contamination models are shown in Figures 59, 63, and 67. As expected, the maximum force calculated by the contamination models increased as the stiffness of the elements increased (1%-5%). The shape of the impact time response predicted from the front layer, back layer and front/back layer models was very similar. The main difference between the curves at each stiffness level was the peak force values. The maximum force values for the front layer and back layer models were identical for each of the three contamination models run (1%, 3%, and 5%). However, the front/back contamination models always predicted a lower maximum percussion force, varied from 0.5-0.7 N lower, compared to the front layer and back layer models. When compared to the experimental data, the results from the 1% front layer and 1% back layer models and 3% front/back layer model corresponded well with the kiss bonded panel.
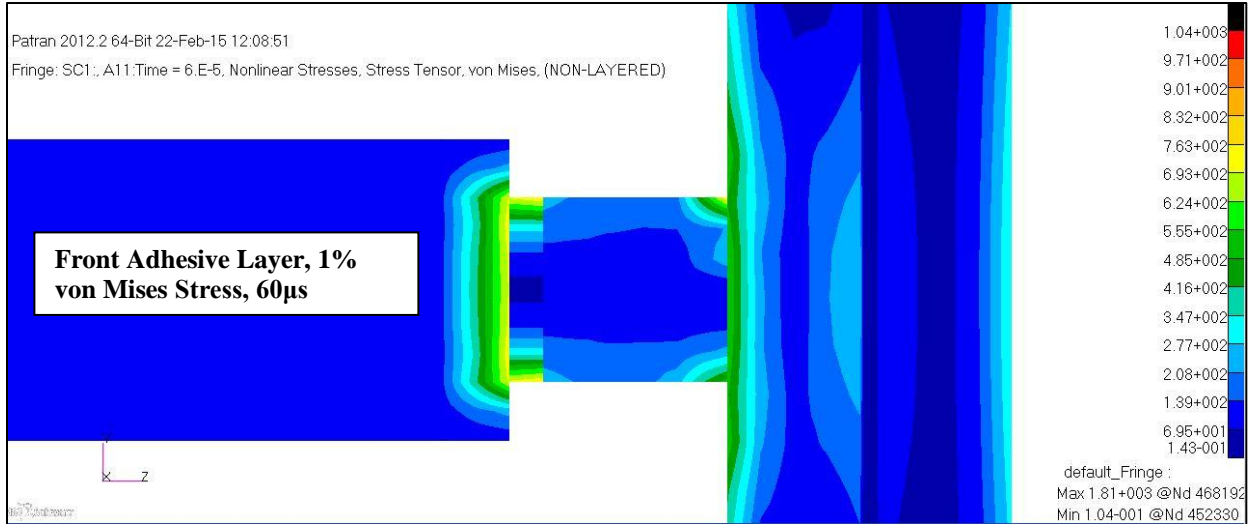
Figure 56 Fringe plot of von Mises Stresses (psi) at 60μs for the Front Adhesive Layer Model (1% modulus).
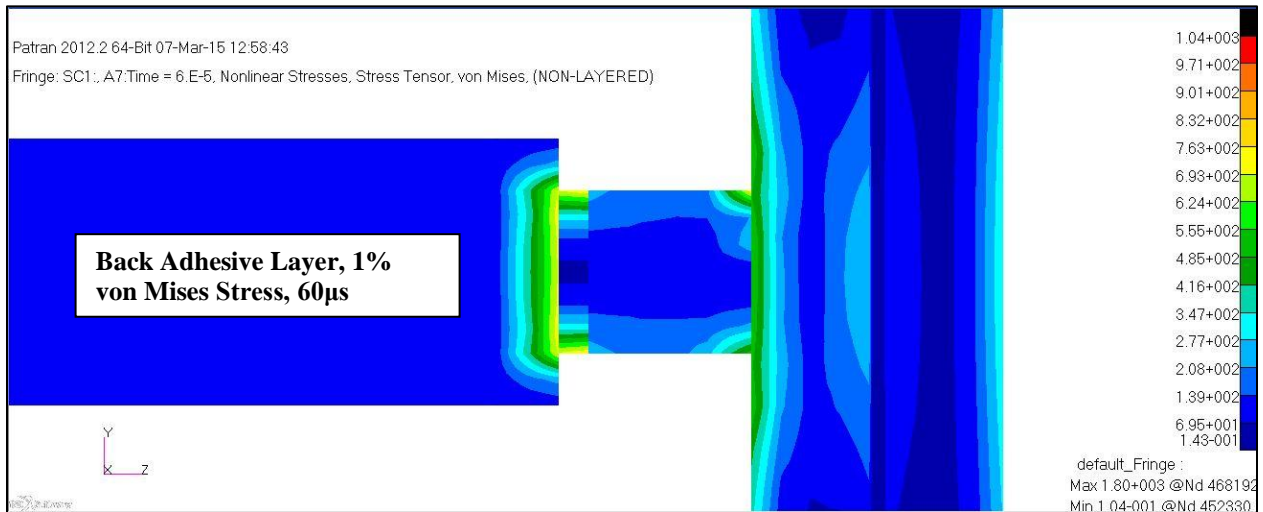
Figure 57 Fringe plot of von Mises Stresses (psi) at 60μs for the Back Adhesive Layer Model (1% modulus).
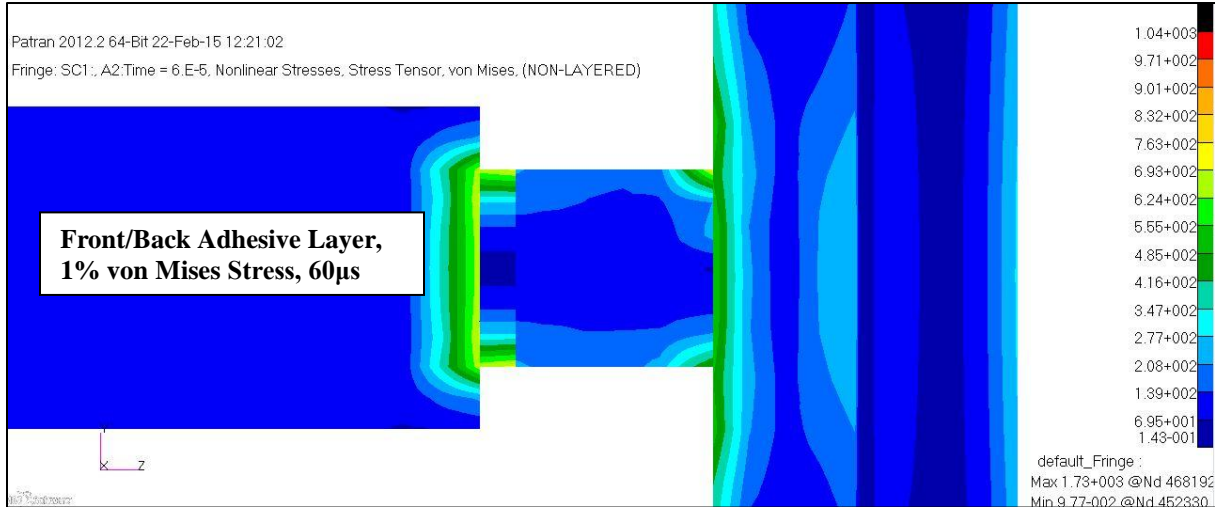
Figure 58 Fringe plot of von Mises Stresses (psi) at 60µs for the Front/Back Adhesive Layer Model (1% modulus).
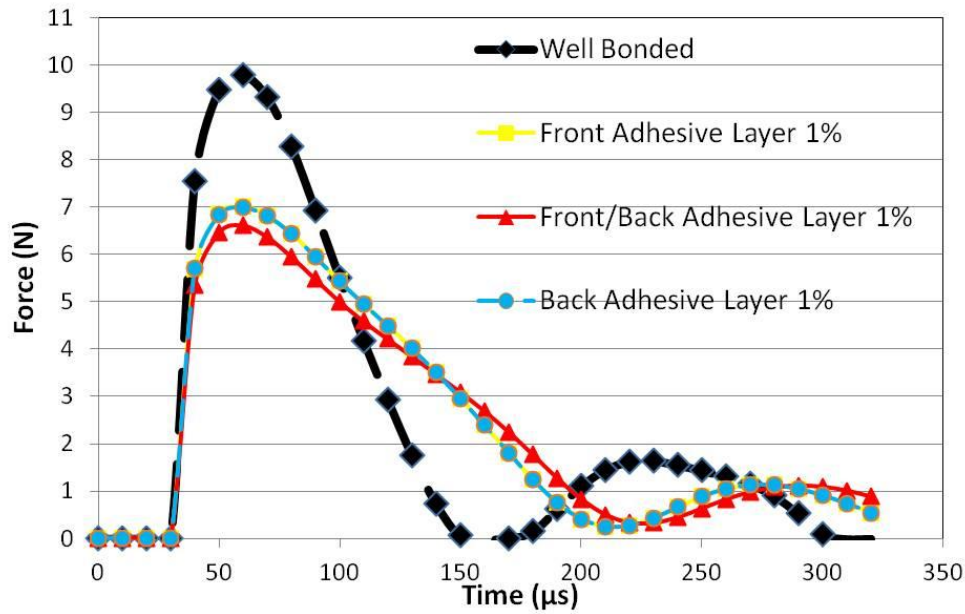
Figure 59 Predicted Force vs Time Curves for Well bonded and 1% Contamination Models.
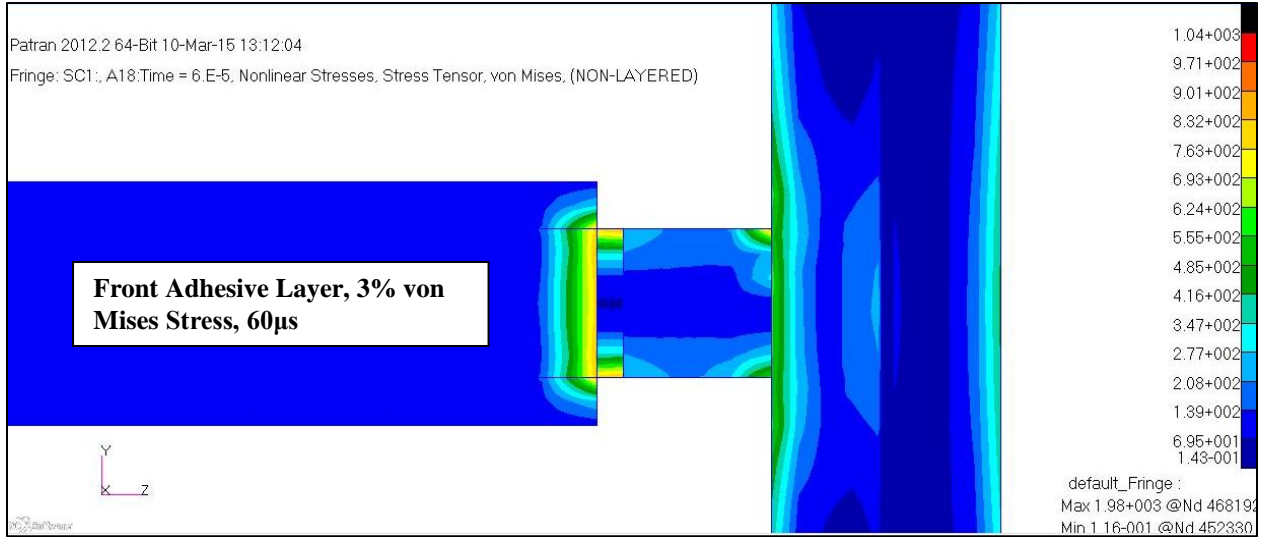
Figure 60 Fringe plot of von Mises Stresses (psi) at 60μs for the Front Adhesive Layer Model (3% modulus).
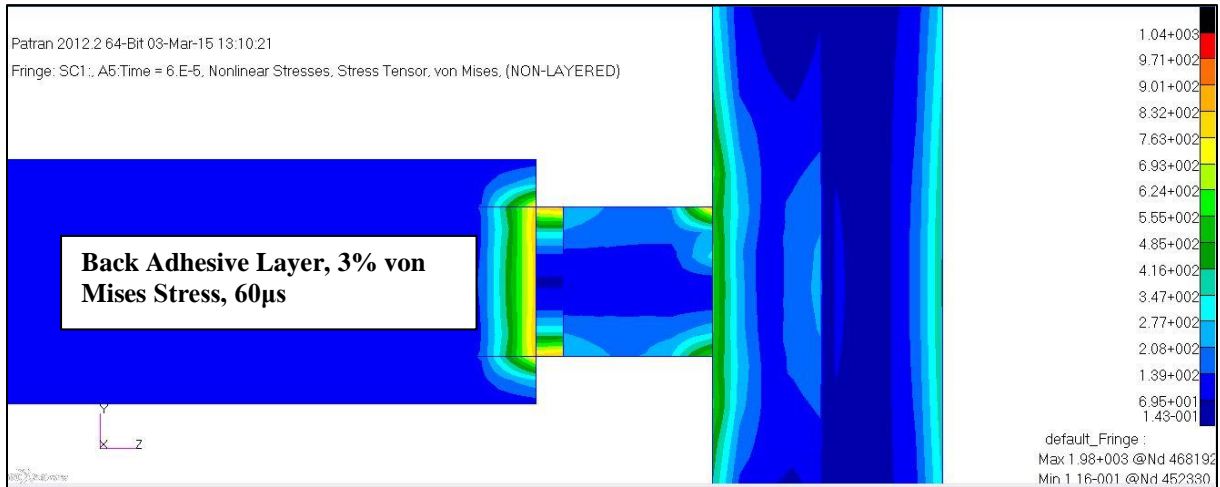
Figure 61 Fringe plot of von Mises Stresses (psi) at 60μs for the Back Adhesive Layer Model (3% modulus).
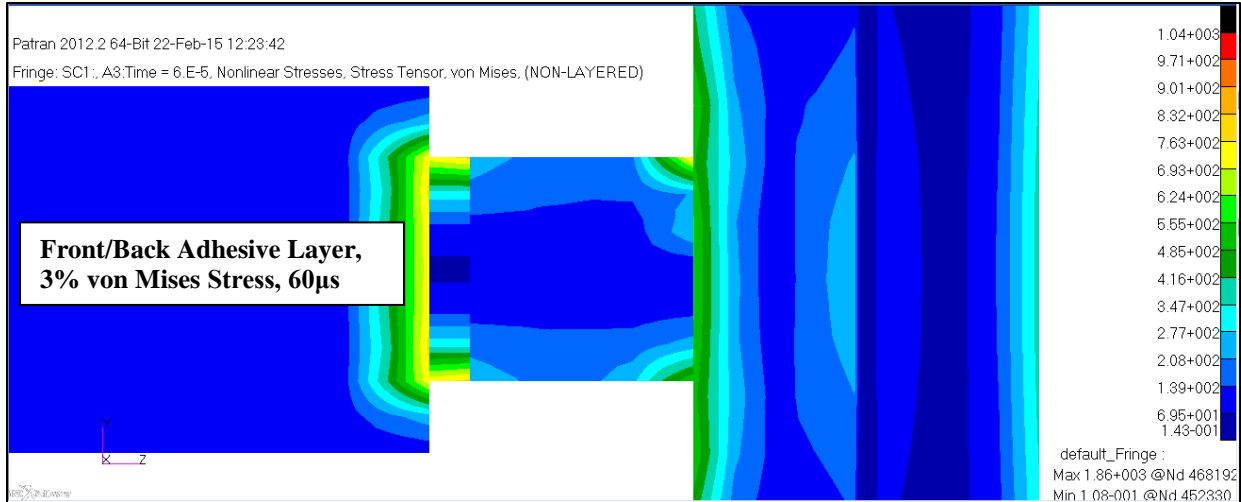
Figure 62 Fringe plot of von Mises Stresses (psi) at 60µs for the Front/Back Adhesive Layer Model (3% modulus).
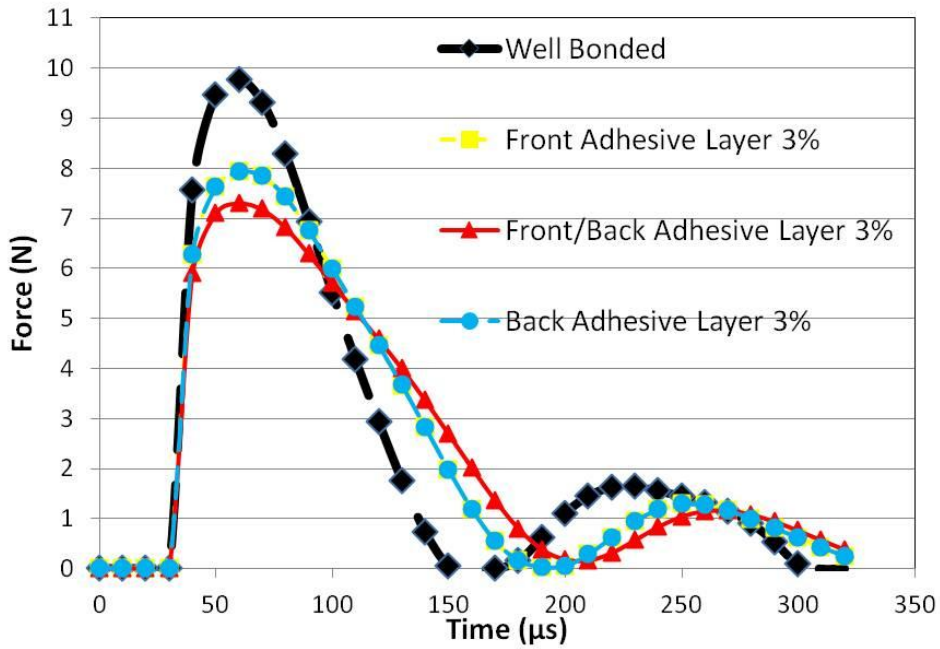
Figure 63 Predicted Force vs Time Curves for Well bonded and 3% Contamination Models.
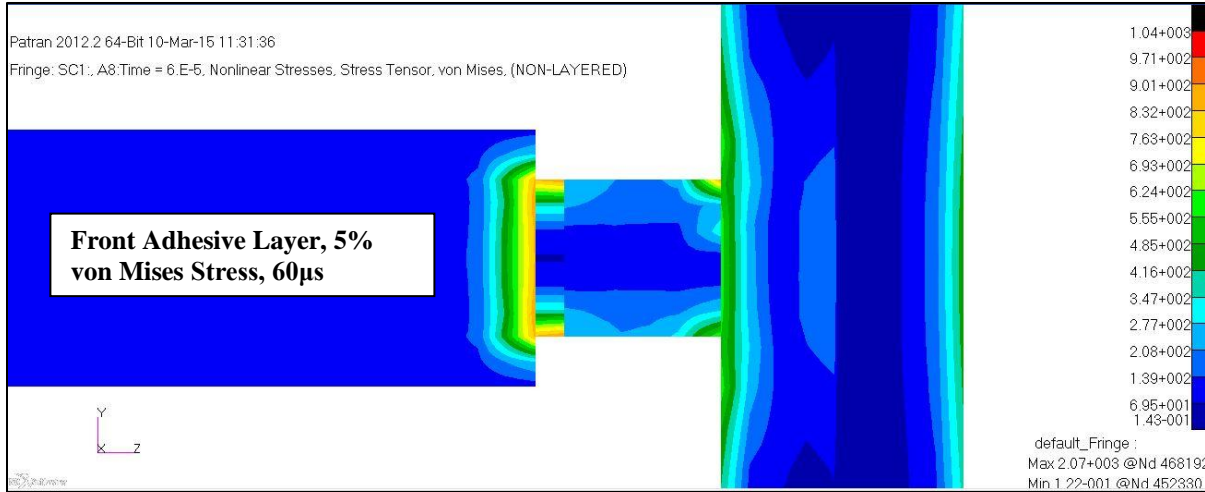
Figure 64 Fringe plot of von Mises Stresses (psi) at 60μs for the Front Adhesive Layer Model (5% modulus).
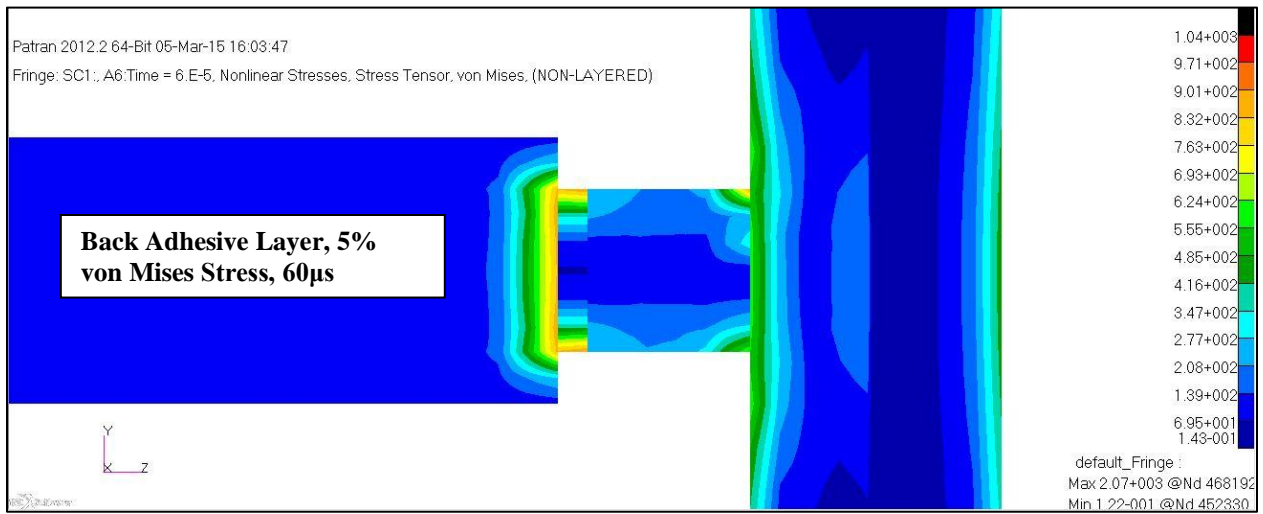
Figure 65 Fringe plot of von Mises Stresses (psi) at 60μs for the Back Adhesive Layer Model (5% modulus).
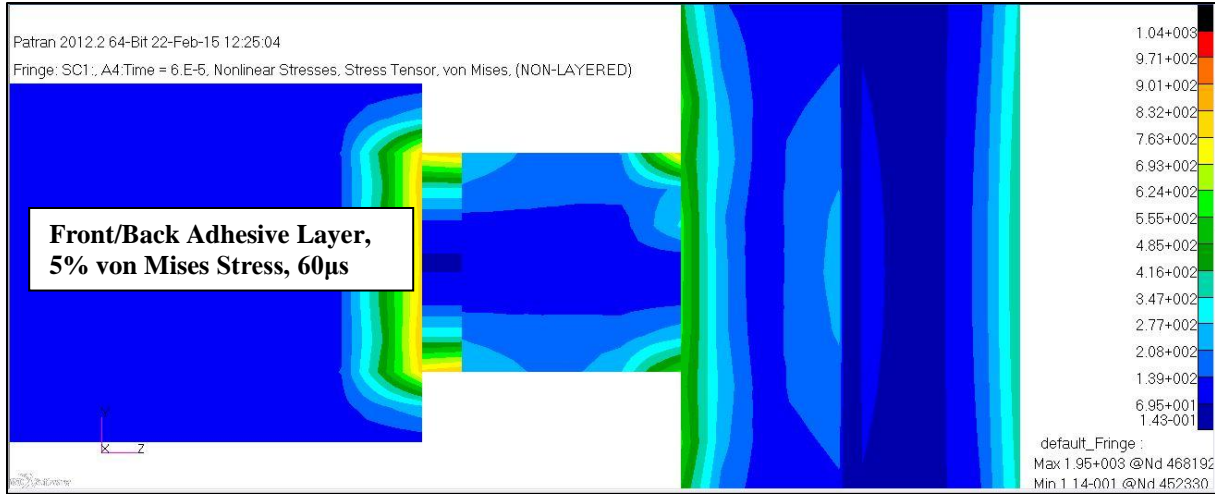
Figure 66 Fringe plot of von Mises Stresses (psi) at 60μs for the Front/Back Adhesive Layer Model (5% modulus).
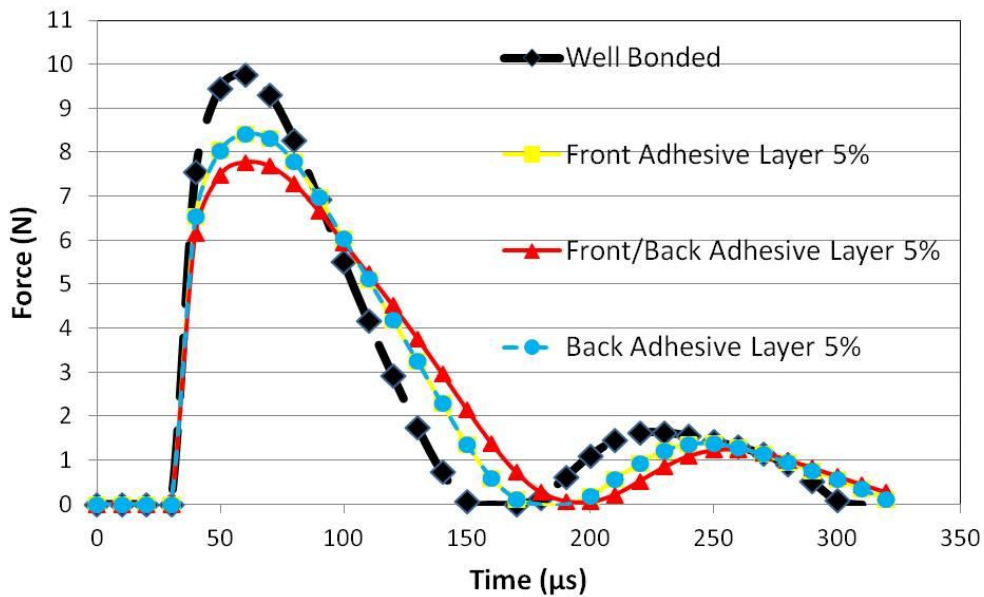
Figure 67 Predicted Force vs Time Curves for Well bonded and 5% Contamination Models.

4.7 Finite Element Analysis Results-Modeling Changes in Kiss Bond Area

In sections 4.5 and 4.6, the kiss bond modeling conditions were based on making changes to the stiffness of the entire 101.6 mm x 101.6 mm (4 in x 4 in) adhesive film surface area. However, the kiss bond area may vary depending on how the kiss bond was created; caused by contamination (local area or entire component affected) or degradation to the bulk adhesive (entire component affected). Also, it is important to understand the resolution of the QPD technique in terms of kiss bond area. To determine this resolution the kiss bond area was decreased from the entire composite panel model all the way down to 2.79 mm x 2.79 mm, which is on the order of the diameter of the percussion rod itself. For this study, an implicit nonlinear analysis was run for the following 5 different conditions using the percussion rod/composite model described in section 4.2.   The stiffness of the adhesive in the kiss bond area was kept constant at 5% of the ultimate value (0.12 GPa). Results will also be compared to the baseline well bonded model illustrated in the previous sections.

- Kiss Bond Area 101.6 mm x 101.6 mm (Entire Panel)

- Kiss Bond Area 76.2 mm x 76.2 mm

- Kiss Bond Area 25.4 mm x 25.4 mm

- Kiss Bond Area 12.7 mm x 12.7 mm

- Kiss Bond Area 2.79 mm x 2.79 mm

    .

The percussion force vs time curves predicted by the FEA kiss bond area models are shown in Figure 68. A summary of the maximum force values predicted for all kiss bond area models compared to the well bonded model are shown Table 8. The maximum force calculated by the kiss bond area models decreased as the area of the kiss bond decreased. As the area decreased from 101.6 mm x 101.6 mm to 76.2 mm x 76.2 mm very little change occurred in the impact time response. A small increase in maximum force (~0.5 N) and a slight shift in the peak of the impact time response occurred when the kiss bond area decreased to 1in. x 1in. However, a 20% difference in peak force values compared to the well bonded model was still observed for the 25.4 mm x 25.4 mm area model. Once the kiss bond area decreased below a 25.4 mm x 25.4 mm area, the maximum force values begin to increase more rapidly. At 12.7 mm x 12.7 mm, the maximum force value predicted was 11% lower than the well bonded panel and is considered to be close to the resolution limit of the QPD technique using the 2 mm diameter size percussion rod. Results for the 2.79 mm x 2.79 mm model show the impact-time response to be similar as the well bonded model and cannot be resolved using the current QPD technique.
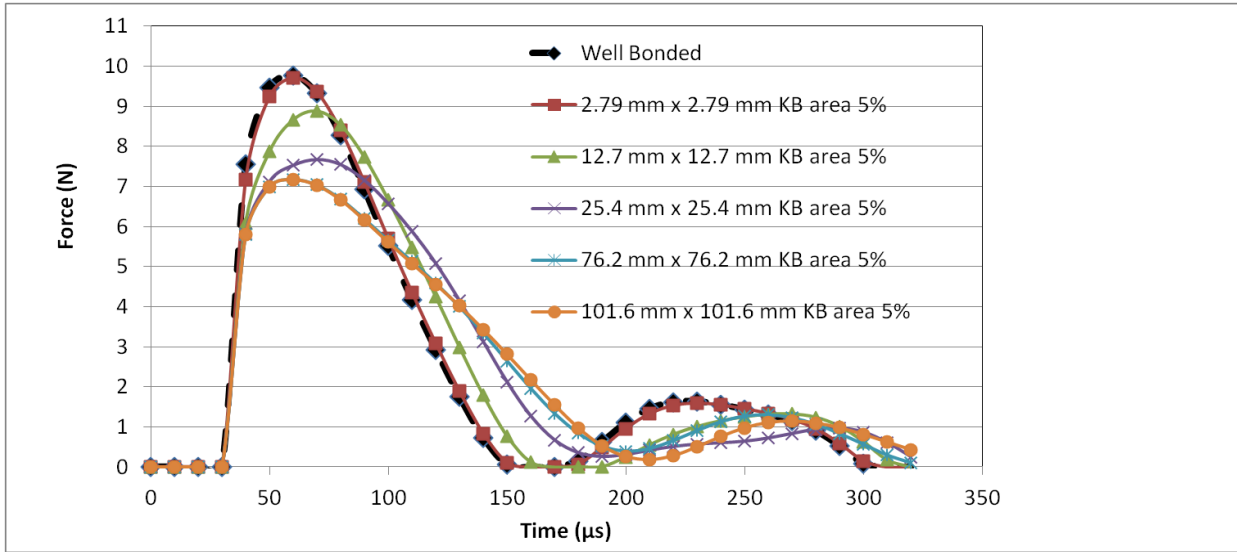
Figure 68 Predicted Force vs Time Curves for well bonded and kiss bond area (KB) models.

Table 8 Summary of maximum force values predicted by kiss bond area models and compared to well bonded model

Panel Description	Max Force (N) at 60μs	% Change from Well Bonded Panel
Kiss Bond Panel 5% modulus (Entire Panel 101.6 mm x 101.6 mm)	7.17	26.58
Kiss Bond Panel (5%) 76.2 mm x 76.2 mm	7.18	26.51
Kiss Bond Panel (5%) 25.4 mm x 25.4 mm	7.67 (Peak at 70μs)	21.49
Kiss Bond Panel (5%) 12.7 mm x 12.7 mm	**8.67 (Peak at 70μs)**	**11.26**
Kiss Bond Panel (5%) 2.79 mm x 2.79 mm	9.71	0.61
Well Bonded Panel	**9.77**	**NA**

4.8 Finite Element Analysis Results-Modeling Changes in Panel Thickness

Another variable that was examined using FEA was the composite panel thickness. It is important to identify a maximum panel thickness above which the QPD technique will not be able to measure significant changes in probe force due to changes in adhesive modulus. To determine the overall thickness limitation, the composite laminate thicknesses were increased from 1.59 mm (0.0625 in.) to 3.18 mm (0.125 in.) while keeping the panel's material properties, and the rods diameter and velocity constant. The total panel thickness in the model was 6.58 mm (0.259 in.). However, to keep the element size more uniform (aspect ratio of 10 to 1 or less) the number of elements created through the thickness of the laminates was changed from 4 to 6 elements making their thickness ~0.51 mm (~0.020 in.). An illustration of a cross section of the thick panel meshed is shown in Figure 69.
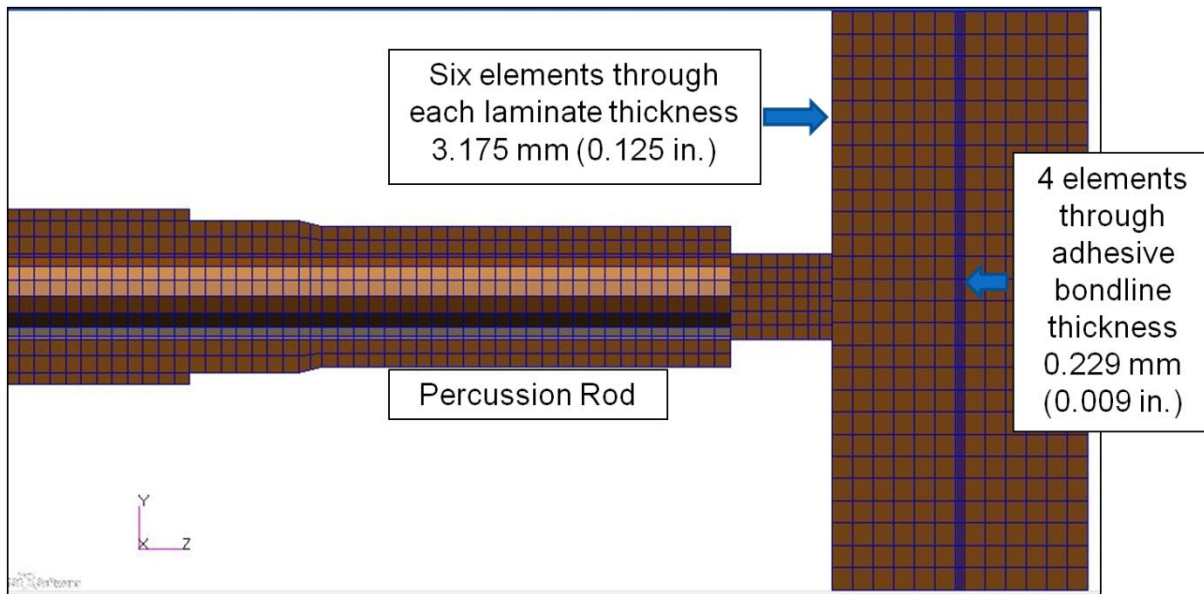
Figure 69 Description of Mesh Details for the Thick Panel Model.

For this study, an implicit nonlinear analysis was run for the well bonded condition and a kiss bonded condition where the stiffness of the adhesive in the kiss bond area was 5% of the ultimate value (0.12 GPa). As a result of the increase in elements through the thickness of the laminates, the total number of elements in the model increased significantly. To reduce the output file to a manageable size, the analysis was run only to 110 μs (instead of 320μs) at the same 10μs time increments performed previously.

First, the von Mises stresses were calculated (psi) vs time and plotted as fringe plots over the percussion rod and composite panel. As previously shown, it was observed that the percussion rod made contact with the composite panel at time increment 40μs and peak stresses occurred at time increment 60μs during the impact. Snapshots of the von Mises stresses at 60μs for the 2 conditions analyzed are shown in Figures 66 and 67. The von Mises fringe plot for the well bonded panel (Figure 70) shows a distribution of stress on the front laminate around the impact area as well as a uniform stress distribution on the back laminate. For the 5% kiss bonded panel (Figure 71), the distribution of stress is also mostly localized on the front laminate near the impact area but there is an increase in stress where the front of the laminate is connected to the bondline indicating lower load transfer across the adhesive. Also, the stresses on the back side of the back laminate are lower for the kiss bonded panel compared to the well bonded panel.
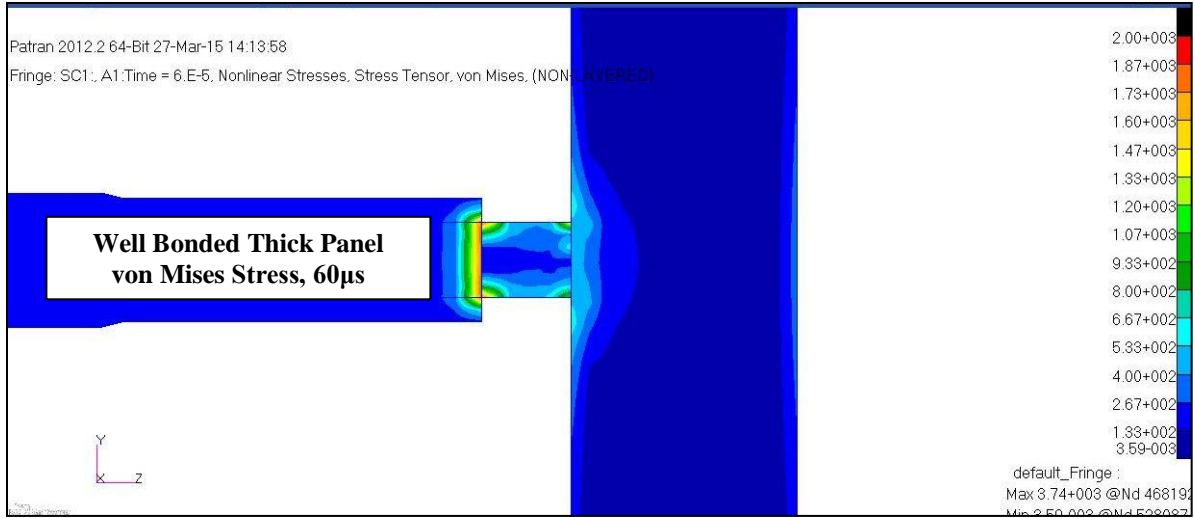
Figure 70 Fringe plot of von Mises Stresses (psi) at 60μs for the Well Bonded Thick Panel Model (6.58 mm thick).
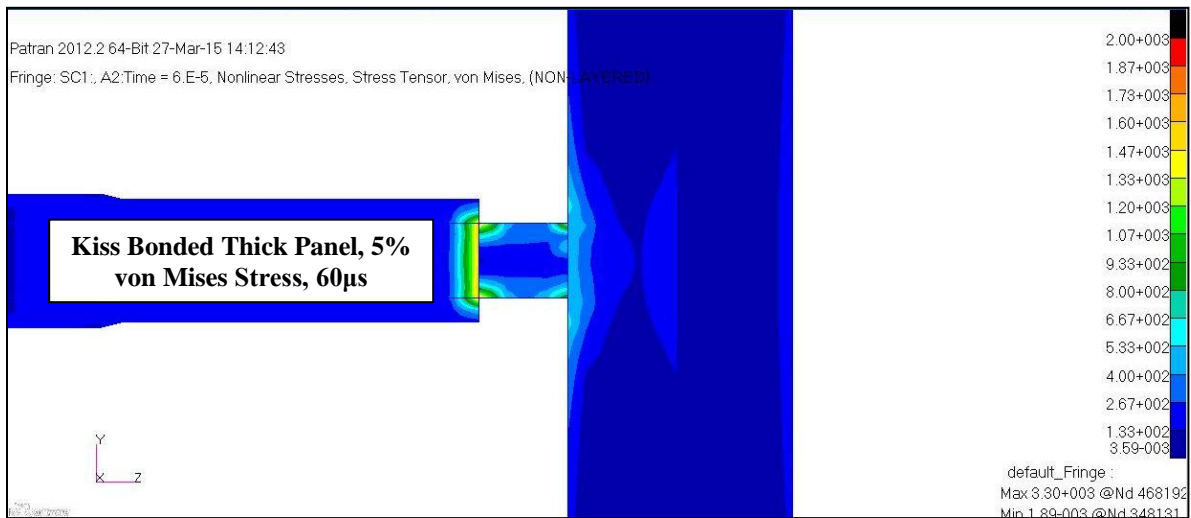
Figure 71 Fringe plot of von Mises Stresses (psi) at 60μs for the Kiss Bonded (5%) Thick Panel Model (6.58 mm thick).

The percussion force vs time curves predicted by the FEA thick panel models are shown in Figure 72. The maximum percussion force for the thick panel models was 20.9 N for the well bonded model and 17.9 N for the 5% kiss bonded model. The difference between the peak force values is 14%. As noted in section 4.5, a change in percussion force of 10% should be observable using QPD.   As a result, the maximum thickness QPD can be used on bonded carbon fiber/epoxy laminates is close to 6.58 mm (0.259 in.) based on a 2 mm diameter rod at 60mm/s velocity. To increase this maximum thickness, a heavier rod or higher velocity would need to be used to increase momentum of the rod.
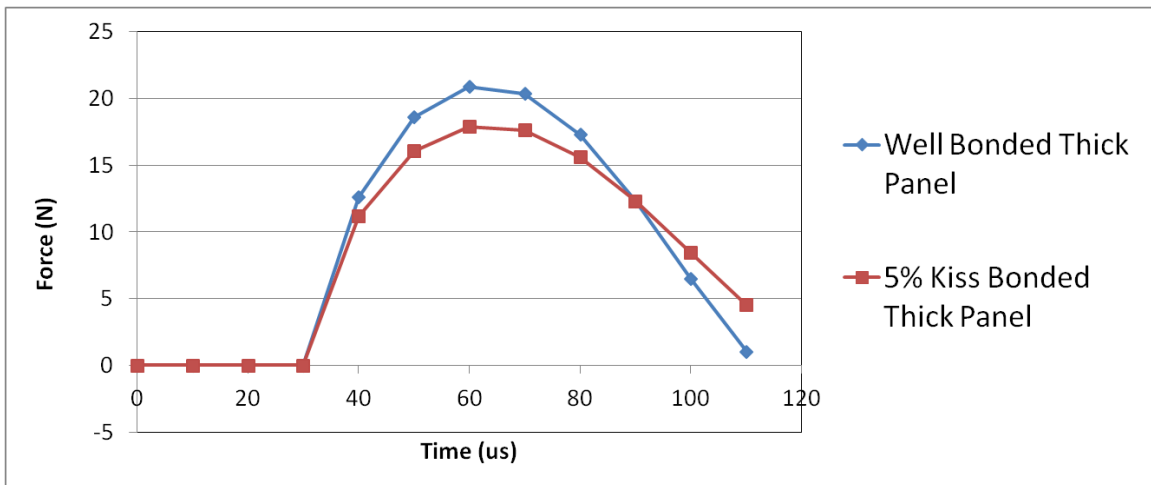
Figure 72 Predicted Force vs Time Curves for Well Bonded and 5% Kiss Bonded Thick Panel Models (6.58 mm thick).

4.9 Finite Element Analysis Results-Concluding Remarks

The following is a summary of the conclusions from the FEA work completed.

• FEA models correctly predict a reduction in measured percussion force (-26.58% to -37.48%) when a kiss bond (5%, 1%, and 0.5%) is introduced. The percussion force decreased as the modulus of the adhesive used to simulate a kiss bond decreased.

• The models indicate that less load transfer into the second panel results in the force reduction predicted and observed experimentally. This is due to a bending moment being applied to the front of the laminate during the impact event for the kiss bonded panel.

• The von Mises, normal, and transverse stresses were significantly higher on the back laminate for the well bonded model when compared to the kiss bonded models. This stress difference may be measured by using a load cell on the back of the panel (transmitted force) during the impact.

• The kiss bond contamination model study illustrated that changing the stiffness of the elements within the adhesive at the laminate/adhesive interface also resulted in significantly lower maximum impact force values. The 1% front layer and back layer models and 3% front/back layer model closely matched experimental data.

• The kiss bond area model of 12.7 mm x 12.7 mm was determined to be the resolution of the QPD technique using a 2mm diameter percussion rod.

• The predicted maximum panel thickness which the current QPD technique can be used to measure changes in adhesive bond integrity is 6.58 mm (0.259 in.). The top and bottom carbon fiber/epoxy laminates are 3.18 mm (0.125 in.) thick and the epoxy film adhesive is 0.229 mm (0.009 in.) thick.

CHAPTER 5: QUANTITATIVE PERCUSSION TESTING OF BOND STRENGTH VARIATION (FILM ADHESIVE ONLY)

5.1 Objectives of Bond Strength Variation Testing

Chapters 2-3 summarized fabrication and experimental QPD work on representative kiss bond panels where release agent was applied to the bonding surfaces. However, low strength bonds can also occur through degradation of properties of the adhesive itself. In this chapter a process to fabricate 'low strength' bonds by varying the cure parameters of FM-300-2K epoxy film adhesive is summarized. Results from QPD measurements of non destructive inspection (NDI) bond strength standards and lap shear strength measurements taken of mechanical test specimens shall then be summarized and discussed.

5.2 Bond Strength NDI Panel Fabrication

Before a NDI technique can be developed to characterize bond integrity, 'low shear strength' bond standards need to be fabricated.   To achieve this objective, processes to fabricate bonded composite panels with known lap shear strength values were developed. The bond strength shall be varied by changing the cure parameters of FM-300-2K epoxy film adhesive. Flat laminates were pre-cured and secondary bonded together using this epoxy film adhesive in an autoclave. Pre-preg material used for this study was IM7 6K PW/8552 graphite/epoxy pre-preg. Each laminate was a 16 ply [0°] lay-up yielding a thickness of 3.18 mm (0.125 in.). The final dimensions of the bonded panels were 254 mm x 254 mm x 6.35 mm (10 in. x 10 in. x 0.25 in.). A 76.2 -101.6 mm (3-4 in.) wide section down the total length of each bonded panel was machined and utilized for lap shear testing.

An illustration of the bonded NDI standard is shown in Figure 73. Notched single lap shear testing was performed per ASTM D 3165 to determine the changes in shear strength for all panels fabricated.

Figure 73. Illustration of a 6.35 mm (0.25 in.) thick secondary bonded composite panel fabricated for bond strength variation study.

5.2.1 Modification of Film Adhesive Cure

By changing the adhesive cure parameters (temperature and time) a correlation between cross link density (extent of cure) of the epoxy film and lap shear strength shall be made. First, a small amount of FM-300-2K adhesive was cured at different time/temperature iterations inside a differential scanning calorimeter (DSC) per ASTM E2160. The samples were then cooled to room temperature and then ramped up to ~204°C (400°F) at 5°C/minute (9°F/minute) and the residual cure heat flow (area underneath the curve) was measured. The samples were then again cooled to room temperature and ramped up to ~204°C (400°F) a third time to ensure that the entire residual cure heat flow was accounted for. All heating and cooling operations were

performed under a nitrogen atmosphere. Based on the percent change in residual cure between specimens, an estimation of the extent of cure was made. Discussions were held with Cytec Industries Inc. (supplier of FM-300-2K) to help guide the DSC analysis in order to successfully reproduce several different shear strength conditions. The cure temperature of 98.9°C (210°F) was chosen and the time was varied from 30 minutes to 240 minutes. The standard cure for FM-300-2K is 121°C (250°F) for 90 minutes.

5.2.2 Fabrication of Film Adhesive Panels

Several FM-300-2K film adhesive samples were cured using a differential scanning calorimeter and the residual cure curve (Heat flow, J/g) was plotted vs temperature. A comparison of the residual cure plots and percent cure data are shown in Figure 74 and Table 9. The standard cure process for the epoxy adhesive, 121°C (250°F) at 90 minutes, displayed a very small residual cure ~ 18 J/g, resulting in a 92% cure, while the 98.9°C (210°F) cure at 30 minutes resulted in the largest residual cure ~ 248 J/g and a 12% cure. A second sample was cured at 98.9°C (210°F) for 30 minutes using a slower ramp rate of 1.7°C/minute (3°F/minute). The resulting residual cure heat flow of ~251 J/g was similar to the original 5°C/minute (9°F/minute) value illustrating that the ramp rate did not have a significant effect on the heat flow data. A good distribution of percent cure values were measured between the different cure times at 98.9°C (210°F) as shown in Table 9 and all temperature/time iterations were used to fabricate 7 bonded NDI panels.
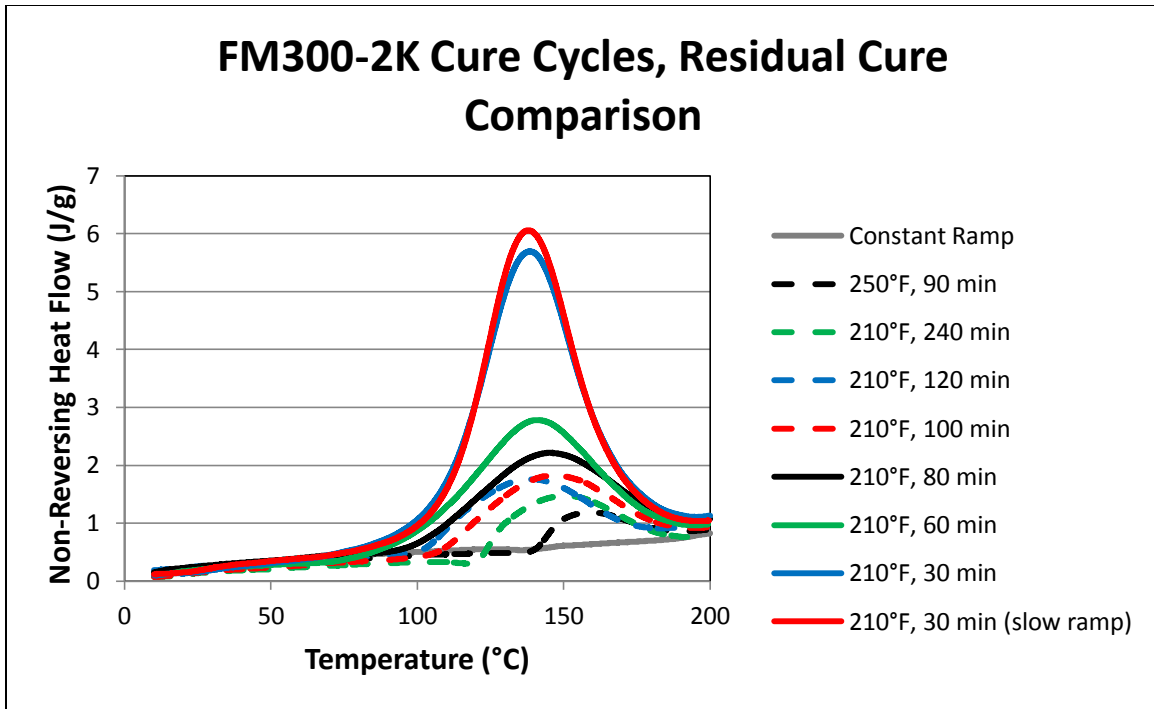
Figure 74. Heat Flow (J/g) vs Temperature (°C) for FM-300-2K cure temperature/time profiles.

Table 9 Summary of Residual Cure and Percent Cure Data Derived from DSC Analysis.

Sample	Temp	Isotherm	Residual Cure (J/g)	% Cure
1	Ramp	-	0	100
2	121°C (250°F)	90 min	18	94
3	98.9°C (210°F)	240 min	49	83
4	98.9°C (210°F)	120 min	60	79
5	98.9°C (210°F)	100 min	70	75
6	98.9°C (210°F)	80 min	94	67
7	98.9°C (210°F)	60 min	136	52
8	98.9°C (210°F) 5°C/minute (9°F/minute)	30 min	248	12
9	98.9°C (210°F) 1.7°C/minute (3°F/minute)	30 min	251	11

5.3 Summary of Lap Shear Results

The lap shear strength was measured for all variable cure NDI standards fabricated per the processes described in the film adhesive panel fabrication section. A summary of the lap shear strength data for the variable cure panels is shown in Table 10. Low lap shear strength was observed for the 30 minute (674 psi) and the 60 minute (1683 psi) cure test specimens. The failure mode for these specimens was also predominantly adhesive. Although the 80 minute to 240 minute cure specimens showed iteratively higher average lap shear strength values, the change in strength was very small from 3646 psi to 4038 psi. These specimens also showed more cohesive/adherend failure modes indicating the performance of the adhesive increased significantly after 60 minutes of cure.

Table 10 Summary of Variable Cure Specimen Lap Shear Strength and Percent Failure Mode

Temp/Time/#	Lap Shear Strength	% Failure Mode		
		Coh	Adh	Adherend
210-30-1	644	20	80	
210-30-2	704	20	80	
AVG	674			
210-60-1	1787	25	75	
210-60-2	1579	25	75	
AVG	1683			
210-80-1	3661	30	70	
210-80-2	3673	30	70	
210-80-3	3603	30	70	
AVG	3646			
210-100-1	4068	35	60	5
210-100-2	3467	40	60	
AVG	3768			
210-120-1	3796	40	60	
210-120-2	3965	35	60	5
210-120-3	3870	40	60	
AVG	3877			
210-240-1	4277	30	40	30
210-240-2	4168	30	50	20
210-240-3	3667	25	50	25
AVG	4038			
250-90-1	4104	30	70	
250-90-2	4614	20	80	
AVG	4359			

5.4 QPD Test Results

Based on the lap shear strength results summarized in the previous section, the focus of the quantitative percussion analysis was on characterizing the 30, 60, and 240 minute NDI panels cured at 98.9°C (210°F) as well as the standard cure (control) NDI panel. The 30 minute and 60 minute cure resulted in low shear strength while the 240 minute and control specimens resulted in high lap shear strength as shown in Table 11.

Table 11 Summary of Lap Shear Strength Data for NDI Panels Characterized using QPD

Specimen Description	% Cure (DSC)	AVG Lap shear Strength (psi)	% Strength
250°F, 90 minutes (Control)	94	4359	100
210°F, 30 minutes	12	674	15.5
210°F, 60 minutes	52	1683	38.6
210°F, 240 minutes	83	4038	92.6

Each panel was placed in a leveled aluminum test fixture as described in Chapter 3. The specimens were again aligned and held in place by rubber hemispherical pads (not in contact with the aluminum) in a 3 point configuration. Images of one of the bonded panels secured in the test fixture are shown in Figures 75 and 76. The distance between the outer and inner aluminum bars on the top and bottom of the fixture were held constant at 21.8 mm (0.860 inches) for each NDI panel tested. This allowed control of the amount of torque applied to each specimen tested. A fine threaded bolt allowed the ability to make fine adjustments to the outer aluminum bars in order to keep the distance between the bars consistent on each side of the fixture.

Figure 75 Control NDI panel attached to the aluminum test fixture.
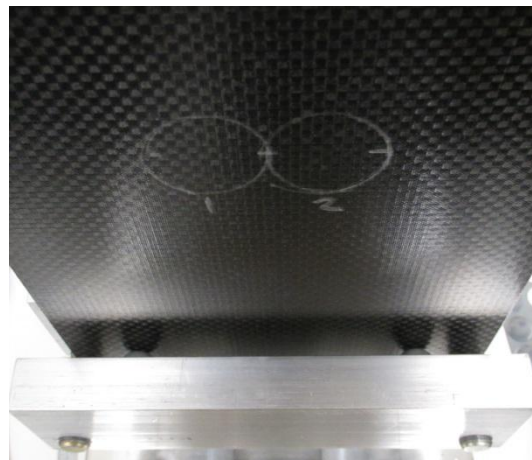
Figure 76 Illustration of bottom hemispherical rubber pads on the bottom outer aluminum block.

Quantitative percussion diagnostics was performed on one center location (location #1) on the panel. First, the loss coefficient (damping capacity) was measured for each specimen. Five percussion measurements were taken at this location six times to gather 300 data points for each panel tested (each of the five measurements gathers 10 data points each).   An average and standard deviation of the loss coefficient taken for each panel is shown in Figure 77. Next, the probe force (force returned to the probe after impact) data was gathered based on the percussion testing performed. A summary of the data can be observed in Figure 78.

The average loss coefficient for the 30 minute and 60 minute specimens were lower than the average loss coefficients for the 240 minute and control specimens. Also, the average maximum probe force for the 30 minute and 60 minute specimens were higher than the average maximum probe force for the 240 minute and control specimens. A single factor analysis of variance (ANOVA) was completed comparing the 30 minute and control data sets and 60 minute and 240 minute data sets. The p values obtained for the loss coefficient and probe force data were less than 0.001 (< 2%) indicating a significant difference between the data sets compared.

The lower damping capacity (higher probe force) for the 30 minute and 60 minute specimens compared to the 240 minute and control specimens was the opposite of what was expected.   As the damping capacity increases there is more energy dissipated from the panel being inspected and this has been related to bond strength degradation. However, parts examined in the past that have had a low bond strength and subsequently higher damping capacity had a release coating layer on the bonding surface which is believed to have caused an increase in energy dissipation. Changing the cure parameters of the

adhesive will result in a different mechanism that is being measured by percussion diagnostics. One potential reason for this trend is that the film adhesive is more brittle at the low temp/time conditions. The reason for the brittle behavior could be that the solvent in the film has evaporated off after the low temp/time conditions but the cure mechanism has not advanced. Another potential reason for the trend is that the adhesive does not wet out the composite laminate bonding surface well at the low temp/time conditions causing the adhesive to not transmit load across the bond joint. If percussion is performed on a well bonded panel, the impact load is transmitted in the longitudinal direction (compressive) and transverse direction (shear) across the bond joint. However, if the adhesive does not carry load (as experienced from the low temp/time conditions) the impact load will only transmit in the longitudinal direction which will significantly decrease the panels damping capacity.
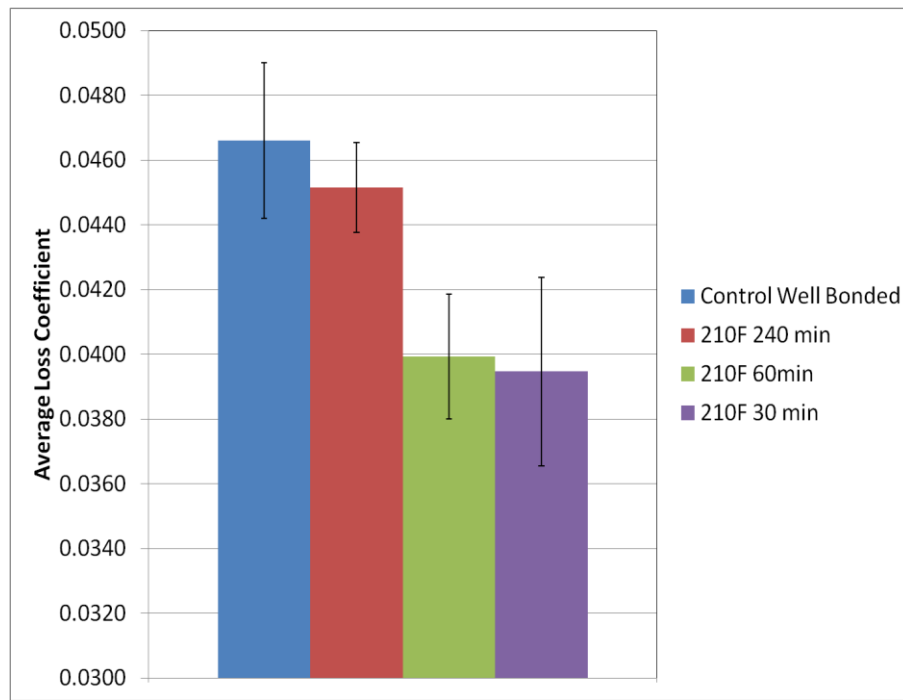
Figure 77 Average Loss Coefficient vs Four Variable Cure NDI Panels.
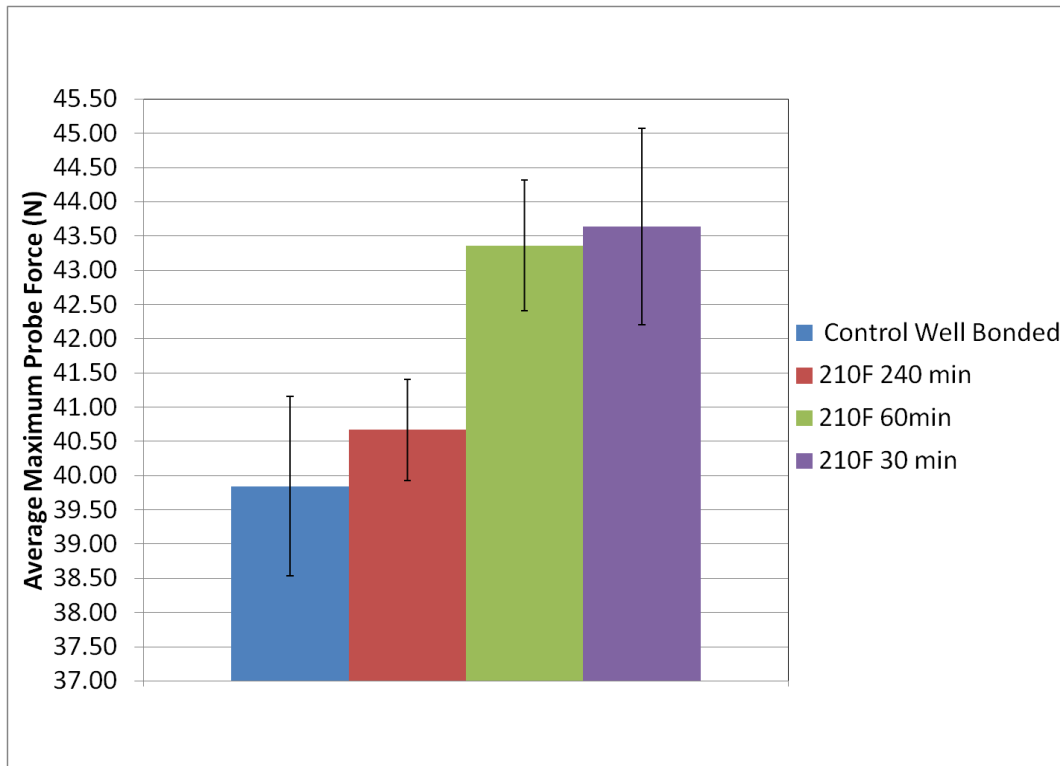
Figure 78 Average Maximum Probe Force vs Four Variable Cure NDI Panels.

5.5 Bond Strength Characterization Conclusions

The following is a summary of the conclusions from the bond strength characterization work completed.

- DSC was successfully used as a tool to create low strength NDI bond standards.

- The average loss coefficient was found to be significantly higher for the standard cure (control) and 240 minute cure film adhesive panels when compared to the 30 minute and 60 minute cure film adhesive panels.

- The average maximum probe force was found to be significantly lower for the standard cure (control) and 240 minute cure film adhesive panels when compared to the 30 minute and 60 minute cure film adhesive panels.

CHAPTER 6: SUMMARY AND FUTURE WORK

6.1 Summary of QPD Project

The feasibility of using quantitative percussion diagnostics to detect 'kiss' bonds and low shear strength adhesive bonds in composite structures was demonstrated for the first time. Processes were developed to fabricate 'kiss' bonds and low shear strength adhesive bond standards using both epoxy film and paste adhesives. Significant differences in loss coefficient and probe force were observed between panels (a) with and without release agent applied to the bonding surface and (b) changes in adhesive cure time/temperature parameters.

6.2 Path Forward for the QPD Project

The following is a list of items that are recommended as a path forward.

- Increase the diameter of the percussion rod to improve measurement sensitivity as well as minimize standard deviation of measurements on rough composite surfaces.

- Structural damping coefficient values will be added into the model to better predict the overall response of the bonded composite panel.

- An explicit non-linear solution (NASTRAN SOL 700) will be used to model the percussion event and compared to the current implicit (NASTRAN SOL 400) solution.

- Develop hybrid approach by working with Advanced Systems and Technologies (AS&T are Phase II NASA NDI winners) and use laser vibrometry to measure small displacement/velocity changes from NDI bond strength panels during percussion measurements.

REFERENCES

1. Barnes, T. a. & Pashby, I. R. Joining techniques for aluminum spaceframes used in automobiles. Part II - adhesive bonding and mechanical fasteners. *J. Mater. Process. Technol.* **99,** 72–79 (2000).
2. Yang, S., Gu, L. & Gibson, R. Nondestructive detection of weak joints in adhesively bonded composite structures. *Compos. Struct.* **51,** 63–71 (2001).
3. Wingfield J.R.J. Treatment of composite surfaces for adhesive bonding. *INT.J.ADHESION Adhes.* **13,** 151–156 (1993).
4. Nagy, P. B. Ultrasonic Detection of Kissing Bonds at Adhesive Interfaces. *J. Adhes. Sci. Technol.* (1991).
5. Cawley, P. & Adams, R. D. Defect types and non-destructive testing techniques for composites and bonded joints. *Mater. Sci. Technol.* **5,** 413–425 (1989).
6. Cawley, P. & Adams, R. D. A review of defect types and non-destructive testing techniques for composites and bonded joints. *NDT Int.* **21,** 208–222 (1988).
7. E. Gros, X. Current and future trends in non-destructive testing of composite materials. *Ann. Chim. Sci. des Matériaux* **25,** 539–544 (2000).
8. Dragan, K. & Swiderski, W. Studying efficiency of NDE techniques applied to composite materials in aerospace applications. *Acta Phys. Pol. A* **117,** 878–883 (2010).
9. Scott, I. G. & Scala, C. M. A review of non-destructive testing of composite materials. *NDT Int.* **15,** 75–86 (1982).
10. Hsu, D. K. Nondestructive inspection of composite structures: methods and practice. in *17th World Conference on Nondestructive Testing* 25–28 (2008).
11. Georgeson, G. Recent Advances in Aerospace Composite NDE. in *NDE and Health Monitoring of Aerospace Materials and Civil Infrastructures* **4704,** 104–115 (2002).
12. Smith, R. Composite Defects and Their Detection. *Mater. Sci. Eng.* **III,** (1997).
13. Roach, D. P. & Scala, C. M. in *Advances in the Bonded Composite Repair of Metallic Aircraft Structure* 659–726 (2002). at <http://www.sciencedirect.com/science/article/pii/B9780080426990500255>
14. Kaczmarek, H. Ultrasonic Detection of Damage in CFRPS. *J. Compos. Mater.* **29,** 59–95 (1995).
15. Fundamentals of Ultrasonic Imaging and Flaw Detection. *National Instruments whitepaper* 1–5 (2010). at <http://www.ni.com/white-paper/3368/en/>
16. Roach, D., Rackow, K., Nelson, C. L., Duvall, R. & Moore, D. *Nondestructive Inspection of Adhesive Metal / Metal Bonds FY 2009 Accomplishments*. *U.S. Automotive Materials Partnership* 1–53 (2009).
17. Vijaya Kumar, R. L., Bhat, M. R. & Murthy, C. R. L. Some studies on evaluation of degradation in composite adhesive joints using ultrasonic techniques. *Ultrasonics* **53,** 1150–1162 (2013).
18. Mayr, G., Plank, B., Sekelja, J. & Hendorfer, G. Active thermography as a quantitative method for non-destructive evaluation of porous carbon fiber reinforced polymers. *NDT E Int.* **44,** 537–543 (2011).
19. Back to Basics:Thermography 101. *MoviTHERM Advanced Thermography Systems* 1–2 (2010). at <http://www.movitherm.com/news/19-lock-in-thermography-for-nondestructive-inspection-of-composite-materials.html>

20. Avdelidis, N. P., Gan, T.-H., Ibarra-Castanedo, C. & Maldague, X. P. V. Infrared lock-in thermography for surface defect imaging in metals for industrial diagnosis. in *Thermosense: Thermal Infrared Applications XXX111* **8013,** 801313–801313–7 (2011).

21. Schroeder, J. a., Ahmed, T., Chaudhry, B. & Shepard, S. Non-destructive testing of structural composites and adhesively bonded composite joints: pulsed thermography. *Compos. Part A Appl. Sci. Manuf.* **33,** 1511–1517 (2002).

22. Vavilov, V. P. Modeling and characterizing impact damage in carbon fiber composites by thermal/infrared non-destructive testing. *Compos. Part B Eng.* **61,** 1–10 (2014).

23. Favro, L. D. *et al.* Infrared imaging of defects heated by a sonic pulse. *Rev. Sci. Instrum.* **71,** 2418–2421 (2000).

24. Tsoi, K. a. & Rajic, N. Non-destructive Evaluation of Aircraft Structural Components and Composite Materials at DSTO Using Sonic Thermography. *DSTO Def. Sci. Technol. Organ.* **0986,** 1–53 (2011).

25. Rantala, J., Wu, D. & Busse, G. Amplitude-Modulated Lock-In Vibrothermography for NDE of Polymers and Composites. *Res. Nondestruct. Eval.* **7,** 215–228 (1996).

26. Bossi, R. H. & Giurgiutiu, V. in *Polymer Composites in the Aerospace Industry* 413–448 (2015). doi:10.1016/B978-0-85709-523-7.00015-3

27. Guo, G., Tu, J., Zhang, Y. & Shi, Y. Inspection of Kissing-bond Defect in Honeycomb Structure by shearography. in *18th World Conference on Nondestructive Testing* 16–20 (2012).

28. Hung Y.Y. Yang L.X. in *Non-destructive evaluation (NDE) of polymer matrix composites* 84–115 (Woodhead Publishing Limited, 2013).

29. Yang, L.X. Hung, Y. Y. Digital Shearography for Nondestructive Evaluation and Application in Automotive and Aerospace Industries. at <http://www.ndt.net/article/wcndt2004/pdf/optical_techniques/534_yang.pdf>

30. Francis, D. in *Non-destructive evaluation (NDE) of polymer matrix composites* 56–83 (2013).

31. Hung, Y. Y. Applications of digital shearography for testing of composite structures. *Compos. Part B Eng.* **30,** 765–773 (1999).

32. Pandurangan, P. & Buckner, G. D. Vibration analysis for damage detection in metal-to-metal adhesive joints. *Exp. Mech.* **46,** 601–607 (2006).

33. Shiloh, K. *et al.* Aging Characterization of Adhesives and Bonded Joints by Non-Destructive Damping Measurements. *J. Intell. Mater. Syst. Struct.* **10,** 353–362 (1999).

34. Srivatsan & T. Electromagnetic measurement of damping capacity to detect damage in adhesively bonded material. *Mater. Eval.* **47,** 564–570 (1989).

35. Chung, D. D. L. Structural composite materials tailored for damping. *J. Alloys Compd.* **355,** 216–223 (2003).

36. Vijaya Kumar, K. R. & Sundareswaran, V. Mechanical and damping properties of epoxy cyanate matrix composite under varied temperatures. *J. Eng. Appl. Sci.* **5,** 106–111 (2010).

37. Cawley, P. & Adams, R. D. The mechanics of the coin-tap method of non-destructive testing. *J. Sound Vib.* **122,** 299–316 (1988).

38. Bossi, Richard, et al. Laser Bond Testing. *Mater. Eval.* 819–827 (2009).

39. Vijaya Kumar, R. L., Bhat, M. R. & Murthy, C. R. L. Evaluation of kissing bond in composite adhesive lap joints using digital image correlation: Preliminary studies. *Int. J. Adhes. Adhes.* **42,** 60–68 (2013).
40. Heller, K., Jacobs, L. J. & Qu, J. Characterization of adhesive bond properties using Lamb waves. *NDT E Int.* **33,** 555–563 (2000).
41. Ramadas, C., Balasubramaniam, K., Hood, A., Joshi, M. & Krishnamurthy, C. V. Modelling of attenuation of lamb waves using rayleigh damping: Numerical and experimental studies. *Compos. Struct.* **93,** 2020–2025 (2011).
42. Su, Z., Ye, L. & Lu, Y. Guided Lamb waves for identification of damage in composite structures: A review. *J. Sound Vib.* **295,** 753–780 (2006).
43. Alleyne, D. N. & Cawley, P. Optimization of lamb wave inspection techniques. *NDT E Int.* **25,** 11–22 (1992).
44. Samaratunga, D. & Jha, R. Lamb wave propagation simulation in smart composite structures. in *SIMULIA Community Conference* 1–11 (2012).
45. Cawley, P. The rapid non-destructive inspection of large composite structures. *Composites* **25,** 351–357 (1994).
46. Diamanti, K. & Soutis, C. Structural health monitoring techniques for aircraft composite structures. *Prog. Aerosp. Sci.* **46,** 342–352 (2010).
47. Georgeson, G. et al. Damage Detection Device and Method. 1–7 (2004).
48. Georgeson, G., Lea, S. & Hansen, J. Electronic Tap Hammer for Composite Damage Assessment. *SPIE* **2945,** 328–338
49. Kunihiro Mitsuhashi et al. Method and Apparatus for Impact-Type Inspection of Structures. 1–17 (1991).
50. Hsu, D. K. et al. Non-Destructive Inspections and the Displae of Inspection Results. 1–5 (2001).
51. P N F4TAP002, RD^3 Electronic Digital Tap Hammer On WichiTech Industries, Inc. (2011). at <http://hotbonders.wichitechindustries.com/category/non-destructive-testing-device-tap-hammer->
52. Earthman, J. C. System and Method for Quantitative Measurements of Energy Damping Capacity. (2000).
53. Stanley, B.D., Bustemente, L., Earthman, J. C. Novel Instrumentation for Rapid Assessment of Internal Damage in Composite Materials. in *The Mineral, Metals,& Materials Society* 97–100 (1997).
54. Brenner, D. A. & Earthman, J. C. Novel instrumentation for quantitative determination of energy damping in materials and structures. *Scripta Metallurgica et Materialia* **31,** 467–471 (1994).
55. Sheets, C. G. & Earthman, J. C. Tooth intrusion in implant-assisted prostheses. *J. Prosthet. Dent.* **77,** 39–45 (1997).
56. Dinh, A., Sheets, C. G. & Earthman, J. C. Analysis of percussion response of dental implants : an in vitro study. *Mater. Sci. Eng. C* 1–26 (2013).
57. VanSchoiack, L. R., Wu, J. C., Sheets, C. G. & Earthman, J. C. Effect of bone density on the damping behavior of dental implants: An in vitro method. *Mater. Sci. Eng. C* **26,** 1307–1311 (2006).
58. Mitchell, D., Lincoln, J., Rieger, L. & Earthman, J. Instrumentation for Determining the Local Damping Capacity in Honeycomb Sandwich Composites. *Journal of Testing and Evaluation* **34,** 12186 (2006).

59. Shields, a. J., Hepburn, D. M., Kemp, I. J. & Cooper, J. M. Absorption of mould release agent by epoxy resin. *Polym. Degrad. Stab.* **70,** 253–258 (2000).
60. Axel, F. Choosing the correct mould release. *Reinf. Plast.* **43,** 24–29 (1999).
61. Mould releases: Products and suppliers. *Reinf. Plast.* **43,** 32–35 (1999).
62. Mould releases – an overview. *Reinf. Plast.* **52,** 32–34 (2008).
63. Goss, B. The effective use of mould release agents. *Reinf. Plast.* **48,** 24–26 (2004).
64. Jeenjitkaew, C., Luklinska, Z. & Guild, F. Morphology and surface chemistry of kissing bonds in adhesive joints produced by surface contamination. *Int. J. Adhes. Adhes.* **30,** 643–653 (2010).
65. Brotherhood, C. J., Drinkwater, B. W. & Dixon, S. The detectability of kissing bonds in adhesive joints using ultrasonic techniques. *Ultrasonics* **41,** 521–529 (2003).
66. Adams, D. E., Sharp, N. D., Myrent, N. & Sterkenburg, R. Inspection for kissing bonds in composite materials using vibration measurements. in *Nondestructive Characterization for Composite Materials* **7983,** 79830W–79830W–8 (2011).
67. Amine Blushing and Blooming of Epoxy Binder Systems. *Dow Technical Bulletin* 1–5 (2007). at <http://msdssearch.dow.com/PublishedLiteratureDOWCOM/dh_00cb/0901b803800cb78d.pdf?filepath=/296-01656.pdf&fromPage=GetDoc>
68. Sapora, A. & Paggi, M. A coupled cohesive zone model for transient analysis of thermoelastic interface debonding. *Comput. Mech.* **53,** 845–857 (2014).
69. Kregting, R. *Cohesive zone models*. 1–31 (2005). at <http://www.mate.tue.nl/mate/pdfs/5169.pdf>
70. Planas, J., Elices, M. & G, J. The cohesive zone model: advantages, limitations and challenges. *Eng. Fract. Mech.* **69,** 137–163 (2002).

APPENDIX 1: DESCRIPTION OF PERIOMETER AND QUANTITATIVE PERCUSSION ANALYSIS IMPORTANT DATA PARAMETERS

1. Loss Coefficient – A measure of how much energy is dissipated

2. Defect Factor – A measure of the asymmetry of the impact/time curve.

3. Probe Force – A measure of the impact force returned to the probe (measured by accelerometer).

Percussion Equipment Parts Description

1. Probe - The probe contains a metal rod that is driven by an electromagnetic coil which provides an initial kinetic energy upon impact with the test specimen. An accelerometer, attached to the rod, measures the amount of force returned to the rod. Based on this measurement the amount of energy dissipated by the test specimen at specific locations can be calculated.   A level is attached to the probe to aid in alignment. Once activated, the probe will actuate 16 times in four seconds.

2. Power Supply - The power supply provides the voltage needed to operate the probe. There is a power button at the side that must be pushed to turn on. The power supply automatically turns off after a few minutes of no use. The user must continually check that the power is on before taking measurements.

3. Computer – Lap-top provided to run the Lab-view application called "Periometer" which is used to operate the percussion instrumentation and measure and collect data.

Initial Experimental Checks

1. Verify that the nozzle around the steel rod is not loose. This can affect data collection. Make note of the nozzle used and calibration should be performed using this nozzle.

2. Minimize pressure when nozzle is in contact with the specimen. The applied pressure from the nozzle can affect data collection and may damage fragile specimens.

3. All percussion measurements shall be taken horizontally, as level as possible. Vertical measurements shall be avoided due to effects from gravity.

4. Specimen shall either be placed in a test fixture or held by the edges by hand before taking percussion measurements.

Experimental Start-up

1. Turn on power supply and wait roughly 10 minutes before use (reduce electronic drift).

2. Turn on computer and enter password.

3. Activate the application: Periometer

4. When the application starts, a pop-up comes up for calibration. Either enter a calibration ID or start a new calibration.

Choosing to Calibrate:

1. Push probe against calibration sample (attached to power supply). Activate probe.

2. Once data is collected, the data will be shown and the program will ask to accept the data. Click yes if the standard deviation is good (roughly less than 1N standard deviation is considered acceptable). Data collection must be done 3 times per calibration sample. (There are 2 calibration samples.)

3. At the end of calibration, enter a save ID. Note: To be consistent, the ID should include the date the data was taken and nozzle description (if desired).

Data Collection

1. The program first asks the user to create a folder to save the percussion data. Label the folder with the date and specimen label.

2. Next, the program allows the user to preset the number of samples to be tested. Presetting allows recording of data at specific locations. Note: Although the program states samples, generally use presetting for locations on one sample. You can add another preset just in case an error was created on a previous preset.

3. Collect data on a preset. If needed, repeat data collection.

4. After completing testing of one sample the user has the option to save or not save the data. Note: Only the raw data of the final data taken of a preset will be saved. The mean loss coefficient, standard deviation, and defect factor will be saved for each measurement.

5. The data will be saved as excel, word, and picture files.

Manipulating data/data labels:

1. Graphs - All graphs are represented as energy vs time. Raw data for 10 energy/time curves will be saved.

2. Superimpose Button – Allows user to combine the ten peaks together to view after each measurement.

3. High Deviation Warning - High standard deviation. Generally should repeat test if this tab is seen. This is observed when the percussion rod does not make good contact with the specimen surface.

APPENDIX 2: EXAMPLE OF ALIGNMENT MEASUREMENTS FOR NEW TEST FIXTURE

|	
Date	
Specimen Test	

Alignment Checklist for Percussion Test Fixture

1) Test Fixture is level (adjust using feet).   □

2) Hex bolts are flush against aluminum rails.   □

3) Panel is level.

Distance from bottom bumpers to panel edge is ~25.4 mm (~1in.)   □

Distance from top bumper to panel edge is ~8.89 mm (~0.35 in.)   □

4) Aluminum rails are equi-distant apart

Top right rail to rail distance   □

Top left rail to rail distance   □

Bottom right rail to rail distance   □

Bottom left rail to rail distance   □

APPENDIX 3: FEA ANALYSIS PROCESS INSTRUCTIONS

The following bullet points outline the process followed to create a percussion

rod/composite bonded panel model using MSC PATRAN/NASTRAN.

- Create composite bonded panel model in Patran.

  - Geometry: Modeled secondary bonded composite laminate by using three rectangular solids. Bond-line thickness = 0.009". Facesheets thickness = 0.062". Use Create/Solid/XYZ and define reference point where solids were formed from. Solid 3 (film adhesive) was created by matching two surfaces from Solids 1 and 2 (top and bottom laminates). Use Create/Solid/Surface.

  - Mesh: Used mesh seeds across both X and Y axis for one of the solid's edges. Choose element length to ensure the same number of elements were across each side. 4 elements were used through the thickness of each laminate. Also, 4 elements were used to mesh the bondline thickness making the element thickness = 0.00225 in. As a result, the largest mesh length that can be used in the entire model is 0.00225 in. X 10 = 0.0225 in. to maintain a 10/1 aspect ratio. The bonded laminate was meshed using 3D Hexagonal 8 elements (6 faces and 8 nodes per element). The top and bottom laminate were created as a separate group and meshed first. Next, the film adhesive was put in its own group and meshed. This was done to make it easier to change the film adhesive properties only (create contamination layer, etc.) later on in the modeling.
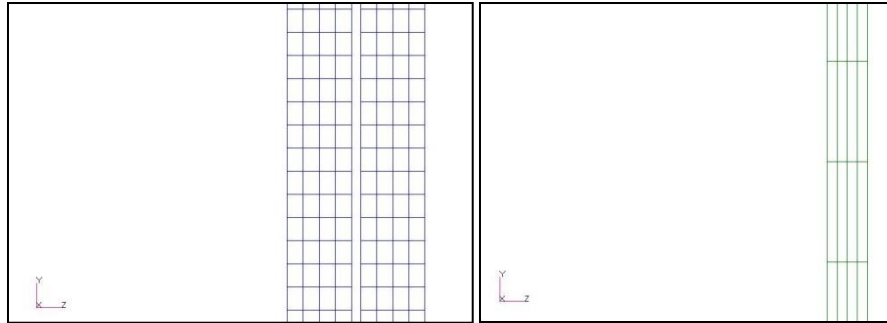
Cross section of top and bottom
laminate showing mesh

Cross section of film
showing mesh

- o After meshing, the entire bonded laminate was 'Equivalenced'

  (Mesh/Equivalence) to remove duplicate nodes. If this step is not done the

  model will not run without errors.
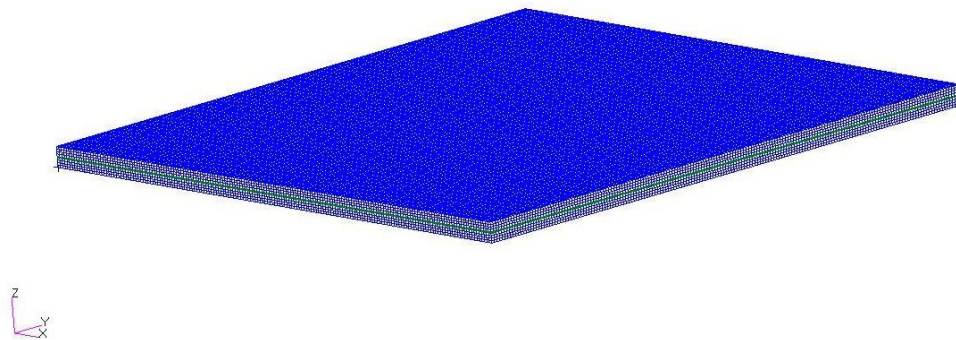
Top and bottom laminate and film meshed and equivalenced

- o Properties: 3D solid elements were used to model the bondline of the

  laminate accurately. The film adhesive was modeled as isotropic and the

  laminates were modeled as 3D orthotropic. Mass density needs to be used

  when inputting properties.

- Next, the percussion rod was imported into PATRAN. Create a new group first, then

  import 'Scaled percussion' rod file into PATRAN with composite bonded panel.

- Rescale Percussion Rod using Group/Transform/Scale (0.0394, 0.0394, 0.0394) to

  convert to inches.

122
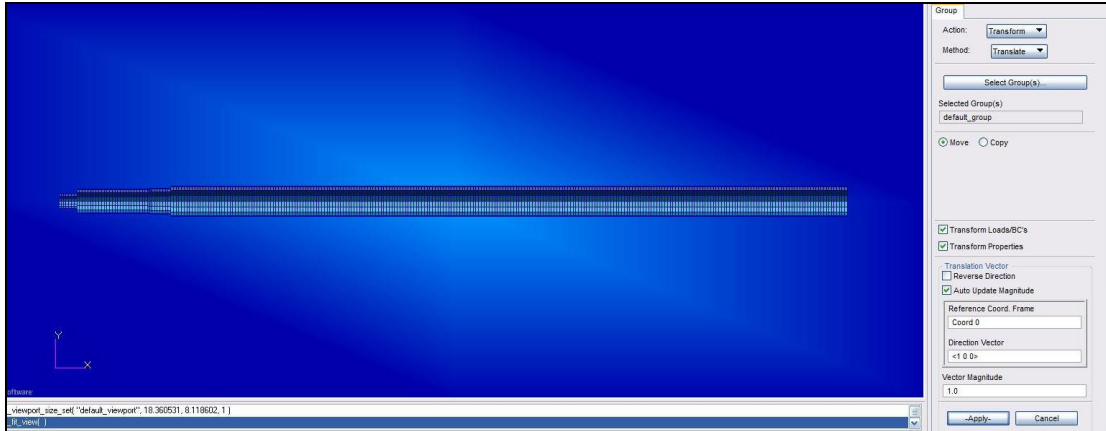
View of full percussion rod with transform action selected on right side

- Post composite panel and percussion rod groups.

- Group/Transform/Translate rod close to Composite bonded panel. Use Display/Coordinate Frames and unpost coordinate frames to rescale images.

- Group/Rotate percussion rod around coord.2 Y-axis 90 degrees.

- Group/Transform/Translate along correct vectors to place rod in center right edge location. Rod should be close to surface of composite panel but not touching. Use Geometry Show Distance between nodes to calculate distances.

- Un-post Composite Panel. Select Percussion Rod and make it a top view and delete half of elements s the Percussion Rod is a half a model.
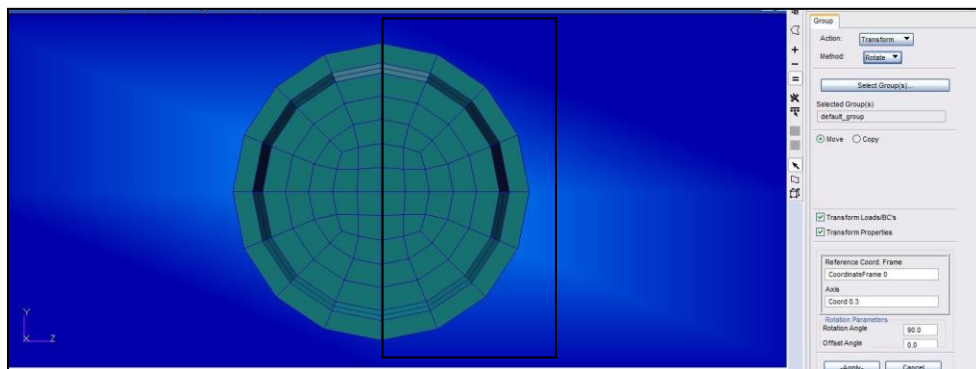

Top view of full percussion rod is shown above. Elements shall be selected that are inside the black box and deleted to create the half model.
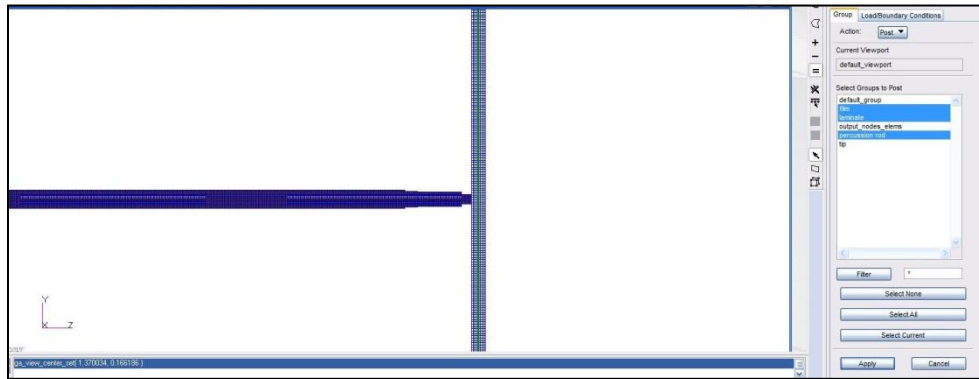
View of cross section of half percussion rod model. Rod is positioned centered along right edge of composite panel.

- Apply boundary conditions to percussion rod. Allow rod to slide in Z direction. Constrain entire rod in X and Y directions (Displacement constraint X=Y=0).

- Apply deformable contact bodies. Select percussion rod. Post just composite laminates. Select composite laminates and apply deformable contact bodies.

- Apply initial velocity -2.36 inch/second to percussion rod.

- Composite panel has two nodal displacement constraints and one symmetry plane. One nodal constraint is in the middle of the bottom of the panel on the back edge (XYZ constrained). The second nodal constraint is the back top left corner (XYZ constrained). The symmetry plane constrained is the entire left side highlighted by the red arrows (shown below). This plane is constrained in the X direction only.
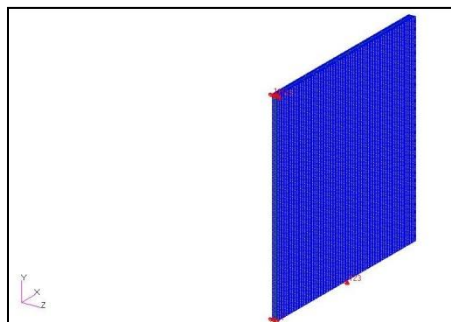
Composite panel showing displacement constraints

- Verify properties are correct. Need to change steel modulus to pounds per square inch for percussion rod (30e6 psi). Also need to change density to mass density. This can be determined by determining the weight of the rod divided by two. Then calculate the volume of rod in Patran. Next, calculate the weight density and then multiply by 0.00259 to get mass density of the rod ½ model.

- Create load case with correct boundary conditions stated in the above bullet points.

- Create new group 'output_nodes_elems'. Select all elements in the percussion rod and a small centered section of the composite panel (shown below). This group will be used to calculate the element stresses and will help reduce model run time.

- Use Implicit Non-Linear-Sol 400 in MSC NASTRAN to run analysis.

- Create new subcase for run. Select time scale of 10us and use 320 time steps. Select element stresses as output and select the group 'output_nodes_elems'

- Choose subcase just created and run analysis.

- Analysis run time is around 36 hours.
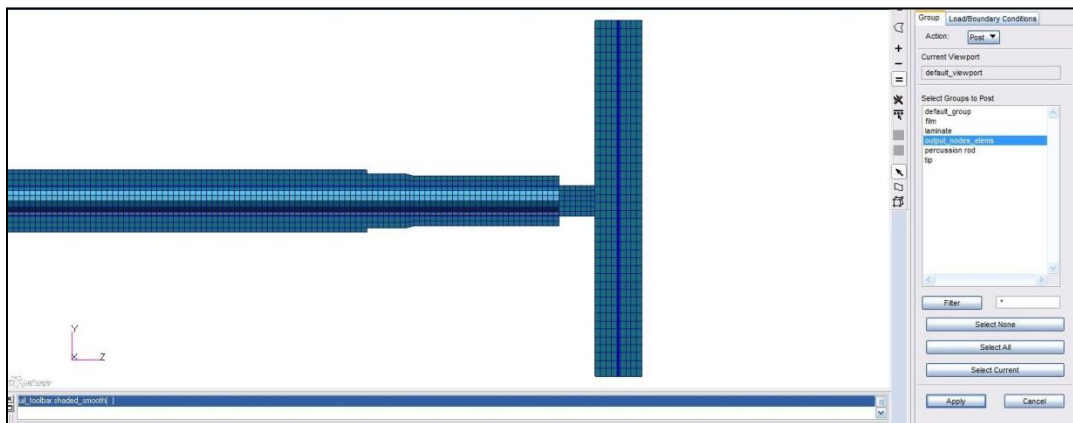
The percussion rod and 'centered' composite panel section within Group 'output_nodes_elems'.